



Master Thesis

Miniaturization of a cerebral Open-Flow Microperfusion probe

Author: Christoph Ober BSc

Institute of Biomechanics
Center of Biomedical Engineering
Graz University of Technology
Kronesgasse 5-I, 8010 Graz, Austria

HEALTH - Institute of Biomedicine and Health Sciences
Biomedical Technology and Monitoring
Joanneum Research Forschungsgesellschaft mbH
Elisabethstrasse 11A, 8010 Graz, Austria

Supervisors (JR): Thomas Birngruber MSc and Thomas Kroath MSc
Evaluator (TUG): Professor Gerhard A. Holzapfel, PhD

July 5, 2013

Contents

1. Introduction	1
1.1. Neurotherapeutics and the Blood-Brain Barrier	1
1.2. Open-Flow Microperfusion	3
1.3. Microfluidics	4
1.3.1. Multiphase flow through microchannels	5
1.3.2. Materials and fabrication techniques	9
1.4. Aim of the Thesis	10
2. Materials and Methods	13
2.1. Cerebral Open-Flow Microperfusion	13
2.2. Rheological Characterization	15
2.2.1. Composition of the fluids	15
2.2.2. Viscosity and rotational rheometry	17
2.3. cOFM Probes	20
2.3.1. Material characteristics	20
2.3.2. Version 1.0	23
2.3.3. Version 2.0	28
2.3.4. Test probes	32
2.3.5. Comparison of the probe types	36
2.4. Performance Comparison In-Vitro	38
2.4.1. Feasibility studies	38
2.4.2. Main studies	44
2.5. Performance Comparison In-Vivo	47
2.5.1. Objective	47
2.5.2. Animals	47
2.5.3. Implantation	48
2.5.4. Marker Injection	51
2.5.5. Sampling and deuterium measurement	51
2.5.6. Quantitative analysis	51
3. Results	53
3.1. Rotational Rheometry	53
3.2. Miniaturization in Theory	55
3.3. Performance Comparison In-Vitro	56
3.3.1. Feasibility studies	56

3.3.2. Main studies	57
3.4. Performance Comparison In-Vivo	62
4. Discussion	65
4.1. Rheological Characterization	65
4.2. cOFM Probes	66
4.3. In-Vitro Performance	69
4.4. In-Vivo Performance	70
4.5. Conclusion	71
4.5.1. Handling optimization	71
4.5.2. Outlook	71
Appendix	81
A. General material properties	82
A.1. PTFE	82
A.2. PI	87
A.3. PEEK	93
A.4. PMMA	96
A.5. FEP	102
B. SOP Rheometer	108

Abstract

Cerebral Open-Flow Microperfusion (cOFM) is a microfluidic system to sample brain interstitial fluid after re-establishment of the Blood-Brain Barrier. Currently, it is used for preclinical studies in rats to evaluate the pharmacodynamics and pharmacokinetics of neurotherapeutic drugs. The intention is to use the same sampling system in other animal models such as mice due to the higher number of pharmacological models available. Therefore, the aim of this thesis was to miniaturize the current cOFM probe V1.0, especially its guide cannula.

The first step was an evaluation of the current cOFM system to get used to the system and to assess miniaturization possibilities. The fluids of interest were rheologically characterized by studying their viscosity, surface tension and composition. Based on the findings, miniaturization boundaries were assessed. Prototypes (V2.0) and test systems (V3.0) were designed and assembled. All three probe types were compared in-vitro by studying the differences of the exchange performance of glucose molecules in an agar network. V1.0 and V2.0 were used in a comparative in-vivo study by choosing the relative recovery (RR) of deuterium as parameter of comparison.

The miniaturization did not decrease the performance of exchange performance of glucose molecules in the in-vitro studies and did not influence the flow behavior. Likewise, miniaturization lead to no differences in the RR of deuterium in the in-vivo studies.

However, the miniaturization affected negatively the handling properties. To enhance the handling capability, a new prototype was designed.

KEYWORDS: cOFM; microfluidics; miniaturization; in-vitro; in-vivo

Kurzfassung

Die zerebrale offene Mikroperfusion (cOFM) ist ein mikrofluidisches System, um interstitielle Flüssigkeit aus dem Hirn nach Wiederherstellung der Blut-Hirn-Schranke zu entnehmen. Diese Methode wird zur Zeit in präklinischen Studien an Ratten angewandt, um die Pharmakodynamik und Pharmakokinetik von neurotherapeutischen Medikamenten zu erforschen. In Zukunft soll das System auch an anderen Tiermodellen wie z.B. an Mäusen angewandt werden, da für diese eine größere Anzahl pharmakologischer Modelle zur Verfügung steht. Das Ziel der Arbeit war es daher, den aktuellen cOFM-Katheter V1.0 und im Speziellen dessen Guide-Kanüle zu miniaturisieren.

Der erste Schritt war eine Evaluierung des aktuellen cOFM-Systems, um Möglichkeiten der Miniaturisierung abschätzen zu können. Es folgte eine rheologische Charakterisierung der Flüssigkeiten, welche bei der cOFM zur Anwendung kommen. Dabei wurden deren Viskositäten, Oberflächenspannungen und Zusammensetzungen erforscht. Nach einer theoretischen Abschätzung der minimalen Dimensionen basierend auf fluidischen Berechnungen wurden miniaturisierte Prototypen (V2.0) und Testsysteme (V3.0) entwickelt. V1.0, V2.0 und V3.0 wurden in einer in-vitro-Studie miteinander verglichen, in der das Austauschverhalten von Glukosemolekülen in einem Agar-Netzwerk erfasst wurde. V1.0 und V2.0 wurden in einer komparativen in-vivo-Studie verwendet, in der die sogenannte Relative Recovery von Deuterium als Vergleichsparameter verwendet wurde.

Die Miniaturisierung hatte in den in-vitro-Studien weder einen Einfluss auf das Austauschverhalten von Glukosemolekülen noch einen Einfluss auf die Fluidik. In den in-vivo-Studien wurde das selbe Ergebnis erzielt.

Im letzten Schritt der Arbeit wurde das Design des miniaturisierten Prototypen überarbeitet, um dessen Gebrauchseigenschaften zu verbessern.

SCHLÜSSELWÖRTER: cOFM; Mikrofluidik; Miniaturisierung; in-vitro; in-vivo

Acknowledgment

I would like to thank Thomas Birngruber, Thomas Kroath, Frank Sinner and Prof. Thomas R. Pieber for giving me the opportunity to write the thesis at the Joanneum Research GmbH - HEALTH and for their outstanding and patient supervision.

I am grateful to Prof. Gerhard A. Holzapfel from the Institute of Biomechanics (TU Graz) for his advice and support and for taking over the evaluation of the thesis. Thanks are also due to Michael Unterberger from the same institute for his supervision of the rheological experiments.

I wish to extend thanks to the staff of the Institute of Biomedical Research from the Medical University of Graz, especially to Günther Rauter, and to Albrecht Leis from the Joanneum Research GmbH - RESOURCES.

Last but not least I address special thanks to my parents for their support and for believing in me during my study years.

List of Abbreviations

- **aOFM**: adipose Open-Flow Microperfusion
- **BBB**: Blood-Brain Barrier
- **BW**: Body Weight
- **cOFM**: cerebral Open-Flow Microperfusion
- **CSF**: Cerebrospinal fluid
- **ddH₂O**: Aqua bidest, distilled water
- **DIE**: Desired Initial Enrichment
- **dOFM**: dermal Open-Flow Microperfusion
- **FEP**: Fluorinated ethylene propylene
- **FMD**: Fentanyl, Midazolam, Domitor
- **ID**: Inner Diameter
- **IE**: Injection Enrichment
- **i.p.**: intraperitoneal
- **ISF**: Interstitial fluid
- **IV**: Injection Volume
- **MD**: Microdialysis
- **Naf**: Sodium fluorescein
- **OD**: Outer Diameter
- **OFM**: Open-Flow Microperfusion
- **PD**: Pharmacodynamics

- **PEEK**: Polyetheretherketone
- **PI**: Polyimide
- **PK**: Pharmacokinetics
- **PMMA**: Polymethylmethacrylate
- **ppm**: parts per million
- **PTFE**: Polytetrafluoroethylene
- **RR**: Relative Recovery
- **s.c.**: subcutaneous
- **SOP**: Standard Operating Procedure
- **SP**: Syringe Pump

1. Introduction

1.1. Neurotherapeutics and the Blood-Brain Barrier

Mental and neurological disorders are a major burden in Europe. In the European Union plus Iceland, Norway and Switzerland (514 million inhabitants) the total number of brain disorder diagnoses was 380 million in 2010. About 33% of the population were diagnosed to have at least one such disorder (Olesen et al., 2012). It was further estimated, that the total (direct, in-direct and non-medical) cost of brain disorders was 798 billion €. This is an average cost per inhabitant of about 5.550 €. Most costly are mood disorders (113.4 bn €), dementia (105.2 bn €) and psychotic disorders (93.9 bn €). The development of neurological therapeutics is hence an important but difficult task.

The Blood-Brain Barrier (BBB) (Fig. 1.1) separates the blood from the interstitial fluid (ISF) in the brain. Its main task is to maintain homeostasis by highly selective and effective influx and efflux mechanisms. It does not only protect the ISF from toxic agents, but hinders also the transport of macromolecules into the brain. Small molecules are transported through the BBB using carrier-mediated or active flux systems. Large molecules like leptin or insulin can pass the BBB via receptor-mediated transport systems, or can be packaged into small 100 nm nanoparticles or liposomes. Nevertheless, more than 98% of small therapeutics and approximately 100% of large therapeutics cannot pass the BBB (Pardridge, 2005).

There is a need for reliable and continuous in-vivo methods to assess the pharmacokinetics (liberation, absorption, distribution, metabolism and elimination, Aktories et al., 2009) and the pharmacodynamics (effect of the drug on the body) of neurotherapeutics. This is done by evaluating the transport over the BBB. A state-of-the-art in-vivo method is the brain microdialysis (Chefer et al., 2009 and Darvesh et al., 2011). Here, a double-lumen probe is implanted into the brain. A perfusate is pushed into the probe, molecules are

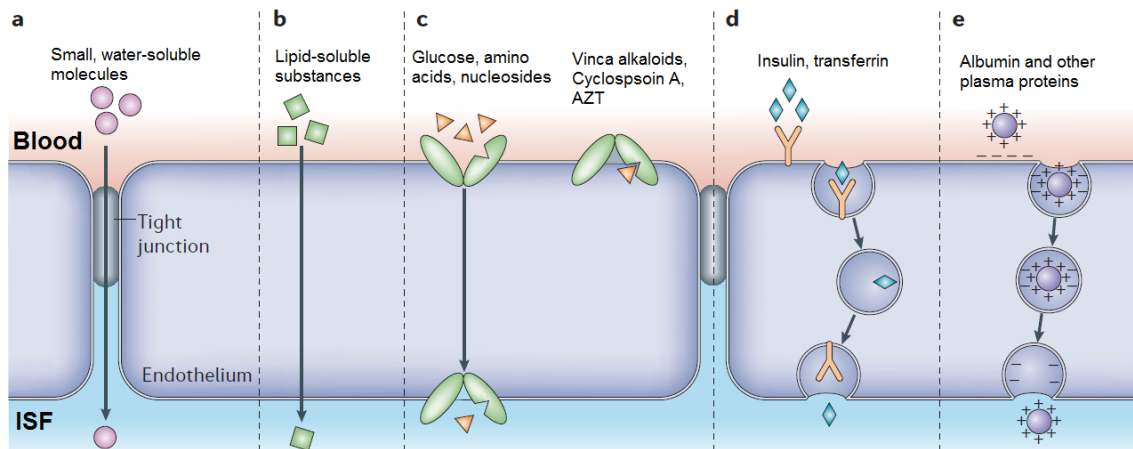


Figure 1.1.: Transport mechanisms through the Blood-Brain Barrier, modified from [Abbott et al., 2006](#) and [Brasnjevic et al., 2009](#). a) Small amounts of water-soluble agents diffuse through tight junctions into the brain (paracellular aqueous pathway). b) Lipid-soluble agents, such as O_2 , CO_2 , alcohol and steroid hormones pass the BBB over the transcellular lipophilic pathway by dissolving into the plasma membrane. c) Nutrients and endogeneous substances, such as glucose, amino acids or AZT, pass the BBB by a saturable, highly specific carrier-mediated transport mechanism. d) Proteins and peptides like insulin are transported using a receptor-mediated transport mechanism. e) Positively charged proteins such as cationic Albumin pass the BBB via adsorptive transcytosis. The efflux transport system, which removes substances from the ISF or the CSF, is not shown.

exchanged over a size-selective membrane and this mixture is stored for further analysis. The membrane at the implanted probe tip protects the fluidic path. It has the disadvantage to hinder the exchange of lipophilic and high-molecular weight substances ([Pieber et al., 2013](#)).

1.2. Open-Flow Microperfusion

Open-Flow Microperfusion (OFM, [Pieber et al., 2013](#)) is a microfluidic sampling system that allows continuous sampling of interstitial fluid (ISF) in various tissues. It is used to assess the pharmacokinetics and pharmacodynamics of tissue-specific therapeutics. *Perfusate* is pumped into the tissue, where substances of the ISF are exchanged with the perfusate due to convection and diffusion through macroscopic openings. This mixture (*sample*) is pulled out for further analysis. A depiction of a sampling system is shown in Fig. 1.2. OFM is a technique similar to microdialysis, without a membrane at the exchange area. Therefore, problems like membrane fouling, clotting or filtering of high-molecular, lipophilic substances are avoided. Furthermore, protein-bound substances and even entire cells can be sampled. A challenge of the OFM method is the quantitative analysis of the complex samples.

Currently, OFM can be applied in three tissues types: adipose tissue (aOFM), dermal tissue (dOFM) and cerebral tissue (cOFM). Sampling in adipose tissue has been developed in 1995 ([Skrabal et al., 1995](#)). Since, aOFM has been applied to quantify different substances for endocrinological purposes in pre-clinical and clinical ex-vivo and in-vivo studies, such as lactate ([Ellmerer et al., 1998](#)), insulines ([Bodenlenz et al., 2005](#)) or cytokines ([Ikoeka et al., 2011](#)). dOFM was introduced in 2010 and has been used in dermatological studies, investigating e.g. inflammatory skin diseases like psoriasis ([Bodenlenz et al., 2012](#)). cOFM is being used in pre-clinical neurological studies in rats since 2010, and is the method of interest in this thesis. Using cOFM, the transport of neurotherapeutic substances over the BBB can be assessed.

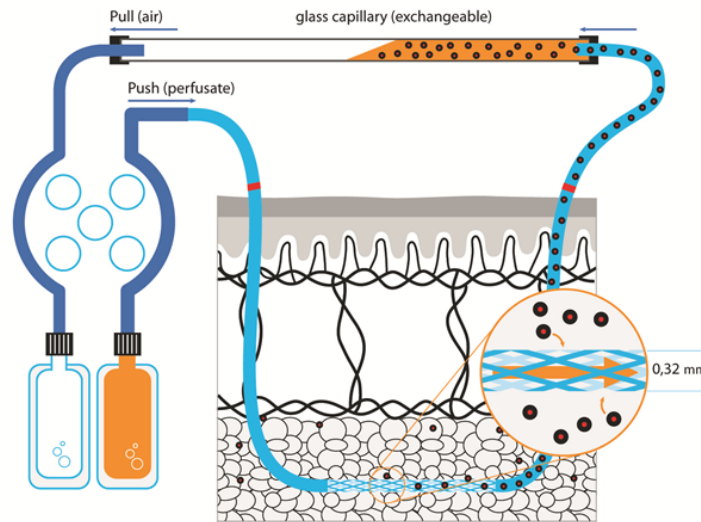


Figure 1.2.: Schematic of a dOFM sampling system, taken from [Pieber et al., 2013](#). The perfusate is pushed into the extracellular matrix by means of a peristaltic pump. Different molecules diffuse through the macroscopic openings and mix with the perfusate. This mixture is pulled out with the same flow rate through polymeric tubes and glass capillaries and sampled.

1.3. Microfluidics

Microfluidic systems process or manipulate fluids at microscale (10^{-9} to 10^{-18} litres). In microchannels, fluid flow behaves differently than conventional fluid flow due to the smaller dimensions (between ten and hundreds micrometers, [Whitesides, 2006](#)).

Fluidic systems at microscale offer several advantages, e.g. time and cost savings due to smaller sample volumes and reagent wastage, high reproducibility due to the increased ability of parallelization or the capability to easily control fluid flow and reactions due to the laminar flow characteristic ([Whitesides, 2006](#), [Rivet et al., 2011](#)).

Research and development of microfluidic systems has grown significantly in the last years. Currently, microfluidic systems are used in a broad range of biomedical applications ([Janasek et al., 2006](#), [Rivet et al., 2011](#), [Yeo et al., 2011](#)). Methods and techniques include e.g. the so-called Lab-on-a-chip, digital, droplet-based microfluidics or optofluidics. These methods are used for the analysis of genes, proteins or cells, for biochemical or pathogen detection in combination with biosensors, for point-of-care diagnostics, biomaterial and tissue engineering, and, like OFM, for drug development and delivery.

1.3.1. Multiphase flow through microchannels

Fluids encountered in OFM studies are generally multiphase. They consist of the water-like perfusate, soluted ISF molecules and particles as well as small gas bubbles.

The flow of single-phase fluids can be predicted by continuum mechanics down to a very small length scale (Nguyen and Wereley, 2006). For a single-phase liquid flowing through a microchannel, continuum approach can be assumed starting from a channel diameter of about 10^{-8} m. A gaseous flow through a microchannel with a diameter of 10^{-6} m can be treated as a continuum (Squires and Quake, 2005). Microfluidic flow behavior differs from nano- and conventional fluidics. Nanofluidics (Bocquet and Charlaix, 2010) is strongly influenced by surface interactions and can be modeled using molecular dynamic simulations. Conventional fluidic flows are influenced by external and volume forces like inertia or gravity and hence are turbulent. Microfluidic flow is influenced mainly by surface tension and viscosity, inertia becomes irrelevant. A length scale comparison is given in Fig. 1.3. The irrelevance from inertia can be expressed by the *Reynolds Number*, which is the ratio of inertial force density f_i to viscous force density f_v :

$$Re = \frac{f_i}{f_v} = \frac{\rho v d}{\eta}, \quad (1.1)$$

where ρ is the density of a fluid, v is the velocity and d is the diameter of a channel. If Re is smaller than 1, the flow is laminar, otherwise it is turbulent. Microfluidic flows are generally laminar.

The general equation of motion for incompressible Newtonian fluids is given by the Navier-Stokes equation. When dealing with microfluidic systems, it is often simplified by working only with pressure gradient and viscosity and by neglecting inertial terms. Further assumptions are a steady, laminar, fully developed and unidirectional flow. The result is an equation which expresses the linear Stokes flow (Bruus, 2008). The solution of this equation is the general Hagen-Poiseuille law, i.e.

$$Q = \frac{\Delta p}{2\eta L} \frac{A^3}{P^2}. \quad (1.2)$$

The flow rate Q is directly proportional to the applied pressure difference Δp and inversely proportional to the viscosity of the fluid η and a channel length L . The flow rate depends on the channel area A^3 and the perimeter of the channel P^2 . The most important assumption

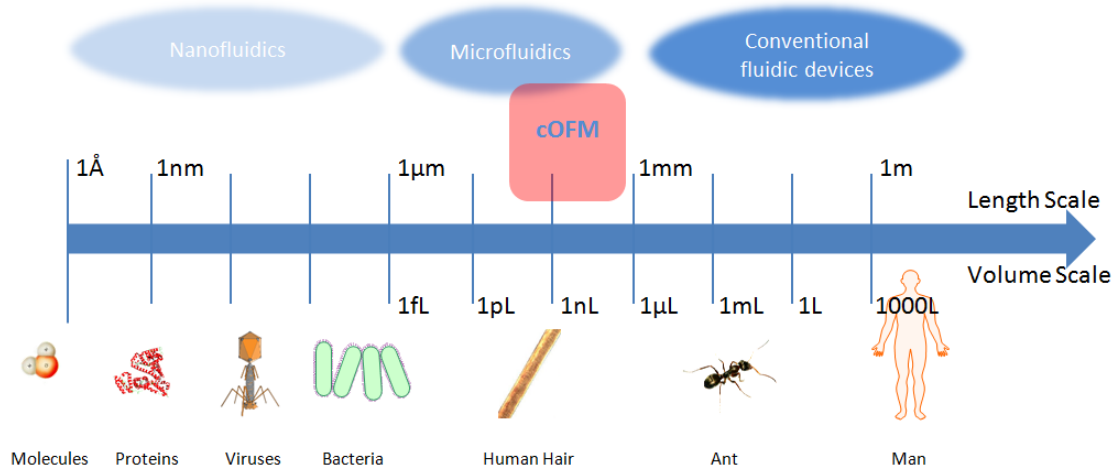


Figure 1.3.: cOFM technology compared to other sizes scales. Microfluidic systems, like the cOFM sampling system, process or manipulate fluids volumes between 10^{-9} and 10^{-18} litres. Microchannels with diameters between 10^{-3} and 10^{-6} mm are used. The range for nanofluidics is below, the range of conventional fluidics above the microfluidic size scale.

of the Hagen-Poiseuille law is the *no-slip boundary condition*, a parabolic flow profile with $v = 0$ at the channel wall boundaries (Lauga et al., 2007). This assumption is not always valid. Dissolved gas, a hydrophobic tubing and increased pressure lead to a higher slipping probability. Other influences are surface roughness, shear rate and electrical properties. The entrance length L_e (Sharp et al. 2005) is the region in a channel, where the fluid flow transitions from the entrance profile to the fully developed parabolic flow profile. The flow is assumed to be fully developed after $L_e = 0.06 Re d$, where d is the diameter of the microchannel.

A two-phase flow (fluid and gas bubbles) differs from conventional flow due to its enhanced compliancy. Important parameters for a gas-liquid flow are the surface tension, the contact angle and the surface roughness.

Surface tension (Fig. 1.4 A, B) is defined as the free energy per area at a certain temperature and pressure at the interface between two different phases. A tension develops due to the different chemical constitutions and bondings of each phase (Bruus, 2008). The *contact angle* θ (Fig. 1.4) of a liquid drop on a solid is measured at the meeting point of the 3 immiscible phases. It can be calculated using the surface tensions between the three

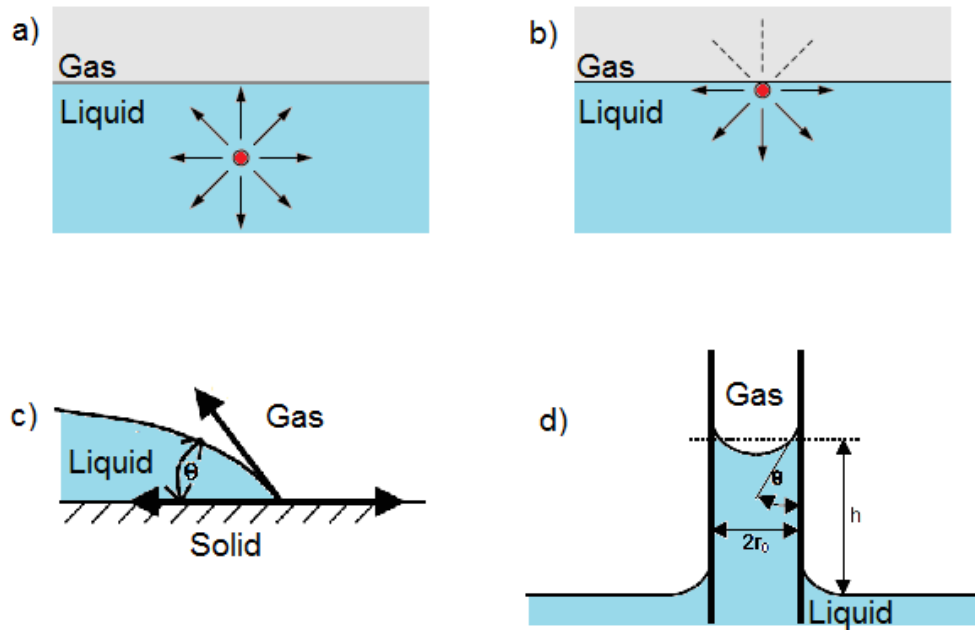


Figure 1.4.: Surface tension, contact angle and capillary effect, modified from [Nguyen and Wereley, 2006](#) and [Bruus, 2008](#). a) and b) surface tension is defined as the free energy per area at the interface between two different phases due to the different chemical constitutions and bondings of each phase; c) the static contact angle of a wetting fluid ($\theta < 90^\circ$) at the meeting point of 3 immiscible phases; d) contact angle and surface tension define the capillary rise height into a microchannel. In this figure, the microchannel is made out of a hydrophilic material. Hence, the fluid shows a wetting behavior, and the capillary rise height is positive.

phases. One distinguishes between static and dynamic contact angle. In contrast to the static contact angle, the dynamic contact angle will change whenever a liquid-gas interface is driven, e.g., over a rough region inside a tubing. A non-wetting liquid has a contact angle of $> 90^\circ$ on a hydrophobic solid. A fully-wetting liquid shows the opposite behavior, the contact angle is $< 90^\circ$. Contact angle and surface tension define the capillary rise height into a microchannel (Fig. 1.4 D).

In extreme cases, channel-spanning bubbles are able to clog the fluidic system. This frequently happens at interfaces between different channel geometries (e.g. contractions). Here, a higher pressure difference is needed to drive the fluid through the channel. This results in increased outgassing of soluted molecules. Combined with the compliancy of air, it leads to unwanted clogging effects.

Molecules diffuse from a region of high concentration to a region of low concentration. Diffusion (Bruus, 2008) is generally described by the Fick's law. The most important influencers are the physico-chemical properties of diffusing molecules and of the tissue, temperature and concentration gradient. If the region of low concentration is in constant movement, the flow rate needs to be taken into account. Once dispensed, the analyte molecules are not dragged through a channel in a parabolic shape, but rather in an evened out plug shape due to the interaction of convection and diffusion (*Taylor Dispersion*, see Fig. 1.5). In some cases, surface-analyte interactions like sedimentation can occur. Hence, the choice of the tubing material is an important issue. Large macromolecules and particles make up the third phase in the multiphase flow. In addition to sedimentation effects, they are able to clog small microchannels and can interact with the analyte molecules (Guenther and Kreutzer, 2009).

The term *Relative Recovery (RR)* (Chefer et al., 2009) is a performance measure of OFM and microdialysis systems. It is used as correction factor to convert analyte concentration in the sample to analyte concentration in the tissue. The RR is defined as

$$RR = \frac{c_{out} - c_{in}}{c_{ext} - c_{in}}, \quad (1.3)$$

where c_{out} is the concentration of analyte in the sample, c_{in} is the concentration of analyte in the perfusate, and c_{ext} is the concentration of analyte in the tissue. The RR is inversely proportional to the flow rate, and depends on analyte properties, temperature, tissue and

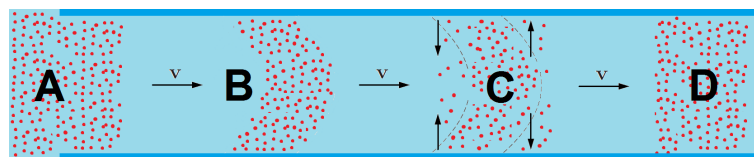


Figure 1.5.: Taylor dispersion, modified from [Bruus, 2008](#). The dispersion of uptaken analyte molecules from a specific compartment (A) in a microfluidic channel develop from a parabolic shape (B) to an evened out plug shape (D) due to convection and diffusion (C).

probe configuration (e.g. exchange area and material properties).

1.3.2. Materials and fabrication techniques

Materials for biological or chemical microfluidic systems should have a variety of important properties ([Bayraktar and Pidugu, 2006](#)). These include optical properties, surface properties (surface-analyte interactions), biocompatibility and machinability. While in the past glass and silicon were widely used, certain polymers are the material of choice nowadays. Such materials are relatively cheap and easy processable. Common polymeric materials are, e.g., Polymethylmethacrylate (PMMA), Polytetrafluoroethylene (PTFE) and Polydimethylsiloxane (PDMS).

Commonly used basic fabrication techniques for microfluidics, microelectromechanical systems (MEMS) and microelectronics ([Nguyen and Wereley, 2006](#)) include lithography, additive techniques such as chemical vapor deposition and subtractive techniques like wet etching and pattern transfer techniques. Techniques used specifically for polymers include bulk and surface micromachining as well as molding techniques. The latter techniques make it possible to produce microfluidic devices in a large scale and with high accuracy by using a *replica master* for the molding process.

1.4. Aim of the Thesis

Currently, cOFM is used for in-vivo studies in rat models and for in-vitro experiments. The intention is to use the same sampling system in different animal models. Compared to rats, the brain volume of e.g. mice is about ten times smaller. Therefore, the aim of this thesis was to miniaturize the current cOFM probe. The main requirements of the miniaturized probe are:

- The implanted tubings should be as small as possible to minimize implantation trauma and to target different brain regions in mice. The current cOFM probe tip has an outer diameter (OD) of 0.8 mm. The target diameter should be smaller than 0.3 mm.
- It should be possible to establish a homogeneous flow rate of at least 1 $\mu\text{l}/\text{min}$ through the microchannels without having unwanted physical effects, such as outgassing of soluted gas molecules. Outgassing occurs when the pressure difference to drive fluids through microchannels is too high.
- The relative recovery (RR) of the probes should not be diminished. This has to be shown in in-vitro and in-vivo studies.

To solve this tasks, the workflow shown in Fig. 1.6 was pursued. The first steps included an evaluation of the current cOFM system to get used to the system and to assess miniaturization possibilities (2.3.2). A literature study on microfluidics was done (1.3). Based on the basic findings and knowledge, the fluids of interest were rheologically characterized (2.2) and boundaries for the miniaturization were assessed (2.3.5). Next, prototypes were designed (2.3.3) and test systems were assembled (2.3.4). The current probe type, the prototype as well as the test systems were compared in-vitro (2.4) and in-vivo (2.5). The design of the new prototype was optimized to ease handling and sampling during implantation and sampling (4.5.1).

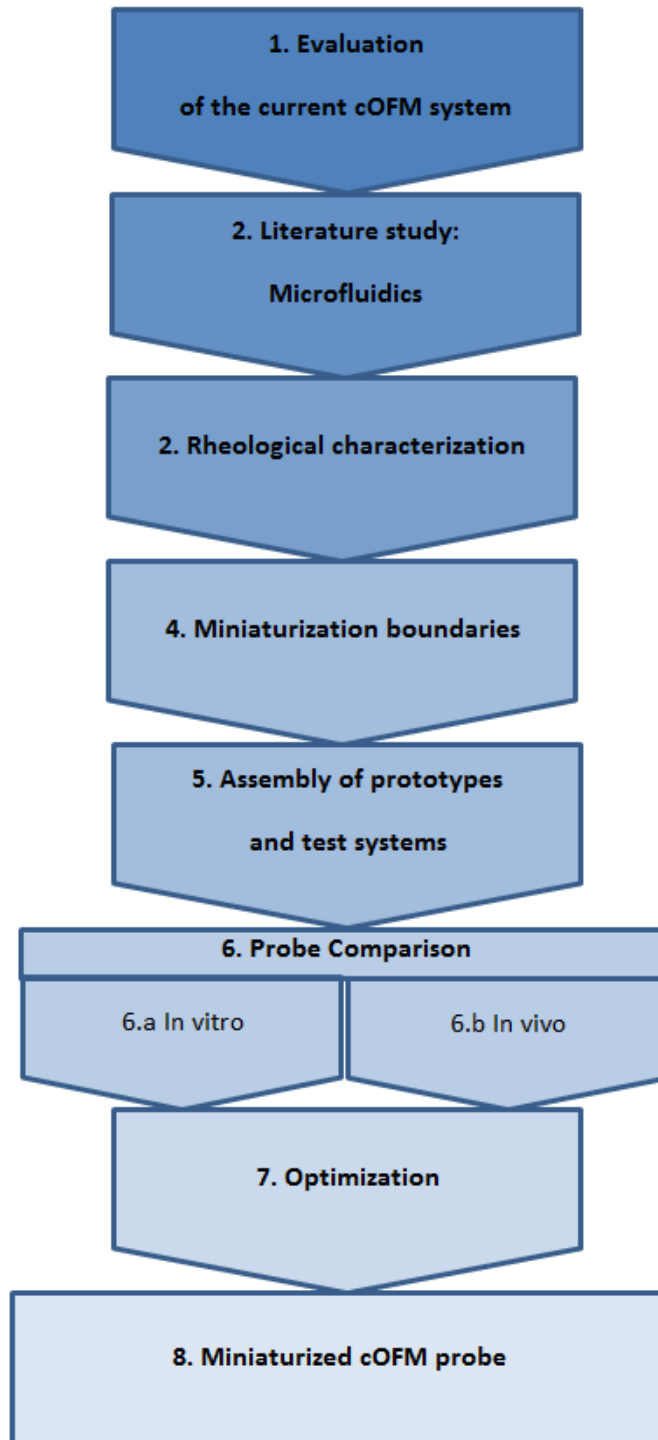


Figure 1.6.: Master Thesis workflow. Firstly, an evaluation of the current cOFM system and a literature study on microfluidics was done. Based on the basic findings and knowledge, the fluids of interest were rheologically characterized and boundaries for the miniaturization were assessed. Then, prototypes were designed and test systems were assembled. Comparisons were done in-vitro and in-vivo. The design of the new prototype was optimized to make the handling and sampling easier.

2. Materials and Methods

2.1. Cerebral Open-Flow Microperfusion

Cerebral Open-Flow Microperfusion (cOFM) is a microfluidic system to sample brain interstitial fluid (ISF) after re-establishment of the Blood-Brain Barrier (BBB) (Kroath, 2011, Pieber et al., 2013). Its main application is the study of pharmacokinetics and pharmacodynamicse of neurotherapeutic drugs. cOFM is currently available for preclinical use only. The general setup is shown in Fig. 2.1. Its central element is a concentric *probe* consisting of a *probe body* and a guide cannula. The probe is implanted combined with an inner removable stainless steel or PEEK rod (*healing dummy*), which prevents tissue migration inside the implanted cOFM tubing tip during implantation and BBB re-establishment. After 2 weeks, the healing dummy is replaced by a tubing system (*probe insert*). The fluidic system is sealed using a commonly used luer locking system (*probe cap*). The probe insert consists of an inflow and an outflow tubing. Before sampling starts, a Run-In phase of about 20 to 30 minutes is performed to minimize the occurrence of biased samples. During sampling, perfusate is pushed through the inflow tubing into the tissue. From here, the sample is pulled out through the space between inflow tubing and guide cannula into the probe, from where it is withdrawn through the outflow tubing. Inflow and outflow tubings are connected to syringes, which are driven by programmable high-precision pumps. Both flow rates are equal to avoid fluid loss into the brain tissue. The sample is stored into vials, frozen, and analyzed in a laboratory.

So far, the cOFM system has been used to demonstrate the re-establishment of the BBB in-vivo using albumin-bound Evans Blue, which yielded the conclusion that the BBB is closed 11 days after implantation. A constant Relative Recovery (RR) over several weeks has been shown by using the extracellular sodium concentration. Currently, the RR of different substances like the antidepressant Amitryptiline are studied. In addition, in-vitro and in-vivo performance comparisons between state-of-art probes and miniaturized prototypes are conducted, which are presented in this thesis.

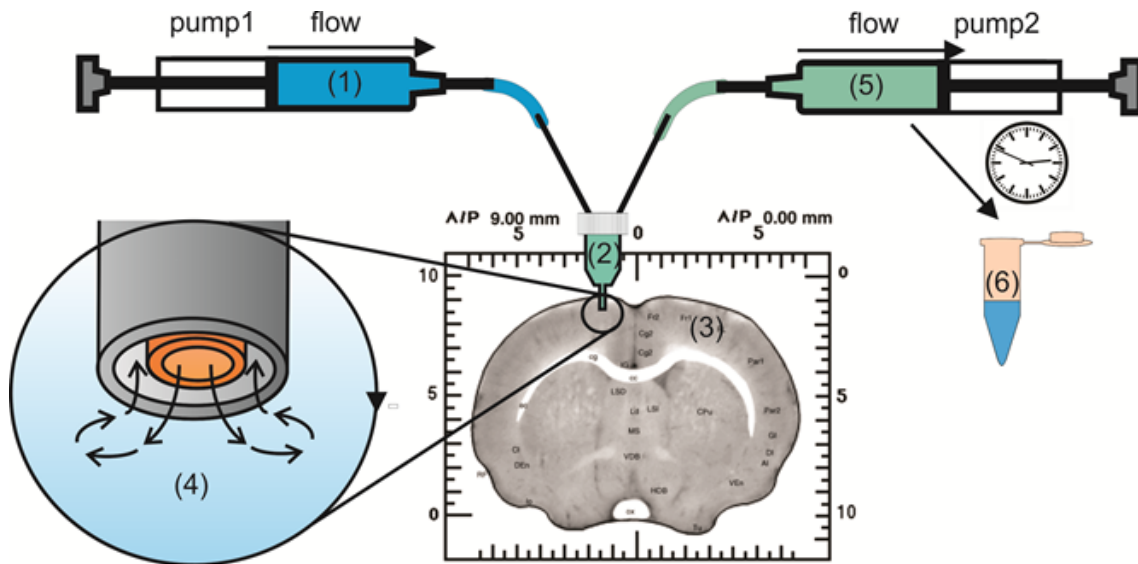


Figure 2.1.: Working principle of the cOFM, taken from [Kroath, 2011](#). Perfusate (1) is pushed through the inflow tubing of the cOFM probe (2) into the extracellular matrix of the brain (3), where it is mixed with ISF at the probe tip (4). The solution is withdrawn (5) and sampled into vials (6).

The flow behavior of perfusate and sample through cOFM probes is influenced by:

- *Rheological properties* of the fluids of interest like viscosity, see next chapter.
- *Surface properties* and *geometries* of the microchannels, see Chapter 2.3.
- *External influences* like temperature, which is kept constant during the sampling.

2.2. Rheological Characterization

Rheological properties of the fluids which influence the flow through cOFM channels are the *composition of the fluids*, their *viscosity* and their *surface tension*.

The composition of the fluids determines, e.g., the viscosity and its dependency on the shear rate (Newtonian or non-Newtonian behavior). Viscosity determines the pressure difference needed to drive a fluid through a microchannel. Surface tension is particularly important whenever different phases are encountered in a fluid flow, e.g., dissolved gas bubbles or two fluids with different rheological parameters. In this thesis, surface tension and viscosity have been evaluated for CSF and water-like liquids with a certain protein content. Parameters for surface tension have been estimated from a literature study (see chapter 4.1), viscosity values were measured and compared with findings in the literature.

2.2.1. Composition of the fluids

An overview on the fluids of interest in cOFM is given in Fig. 2.2. The *cerebrospinal fluid* (CSF) occupies the sub-arachnoidal and the ventricular space of the brain, and is separated from the blood by the so called Blood Cerebrospinal Fluid Barrier (BCSFB), which is formed by the choroid plexus epithelium. The *interstitial fluid* (ISF) occupies the extracellular space in the tissue of the brain. It is protected by the capillary structure Blood-Brain Barrier (BBB). Substances can be exchanged between ISF and CSF over ependyma glia. The *intracellular fluid* (ICF) is the fluid inside the brain cells. Both CSF and ISF are water-like substances with soluted metabolites, sparsely occurring plasma cells and a lower amount of proteins compared to the blood plasma (about 0.45 g/l, which is ca. 1% to that in blood plasma) (Brydon et al., 1995). Nevertheless, CSF and ISF compositions can differ, especially if the transport of neurotherapeutic substances are studied (Hammarlund-Udenaes et al., 2008).

The cOFM perfusate is injected into the ISF, and is composed to match the ISF in order to avoid chemical stresses for the BBB. An exemplary composition, modified from McNay and Sherwin, 2004, is shown in Table 2.1.

The sample is equal to the ISF, but with a lower amount of proteins and cells.

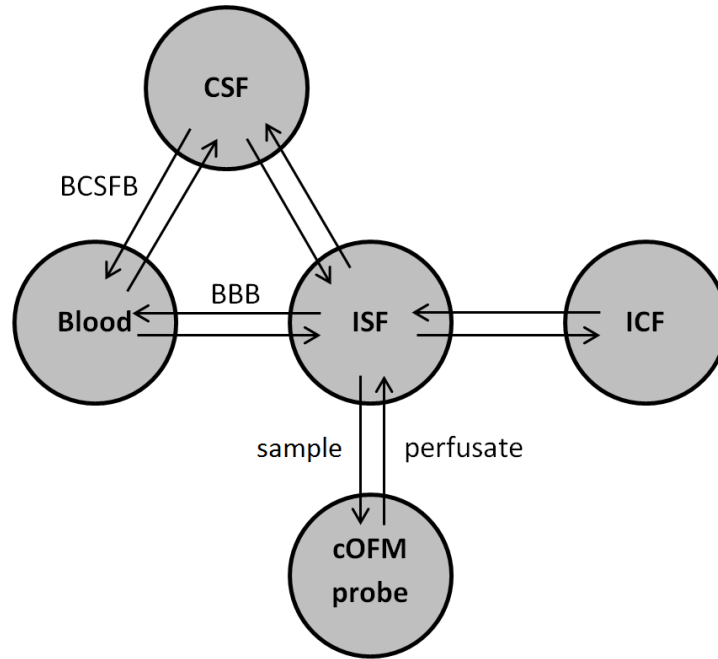


Figure 2.2.: Fluids of interest in a simplified compartment structure (modified from [Hammarlund-Udenaes et al., 2008](#)). The *cerebrospinal fluid* (CSF) occupies the sub-arachnoidal and the ventricular space, and is separated from the blood by the so called Blood Cerebrospinal Fluid Barrier (BCSFB), which is formed by the choroid plexus epithelium. The *interstitial fluid* (ISF) occupies the extracellular space in the tissue of the brain. It is protected by the capillary structure Blood-Brain Barrier (BBB). Substances can be exchanged between ISF and CSF over ependyma glia. The *intracellular fluid* (ICF) is the fluid inside the brain cells. cOFM systems sample ISF by pushing *perfusate* into the tissue and by withdrawing a *sample* at the same flow rates.

Substance	Concentration (mM)
NaCl	123
MgCl ₂	0.4 (purity \geq 98%)
CaCl ₂	0.7 (purity \geq 93%)
KCl	4.3
NaH ₂ PO ₄	1.3
Na ₂ HPO ₄	21
Glucose	4

Table 2.1.: Exemplar composition of a cOFM perfusate, modified from [McNay and Sherwin, 2004](#). All reagents are dissolved in sterile water, purity \geq 99% unless stated otherwise.

2.2.2. Viscosity and rotational rheometry

Viscosity is often called the inner resistance of the fluid. It determines the influence of the liquid on the pressure difference needed to drive the liquid through a microchannel and can be measured by using rotational rheometry (Mezger, 2006). This method is based on the two-plates model, see Fig. 2.3a. When the upper one of the two plates moves, it causes a shear stress τ that is parallel to the liquid's surface. The shear rate $\dot{\gamma}$ is defined by the speed the upper plate is moved. The shear rate in a circular channel with a channel diameter d can be estimated using the following formula:

$$\dot{\gamma} = \frac{8v}{d} \left[\frac{1}{s} \right]. \quad (2.1)$$

Newton's law states that shear stress is shear rate times viscosity. Thus, the viscosity η is

$$\eta = \frac{\tau}{\dot{\gamma}} [Pas]. \quad (2.2)$$

Non-Newtonian fluids are subjected to time-dependent structural changes and are therefore dependent on the shear rate. Newtonian fluids are independent of the shear rate. The two greatest influencers on viscosity are temperature and time.

In rotational rheometry, liquids are stirred and turned by a parallel-plate system (Fig. 2.3b). It consists of a measuring bob and a lower plate. The measuring bob is turned by the instrument's motor, the lower plate stand still. The measurement preset is the decision how fast the measuring bob should rotate. Depending on the liquid's viscosity, the measuring bob will require a certain amount of torque. The required torque is the measuring result.

Samples

In the feasibility studies, standard cOFM perfusate and a solution with 200 g/l human proteins (HSA, albumin, *Actapharma Wien, Austria*) were compared at different temperatures with shear rates between 0 and 100 1/s. For the main studies, 3 mL of CSF was extracted from 6 healthy, 11-12 months old Sprague-Dawley rats. The fluid was extracted from their Cisterna Magna and stored 5 days at -22°C before being used for the measurements. Aqua bidest was provided by the Institute of Biomechanics as reference liquid. The

shear rates ranged between 40 and 1000 1/s. The shear rate in cOFM tubings was estimated to be between 200 and 300 1/s.

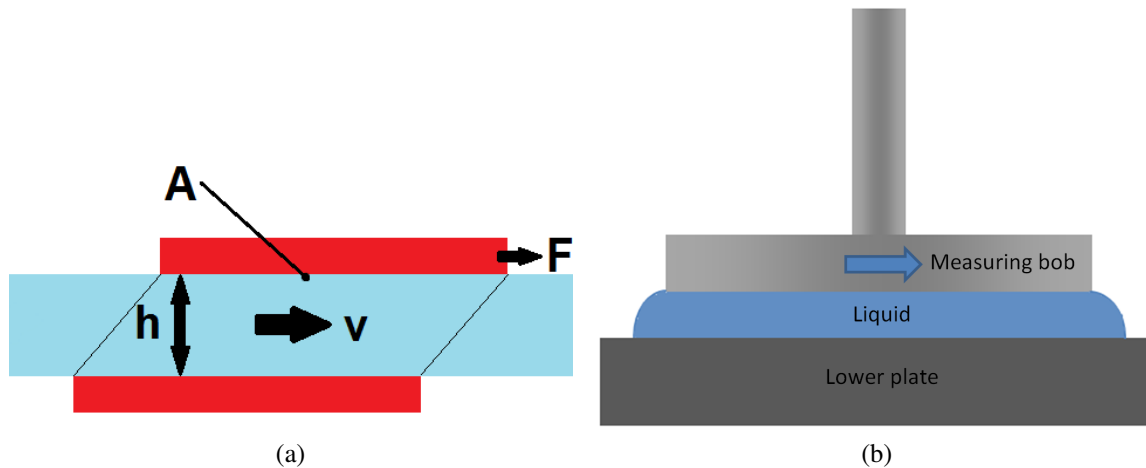


Figure 2.3.: Rotational rheometry: (a) the two-plates model to determine viscosity. When the upper one of the two plates moves, it causes stress that is parallel to the liquid's surface. This is called shear stress τ , and is defined by applied force F divided by an area A , which is parallel to the liquid's surface. The shear rate $\dot{\gamma}$ is defined by the speed the upper plate is stressed. Newton's law states that shear stress is shear rate times viscosity; (b) the parallel-plate system for rotational rheometry. The measuring plate is turned by the instrument's motor, the lower plate stand still. The measurement preset is the decision how fast the measuring bob should rotate. Depending on the liquid's viscosity, the measuring bob will require a certain amount of torque. The required torque is the measuring result. To get reliable measurement results, the measuring plate has to be fully wetted.

Measurements

The measurements at the rheometer were supervised by Michael Unterberger MSc (Institute of Biomechanics, TU Graz) and were done according to a Standard Operating Procedure (SOP), which was created during this thesis for the institute, see Appendix.

To get reliable measurement results, the measuring bob had to be fully wetted. Therefore, about 0.5 ml liquid had to be dropped onto the lower plate. Dynamic viscosity values at different shear rates were calculated by the rheometer by using the resistance to the torque at different rotational speeds.

To account for measurement insecurities, each experiment was repeated three times. The

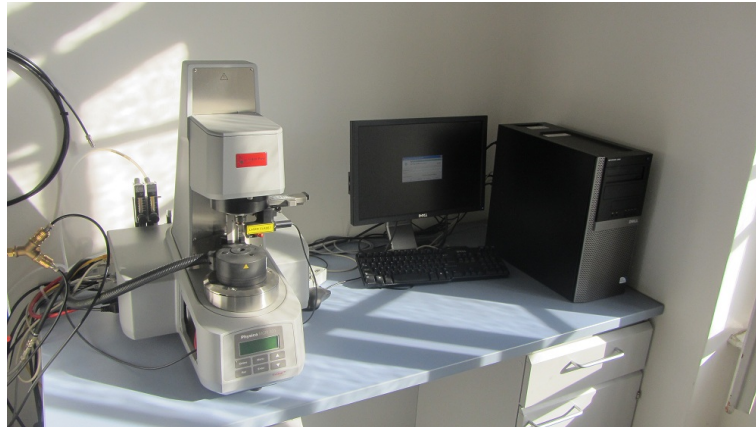


Figure 2.4.: The rheometer at the Institute of Biomechanics.

results were provided by the Software RheoPlus as Excel sheet.

Statistical methods

To show the independency between dynamic viscosity and shear rate and to show the consistency of the same viscosity values over different shear rates, a linear regression test was done. Furthermore, mean, standard deviation, median, minimum and maximum were calculated.

Required Materials

1. Tools and devices.

- Rheometer Physics MCR 301 (*Anton Paar GmbH, Graz, Austria*). It consists of a central measurement device, a compressor, a heating-cooling unit and a PC.
- Syringes
- Cleaning Sheets

2. Chemicals.

- Ethanol
- Aqua bidest

2.3. cOFM Probes

The following chapter describes material characteristics, design, manufacturing and working principle of the following probe types:

- Version 1.0 (state-of-art probe, currently in use for in-vivo and in-vitro experiments)
- Version 2.0 (miniaturized prototype with smaller probe body and reduced tubing dimensions)
- Versions 3.0 and 3.1 (test systems with the smallest tubing diameters commercially available)

Version 2.1 is a re-designed prototype to enhance the handling capability during implantation. The probe type is discussed in the outlook of the thesis (see chapter 4.5.1).

2.3.1. Material characteristics

The probes are made of different polymeric materials (Park and Lakes, 2007, Ha et al., 2009), a comparison of important properties is given in Fig. 2.5. In addition, the state-of-art probe V1.0 contains parts made of stainless steel.

Polytetrafluoroethylen (PTFE) is a flexible and transparent fluoro-carbon thermoplastic with a very low friction coefficient. Due to the high electronegativity of fluor and the resulting strong bonds between the carbon and fluor atoms, it is highly hydrophobic and chemically nearly inert. Thus, the adhesion of gas bubbles and the adsorption of hydrophilic molecules on the material is minimized. It is the material of choice for cOFM tubings, which are in contact with the withdrawn liquid during sampling.

The chemical structure of the copolymer **Fluorinated ethylene propylene (FEP)** is similar to PTFE, but it additionally contains hexafluoropropylene mers. Its physical properties are equal to PTFE, FEP is hence used likewise in cOFM probes.

On the contrary, the thermosetting polymer **Polyimide (PI)** is a very stiff material, opaque (amber), and is more hydrophilic than PTFE and FEP. PI networks gain remarkable stiffness due to the formation of a crosslinked 3D network during synthesis, after which it is irreversibly cured. To improve their surface properties, PI tubings can be coated with a PTFE film. Industrially produced PI tubings can be realized with very thin walls down to 6.35 μm . In cOFM probes, PTFE coated PI tubings are used as part of the miniaturized

fluidic pathway, where small dimensions, easy handling properties and optimized surface characteristics are needed.

Polyetheretherketone (PEEK) is a crystalline, thermoplastic polymer. It is stiff, easy processable and chemically inert. The surface characteristics are not as good as PTFE, but better than PI. Due to its stiffness it is used as healing dummy of the new cOFM prototypes, and is additionally the bulk material of the improved prototype.

Polymethylmethacrylate (PMMA) has been used as bulk material of the first prototype due to its easy processability. It is stiff, hydrophilic and has a moderate surface roughness. In contrast to the other materials, chemical inertness is given only for weak acids and bases as well as for salt solutions.

Flexible **Tygon** tubings are used to connect the PTFE tubings to the syringe needles. Due to their high hydrophilicity the contact to the withdrawn sample is kept minimal.

Medical grade stainless steel (316L) is an alloy made mostly of iron, chromium and nickel. Chromium increases the resistance to corrosion, nickel stabilizes the austenitic, nonmagnetic phase, and molybdenum protects the material against pitting corrosion in salt water. Due to its biocompatibility and its stiffness, medical grade stainless steel is often used as screw or fitting for surgical applications. In the cOFM probe V1.0, it is used as healing dummy and as part of the probe insert.


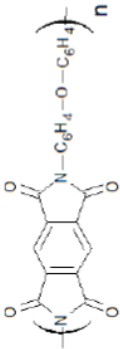
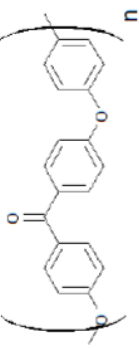
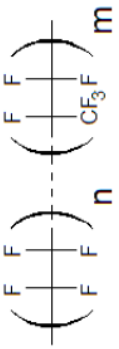
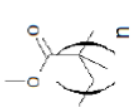
Material	Molecular formula	Mechanical properties	Fluidic properties	
			Contact angle with water [°]	Coefficient of friction
PTFE (Polytetrafluoroethylene)		407 - 750	100 - 117	0.05 - 0.08
PI (Polyimide)		1972 - 3100	70 - 75	0.15 - 0.29
PEEK (Polyetheretherketone)		3650 - 3700	88 - 91	0.34
FEP (Fluorinated ethylene propylene)		480	103 - 112	0.3
PMMA (Polymethyl Methacrylate)		1800 - 3100	60 - 80	0.54

Figure 2.5.: Important polymer properties for cOFM probes. All data and formulas are taken from [Park and Lakes, 2007](#), [Ha et al., 2009](#) as well as from material data sheets, see the Appendix.

2.3.2. Version 1.0

The cOFM probe Version 1.0 (Fig. 2.6) is the state-of-art probe, which is currently used in pre-clinical in-vivo and ex-vivo studies in rats. It is produced in-house. This probe type is the starting point of the miniaturization process, where tubing diameters of the guide cannula (currently OD = 0.80 mm) and probe body dimensions are miniaturized.

Manufacturing

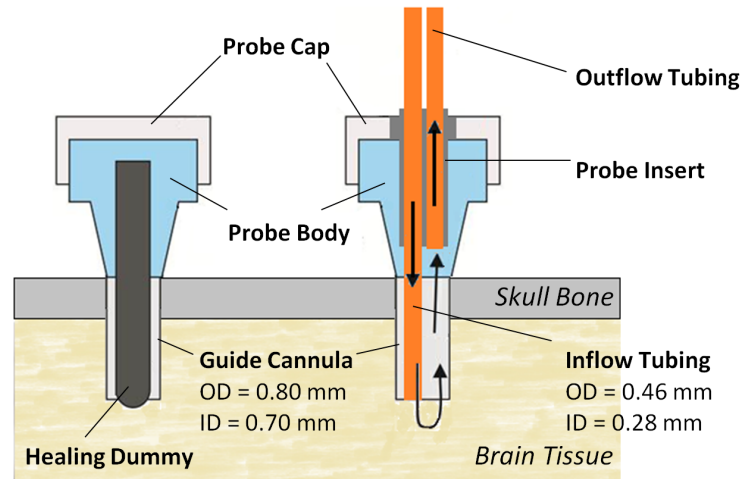
This probe consists of a probe body with guide cannula, a healing dummy, a probe insert and a probe cap (see Fig. 2.7).

For the **probe body** and its FEP guide cannula (OD = 0.80 mm), the Angiocath (a peripheral venous catheter) is used. The FEP tubing is shortened to a individually defined length under the microscope. Fine 1 mm bores are made at the body to be able to stabilize the probe during implantation using dental cement.

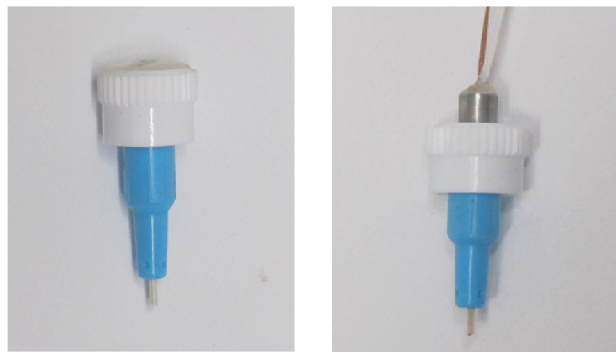
The **healing dummy** ensures mechanical stability during implantation, and prevents tissue migration into the probe. It consists of the mandrin needle of the Angiocath, which is bonded to a Luer plug. The Luer plug is a commonly used locking system for medical applications. When probe body and healing dummy are assembled, the needle has to be as long as the FEP tubing to prevent tissue damage. Furthermore, the tip of the needle is polished to a hemispherical shape.

The **probe insert** replaces the healing dummy during sampling. It consists of a cylindrical body made of stainless steel and 2 tubings: a 120 mm long PTFE outflow tubing and a 80 mm long PTFE-coated PI inflow tubing. The inflow tubing is inserted into the FEP tubing of the probe body during sampling, and must hence be cut to a specific length. If the inflow tubing is longer then the FEP tubing during sampling, the tissue could be damaged. If it is shorter, the performance of the cOFM probe is decreased (Kroath, 2011). Flexible Tygon tubings are imposed on the ends of the inflow and outflow tubings to be able to connect the tubings to syringe pumps. During sampling, the probe insert is locked to the probe body using the Luer-based **probe cap** to seal the fluidic pathway.

All parts are bonded using cyanoacrylic and UV-curing adhesive. Excess adhesive rests are removed using a razor blade and acetone. After assembling the different parts, they are cleaned for 30 minutes in a mixture of alcohol and ddH₂O at 60°C using an ultrasound cleaner. Finally, the parts are assembled for implantation and sealed into sterile foil bags.



A)



B)

Figure 2.6.: The cOFM probe V1.0 in healing (left) and sampling configuration (right). The healing configuration consists of assembled probe body with guide cannula and healing dummy with probe cap. The sampling configuration consists of the probe insert with inflow and outflow tubing, as well as probe body and probe cap: (A) schematic depiction and fluidic pathway of an implanted probe, OD and ID of guide cannula and inflow PI tubing are given. Perfusate is pushed through the inflow tubing into the brain tissue, and withdrawn between inflow tubing and guide cannula, probe and outflow tubing into a syringe; (B) photos of the cOFM probe.

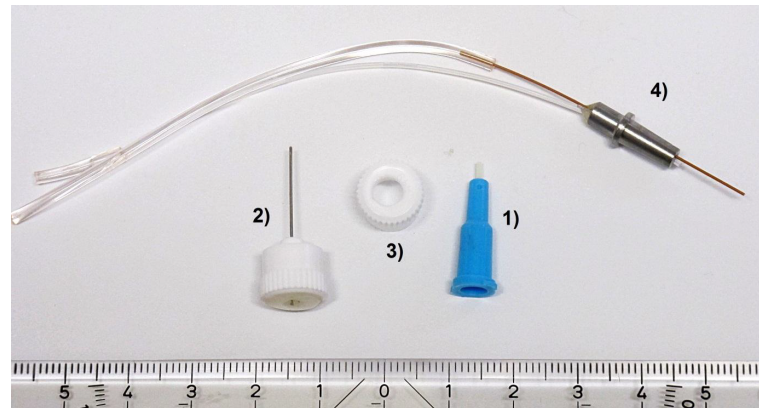


Figure 2.7.: Different parts of the cOFM probe V1.0: (1) is the probe body (blue) with a FEP guide cannula tubing at its tip; (2) is the healing dummy; (3) the probe cap; (4) the probe insert made of stainless steel with PI inflow tubing (red), PTFE outflow tubing (transparent) and Tygon connecting tubings (transparent).

Implantation and Working principle

Healing dummy and probe body are assembled and implanted into the brain. To do so, 3 bores are drilled into the skull. One is used for the probe, the other ones for anchor screws. UV curing dental cement is used to fix the dummy on the skull, see Fig. 2.8. After a 2 week healing phase, the dummy is replaced by the probe insert. Therefore, all tubings and the probe body are filled with perfusate to minimize the occurrence of gas bubbles in the fluidic pathway. During sampling, perfusate is pushed from a single-use syringe through a Tygon and a PI tubing into the tissue, where it is mixed with ISF. The sample is withdrawn through the annular space between PI and FEP tubing into the probe body, and through a PTFE tubing into a gastight syringe. The outflowing liquid is therefore only in contact with hydrophobic, biocompatible materials (FEP, PTFE-coated PI, stainless steel and PTFE). The probability of macromolecule adsorption is hence minimized. Perfusate and sampled liquid are pushed and pulled through the system with the same flow rate (1 $\mu\text{l}/\text{min}$) to prevent the development of edema.

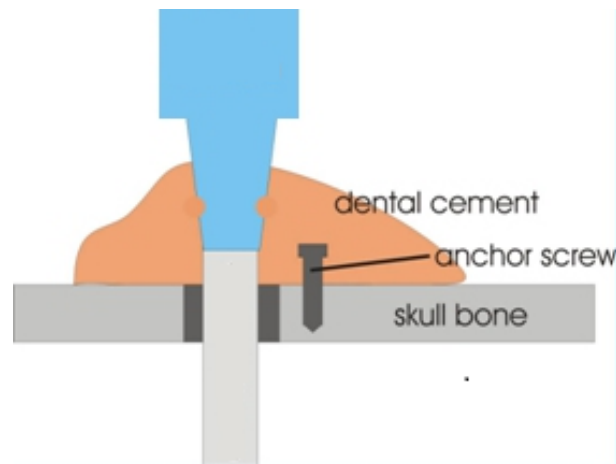


Figure 2.8.: Schematic of a fixed cOFM probe. The probe and anchor screws are fixed using dental cement. The probe is stabilized by small bores at its outer surface.

Required Materials

1. Raw Material.

- BD Angiocath(TM) 22G (*BD Becton Dickinson GmbH, Schwechat, Austria*), used to create healing dummy and probe body.
- BD Luer Plugs (*BD Becton Dickinson GmbH, Schwechat, Austria*), to seal the probe during implantation and sampling.
- PI Tubing; OD=0.46mm, ID=0.28mm, L=80mm, Low friction outside (*Karl Schupp AG, Zollikerberg, Switzerland*), the inflow tubing.
- PTFE Tubing; OD=0.76mm, ID=0.31mm, L=120mm (*Cole-Parmer, distributed by Amex Import-Export, Vienna, Austria*), a part of the outflow tubing.
- Tygon Tubing; OD=2.00mm, ID=0.19mm, L=100mm (*Cole-Parmer, distributed by Amex Import-Export, Vienna, Austria*), connects the inflow tubing to the pushing syringe.
- Tygon Tubing; OD=2.00mm, ID=0.19mm, L=20mm (*Cole-Parmer, distributed by Amex Import-Export, Vienna, Austria*), connects the outflow tubing to the pulling syringe.
- Stainless Steel Probe Insert Body (*Joanneum Research GmbH, Graz, Austria*), a part of the probe insert. It holds inflow and outflow tubing.

2. Tools and devices.

- Drill Machine IB/E (*Proxxon, Unterweikersdorf, Austria*)

- 0.5mm Dental Drill (*Komet Dental, Salzburg, Austria*)
- 1mm Dental Drill (*Komet Dental, Salzburg, Austria*)
- Centring and Clamping Device, used for precise drilling.
- Jet Reamers, small stainless-steel rods used for mechanical cleaning.
- Cutting Device (*BW-TEC GmbH, Hoeri, Switzerland*) to precisely cut to length the tubings.
- Ultrasound Cleaner Elmasonic S10H (*Elma Hans Schmidbauer GmbH Co. KG, Singen, Germany*)
- Sealing Device MELAseal 101 comfort (*MELAG, Berlin, Germany*)
- Microscope EMZ-TR (*Meiji, Saitama, Japan*)
- UV Spot Light System BlueWave50 (*Dymax Corporation, Torrington, USA*)
- Scalpel (Handle and blades)
- Different forceps
- Pin needle
- High accuracy lineal
- Different syringes and cannulas
- Wire cutter
- File (medium, fine)
- Steripacks

3. Chemicals.

- Cyanoacrylic adhesive Cyanolit 241F (*Panacol GmbH, Steinbach/Taunus, Germany*)
- UV light curing adhesive (*Vitralit 1702*)
- Alcohol (2-Propanol)
- Aqua bidest (ddH₂O)
- Acetone

2.3.3. Version 2.0

In contrast to the afore presented probe type, the miniaturized prototype Version 2.0 (Fig. 2.9) consists of a re-designed, smaller probe body and decreased tubing diameters (Guide cannula OD = 0.53 mm). To enhance machinability precision, the assembly was outsourced to Biegler Medizinelektronik GmbH.

So far, the probes were used in-vitro and in-vivo to compare their RR performance and handling ability to the state-of-art probe. The different experiments and results are shown in this thesis.

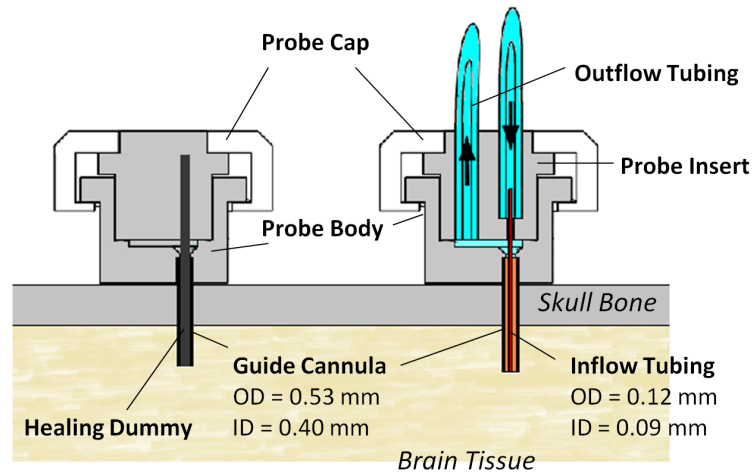
Manufacturing

The probe consists of a probe body with guide cannula, a healing dummy, a probe insert and a probe cap, see Fig. 2.10.

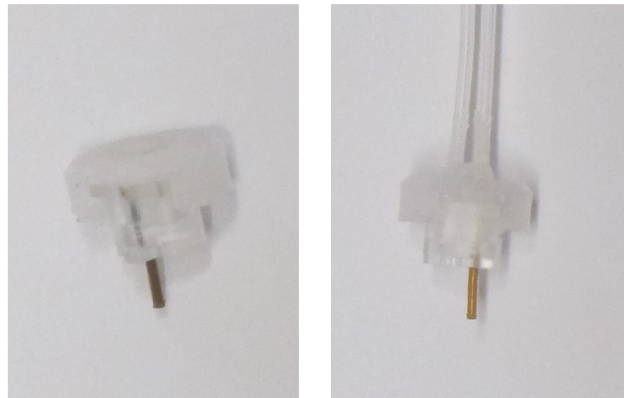
The basic bulk of the **probe body** is milled out of PMMA. It is designed to be able to connect it to a Luer cap at the upper side. Furthermore, it possesses two feet at the lower side to stabilize it in the dental cement during implantation. Inside the probe body, an extrusion is milled out. It serves as part of the outflow pathway. A small 0.53 mm hole is bored through the basement of the probe body. Herein, a 0.53 mm PI tubing is glued. It is shortened to 3 mm. To facilitate insertion of the small inflow tubing, a cone is milled, whose smaller exit has the same diameter as the ID of the PI tubing (0.40 mm).

The body of the **healing dummy** consists of PMMA too. At the lower side, a small bulk fits exactly into the afore described extrusion. At the upper side it is designed to be compatible with the Luer cap. A 0.41 mm hole is bored into the body, which holds a PEEK fiber.

The PMMA **probe insert** is designed likewise, but it lacks the small bulk at the lower side and has two channels for the inflow and outflow tubings. The outflow channel is a 0.76 mm hole, a PTFE tubing is glued into it. The inflow channel has a diameter of 0.76 mm at the upper side, and a diameter of 0.12 mm at the lower side. The inflow tubing consists of a 0.76 mm PTFE tubing which fits into the upper part of the channel, and a 0.12 mm PI tubing, which fits into the lower part. Both PTFE tubings can be connected to syringes via Tygon tubings.



A)



B)

Figure 2.9.: The cOFM probe V2.0 in healing (left) and sampling configuration (right). The healing configuration consists of assembled probe body with guide cannula, healing dummy and probe cap. The sampling configuration consists of the probe insert with inflow and outflow tubing, as well as probe body and probe cap: (A) schematic and fluidic pathway of an implanted probe, OD and ID of guide cannula and inflow PI tubing are given. The perfusate is pumped through the inflow PTFE tubing and the small PI tubing into the tissue. From here, the sample is withdrawn through the PTFE-coated annular space between inner and outer PI tubing, along the channel which is formed between the extrusion and the probe insert, and through the outflow PTFE tubing into a syringe; (B) photos of the cOFM probe.

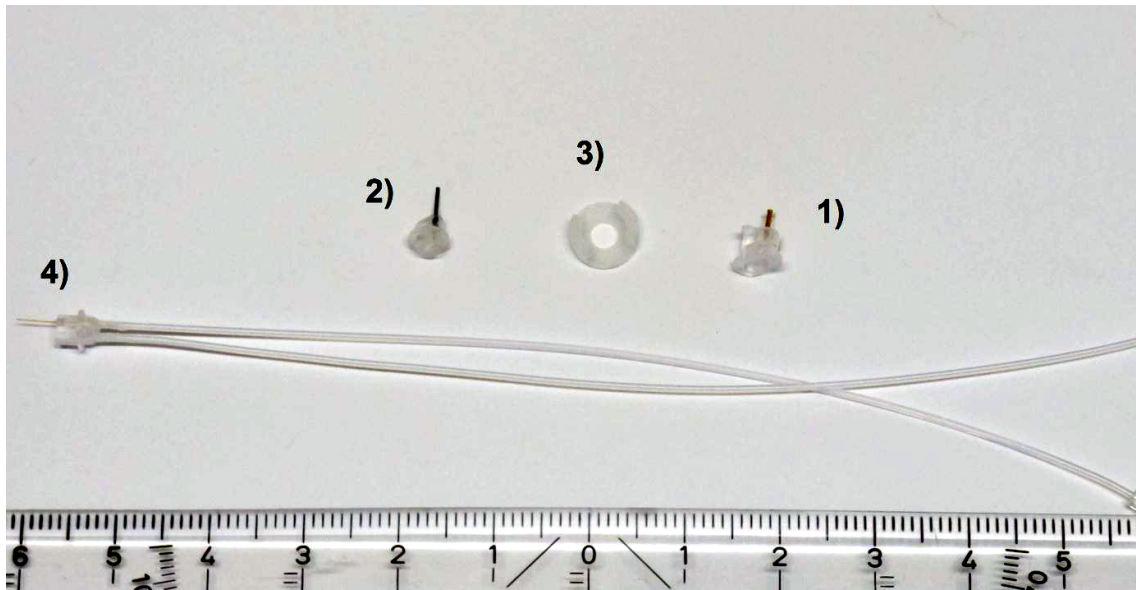


Figure 2.10.: The different parts the cOFM probe V2.0: (1) is the probe body with a Polyimide tubing tip (orange); (2) is the healing dummy; (3) the probe cap; (4) the probe insert, which consists of a PTFE inflow tubing with minimized Polyimide tip (orange) and the transparent PTFE outflow tubing.

Implantation and Working Principle

The cOFM probe V2.0 is implanted like V1.0 using dental cement and anchor screws. Due to the small probe height, the scalps of rats can be imposed on the probes after the surgery. The sampling procedure is similar to V1.0. It occurs 2 weeks after implantation, the tubings and the probe body are filled with perfusate before starting, probe insert and probe body are locked together using a Luer cap. The perfusate is pumped through the inflow PTFE tubing and the small PI tubing into the tissue. From here, the sample is withdrawn through the PTFE-coated annular space between inner and outer PI tubing, along the channel which is formed between the extrusion and the probe insert, and through the outflow PTFE tubing into a syringe.

Required Materials

1. Raw Material.

- PMMA bulk, the basic material of the probe body, the healing dummy and the probe insert.
- PEEK fiber OD=0.41mm (*Zeus Inc., Orangeburg, USA*), the healing dummy needle material.
- PTFE tubing OD=0.76mm, ID=0.31mm (*Cole Parmer, distributed by Amex Import-Export, Vienna, Austria*), the inflow and outflow tubings between syringes and probe insert.
- Polyimide Tubing OD=0.53mm, ID=0.40mm, Low friction inside (*Microlumen Inc., Oldsmar, USA*), the guide cannula.
- Polyimide Tubing OD=0.12mm, ID=0.09mm, Low friction outside (*Microlumen Inc., Oldsmar, USA*), part of the the inflow tubing.
- Tygon Tubing OD=2.00mm, ID=0.19mm, (*Cole-Parmer, distributed by Amex Import-Export, Vienna, Austria*), connects the tubings to the syringes.

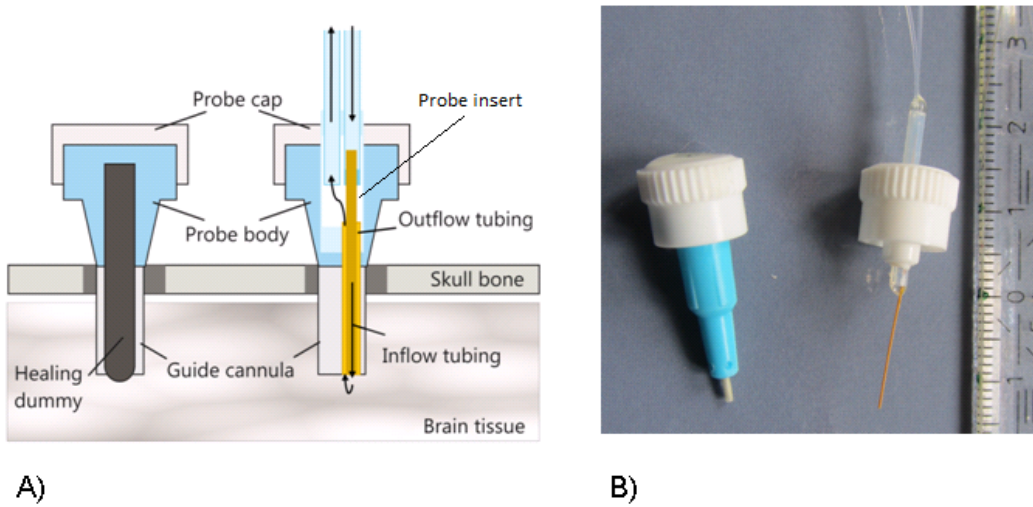


Figure 2.11.: Schematic and image of the test system 3.0: (A) schematic of the system. Left: Configuration during the healing phase, probe body and healing dummy are put together. Right: Sampling configuration and fluidic pathway; (B) image of a realized test system.

2.3.4. Test probes

The test systems simulate cOFM probes with the smallest PI tubing diameters commercially available. The minimized OD of the guide cannula is 0.25 mm, which is a third of the guide cannula of Version 1.0 (0.80 mm). The test probes were assembled in house. Version 3.0 was used in in-vitro feasibility studies, Version 3.1 in the in-vitro main studies.

Version 3.0

This test system features three parts, see Fig. 2.11: probe body, healing dummy and probe insert.

Probe body and healing dummy are unused parts of the cOFM V1.0 probe. The **probe insert** consists of a central 2 cm PTFE-FEP tubing. Herein, outflow and inflow PTFE channels with Tygon connectors are inserted at one site, and concentrically aligned outflow and inflow PI tubings on the other. The inflow PI tubing is bond into the inflow PTFE tubing. The whole module is connected to a luer probe cap, and inserted into the probe body after removing the healing dummy.

The perfusate is pushed through the inflow PTFE and PI tubings into the brain tissue. From here, the sample is pulled out through the space between inner and outer PI tubing, through the central PTFE-FEP module, and finally through the outflow PTFE tubing. Due to the PTFE coatings on the PI walls, the liquid is hence driven through hydrophobic PTFE and FEP channels.

1. Raw Material.

- PTFE/FEP tubing OD=1.75, ID=1.00mm (*Cole Parmer, distributed by Amex Import-Export, Vienna, Austria*), the central element of the probe insert.
- PTFE tubing OD=0.45mm, ID=0.20mm (*Cole Parmer, distributed by Amex Import-Export, Vienna, Austria*), inflow and outflow tubings, connected via Tygon tubings to the syringes.
- PI Tubing OD=0.25mm, ID=0.18mm, Low friction inside (*Microlumen Inc., Oldsmar, USA*), outer PI tubing at the probe tip.
- PI Tubing OD=0.12mm, ID=0.09mm, Low friction inside and outside (*Microlumen Inc., Oldsmar, USA*), inflow PI tubing at the probe tip, smallest PI tubing which is commercially available.
- Tygon Tubing OD=2.00mm, ID=0.19mm, (*Cole-Parmer, distributed by Amex Import-Export, Vienna, Austria*), connects the PTFE tubings to the syringes.
- BD Luer Plugs (*BD Becton Dickinson GmbH, Schwechat, Austria*), seal the probes.
- Probe body and healing dummy of the cOFM probe V1.0.

2. Tools and devices.

- Jet Reamers, for mechanical cleaning.
- Cutting device (*BW-TEC GmbH, Hoeri, Switzerland*)
- Ultrasound Cleaner Elmasonic S10H (*Elma Hans Schmidbauer GmbH Co. KG, Singen, Germany*)
- Microscope EMZ-TR (*Meiji, Saitama, Japan*)
- UV Spot Light System BlueWave50 (*Dymax Corporation, Torrington, USA*)
- High Precision Dispenser Performus III (*Nordson Deutschland GmbH, Erkrath, Germany*), to precisely glue small amounts of adhesive.
- Scalpel (Handle and blades), different forceps, pin, high accuracy lineal, different syringes and cannulas, wire cutter

3. Chemicals.

- see cOFM probe V1.0

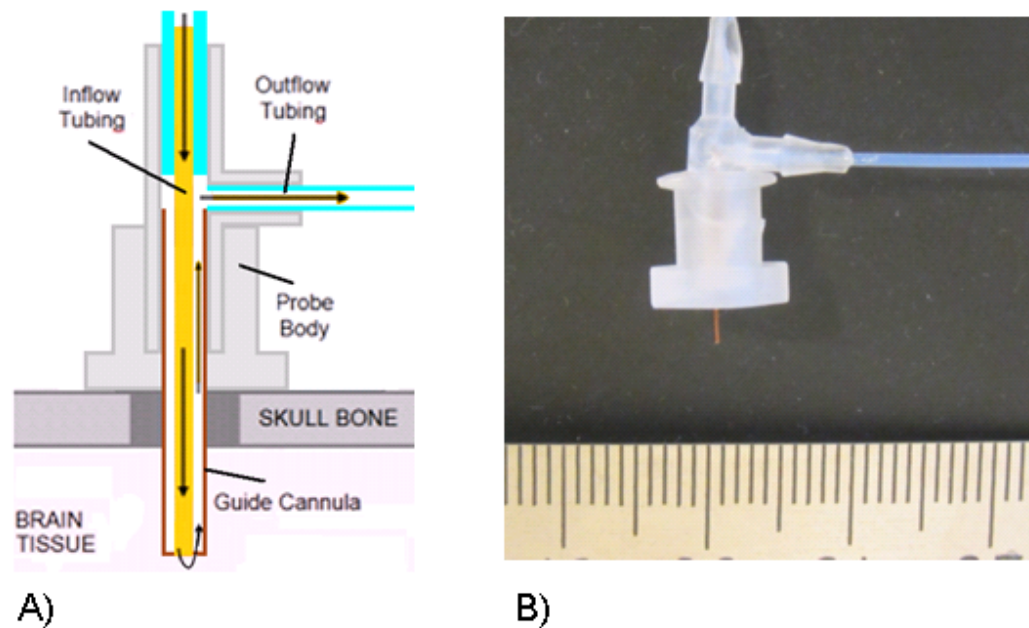


Figure 2.12.: Schematic and image of the test system 3.1: (A) schematic of the system. Sampling configuration and fluidic pathway; (B) image of a realized test system.

Version 3.1

Version 3.1 is a simple, one-part test system (Fig. 2.12). It lacks of a healing dummy. The tubing dimensions are equal to V3.1, the design is different. The central element of V3.1 is a T piece. 2 exits are used for inflow and outflow PTFE tubings, which are connected to syringes via Tygon tubings. The miniaturized concentric probe tip is glued into the third exit, its inflow PI tubing is connected to the inflow PTFE tubing. This assembled module is bonded to a polymeric fitting to be able to fix it during sampling. Here, the perfusate is driven through inflow PTFE and inflow PI tubing to the exchange area, from where it is withdrawn through the outer lumen of the guide cannula into the T-piece, and through the outflow PTFE tubing into the pulling syringe.

1. Raw Material.

- T piece 1/16" (*Cole Parmer, distributed by Amex Import-Export, Vienna, Austria*), the central element of the probe type.

- Fittings luer 3/32" (*Cole Parmer, distributed by Amex Import-Export, Vienna, Austria*), holds the central module and fixes the probe during sampling.
- PTFE tubing OD=0.45mm, ID=0.20mm (*Cole Parmer, distributed by Amex Import-Export, Vienna, Austria*), inflow and outflow tubings connected to the syringes via Tygon tubings.
- PI Tubing OD=0.25mm, ID=0.18mm, Low friction inside (*Microlumen Inc., Oldsmar, USA*), outer tubing of the probe tip.
- PI Tubing OD=0.12mm, ID=0.09mm, Low friction inside and outside (*Microlumen Inc., Oldsmar, USA*), inflow tubing inside the probe tip.
- Tygon Tubing OD=2.00mm, ID=0.19mm, (*Cole-Parmer, distributed by Amex Import-Export, Vienna, Austria*), connects the PTFE tubings to the syringes.

2. Tools, devices and chemicals.

- see test probe 3.0

Probe Type	Tubing	Material	PTFE layer	OD in mm	ID in mm
cOFM V1.0					
	Outer	FEP	none	0.80	0.70
	Inner	PI	OD	0.46	0.28
cOFM V2.0					
	Outer	PI	ID	0.53	0.40
	Inner	PI	OD	0.12	0.09
cOFM V3.0 and V3.1					
	Outer	PI	ID	0.25	0.18
	Inner	PI	OD	0.12	0.09

Table 2.2.: Probe tip comparison.

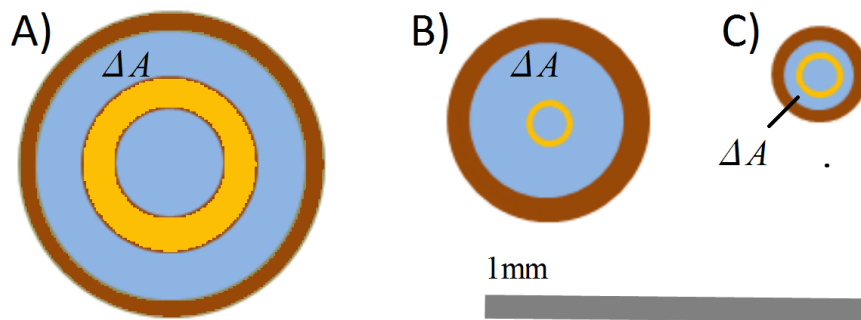


Figure 2.13.: Probe tip comparison: A) is the probe tip of version 1.0; B) of version 2.0; C) of the test systems. ΔA is the area between outer and inner tubing. Compared to version 1.0, the ΔA of the test systems is about 95% smaller.

2.3.5. Comparison of the probe types

Table 2.2 shows the channel diameters at the tips of the three afore presented probe types, and Fig. 2.13 gives a schematic comparison. Let ΔA be the area between outer and inner tubing, through which the sample is withdrawn. Compared to the state-of-art probe ($\Delta A = 0.22 \text{ mm}^2$), the ΔA of the smaller probe V2.0 is about half as small ($\Delta A = 0.12 \text{ mm}^2$). The minimized probe has a ΔA of 0.01 mm^2 , which is only about 5% in comparison to the V1.0 probe.

The flow behavior was estimated theoretically to evaluate the pressure difference needed to drive a liquid through the small microchannels. This was necessary to assess the probability of unwanted outgassing of soluted gases due to a high pressure difference in the outflow channel.

The liquid was assumed to be homogeneous with a certain dynamic viscosity. Furthermore, the no-slip boundary condition was assumed, so that the Hagen-Poiseuille law could be applied. The Hagen-Poiseuille law states that the pressure needed to drive a fluid through a microchannel gets higher when the channel dimensions get smaller. Other parameters like tubing length or viscosity play a minor role. In cOFM systems, the smallest channel diameter the withdrawn fluids pass through is the annular space at the probe tip. A miniaturization boundary was therefore the smallest possible tubing size, where the pressure difference to withdraw a liquid is still low.

The Hagen-Poiseuille law can be rewritten as (Bruus, 2008; Wilkes, 2005)

$$\Delta p = -R_{hydr}Q, \quad (2.3)$$

where Δp is the pressure difference, R_{hydr} is the hydraulic resistance and Q is the flow rate. The hydraulic resistance after the entrance length L_e for a flow through a circular tubing is

$$R_{hydr} = \frac{8\eta\Delta L}{\pi R^4}, \quad (2.4)$$

where η is the viscosity, L is the channel length and R is the radius of the channel. The hydraulic resistance to a flow through an annular channel is

$$R_{hydr} = \frac{8\eta\Delta L}{\pi(R^2 - r^2)} \left\{ \frac{1}{R^2 + r^2 - \frac{R^2 - r^2}{\ln \frac{R}{r}}} \right\}, \quad (2.5)$$

where R is the outer, and r the inner radius.

The estimation was done by calculating the hydraulic resistance in a $\Delta L = 30$ mm long annular tubing with $r = 0.06$ mm and R between 0.06 and 0.16 mm for 3 different viscosity values.

In the in-vitro and in-vivo studies, the mean flow rates through the different probe types were measured by using the weighting method, which is presented in the next chapter.

2.4. Performance Comparison In-Vitro

The aim of the following in-vitro experiments was to study the differences of the exchange performance of glucose molecules between the different probe types and to evaluate the flow behavior. The specific intention was to assess whether smaller tubing geometries influence the exchange behavior at the probe tip by keeping the other influencing parameters constant (flow rate, analyte properties, tubing properties, temperature and tissue). So far it has been shown that longer inflow tubings enhance the performance, but may damage the tissue during sampling. If the inflow tubing is shorter than the guide cannula, the performance is decreased (Kroath, 2011).

To model the brain tissue, an agar network has been used (Chen et al., 2004). This network was mixed with a specific amount of glucose, which diffuses freely in gel networks (Weng et al., 2005).

2.4.1. Feasibility studies

The following probe types were compared:

- 3 cOFM probes Version 1.0 (state-of-art, guide cannula OD = 0.80 mm)
- 3 cOFM probes Version 2.0 (prototype with smaller probe body and decreased tubing dimensions, guide cannula OD = 0.53 mm)
- 3 cOFM probes Version 3.0 (test system with the smallest tubing diameters commercially available, guide cannula OD = 0.25 mm)

Samples

The perfusate consisted of the fluorophore Naf dissolved in saline. The withdrawn sample was therefore a mixture of a Naf, saline and glucose. Naf was used to mark the perfusate flow through the microchannels.

Influence of Naf on the glucose measurements

34 μl ddH₂O was added to $V_0 = 1700 \mu\text{l}$ glucose solution ($c_0 = 2.16 \text{ g/l}$). These mixtures were prepared 5 times. Likewise, 5 solutions containing 34 μl Naf were created. The glucose concentration of the mixtures were measured using the glucose analyzer. The expected concentration (c) was 2.12 g/l:

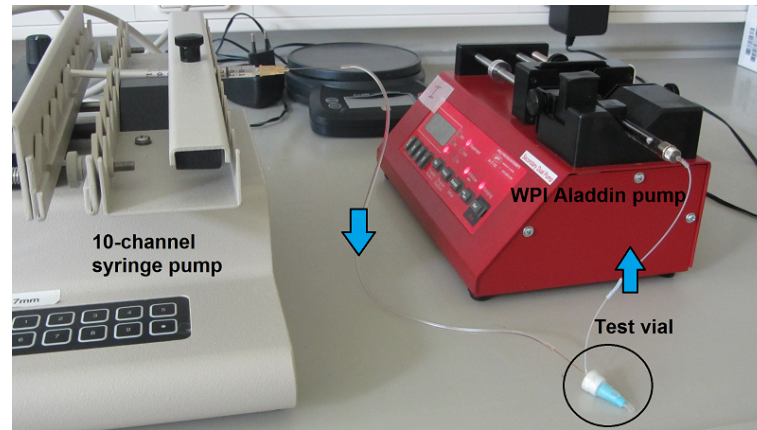


Figure 2.14.: Fluidic system for the flow rate estimation of the 10-channel syringe pump. A 10-channel syringe pump pushes water into the test vial, the WPI Aladdin pump withdraws the liquid.

$$c = \frac{V_0}{V} c_0 = \frac{1700\mu l}{1734\mu l} 2.16g/l = 2.12g/l. \quad (2.6)$$

Flow rate estimation of the 10-channel syringe pump

In a second study, the flow rate of the 10-channel syringe pump was verified. Therefore, a test vial with sealed, water-filled exchange area, was connected to the 10-channel syringe pump on the push end, and to the WPI Aladdin pump on the pull side, see Fig. 2.14. By weighting the syringes and the test probe before and after a perfusion time T_p of 60 min. with water, the mean flow rates Q of both pumps were estimated.

$$Q = \frac{V(t) - V(t + T_p)}{T_p}. \quad (2.7)$$

Matrix plate and measurement setup

Figure 2.15 and Figure 2.16 show the measurement setup. First, the different probe types with healing dummies were fixed on a matrix plate made of PMMA. This plate yields the possibility to test different probes simultaneously, each of them having the same deepness level in the network. The probe bodies of V1.0 and V3.0 were fixed into 3.5mm bores using Cyanoacrylate. The probe bodies of V2.0 could not be fixed likewise, because they have a different design and had to be used in further studies afterwards. To fix and stabilize

them onto the plate, a double-sided adhesive strip was used as well as rods out of stainless steel. Next, the matrix plate was put on the agarose gel, so that the tips of the probes could penetrate the agar block. The push tubings were filled with Naf, the pull tubings with ddH₂O. Before inserting the inflow-outflow tubings into the probe bodies, the latter were filled with ddH₂O. After sealing the probes with the luer caps, the tubings were connected to the pulling and pushing syringes. The connections were realized by expanding the standard tubings of the probes with PTFE tubings, which were stuck to the standard tubings using Tygon and small stainless-steel channels. The flow rates were set to 1 $\mu\text{l}/\text{min}$, and the perfusions started simultaneously. As soon as the red colored Naf solution reached the pulling syringes, the first samples were discarded, and the sampling of the glucose solutions started. The measurements were made in a time period of 7 hours, with sampling at 30 minutes each, see Fig. 2.17. At each sampling step, the gel temperature, which was kept at room temperature, was measured.

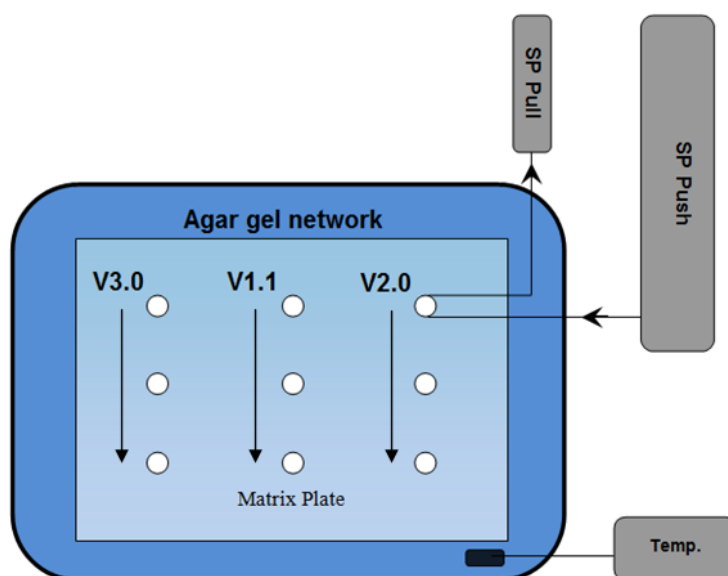


Figure 2.15.: Perfusion system consisting of the agar gel network (dark blue), the matrix plate (light blue) with the different probe types (white) and the PTFE tubes with arrows indicating the flow directions. The push-pull setup with pulling syringe pump (SP Pull) and the 10-channel pushing syringe pump (SP Push) is shown exemplarily for V2.0, and was realized for all other probes in a similar manner.



Figure 2.16.: Measurement setup of the in-vitro feasibility studies. The 8 pulling AL-ADDIN syringe pumps (red), the pulling HARVARD pump (black) and the pushing 10-channel syringe pump (white) surround the laboratory dish with gel network, matrix plate and probe types.

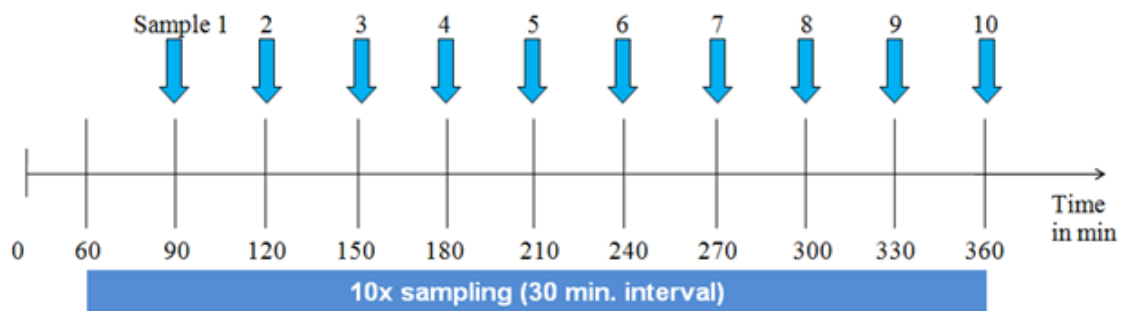


Figure 2.17.: Time line for the in-vitro sampling.

Agar diffusion model

To model the brain tissue, an 1% agarose network was used, which had a glucose concentration of 2.5% (equal to 2500 mg/dl or 139 mmol/l).

5g agarose was mixed with 125 ml of a 10% glucose solution. The volume was filled up to 500 ml with ddH₂O to get the desired concentration. This solution was heated up to its boiling point. As soon as the agarose powder was completely diluted, the solution was poured into a laboratory dish, and stored at room temperature overnight.

The agarose gel network consists of randomly orientated and mixed sized polysaccharide rods, which are formed during cooling down the agar solution. This network builds up a

resistance to the diffusion of molecules. Due to the lack of active transports in this network, a significant diminishment of glucose molecules around the exchange area, expressed by a primary peak in a concentration-time plot, is expected.

Measurement of glucose concentrations

The measurements were performed with the Super GL glucose analyzer (Fig. 2.18). The analyzer needs 10 μl sample fluid to measure accurately. This constraint was satisfied by sampling 30 μl at each time point. The measured glucose concentrations were plotted in a concentration-time-plot.



Figure 2.18.: Glucose measurement setup, the Super GL analyzer.

Required Materials

1. Materials and devices.

- Glass laboratory dish (WxLxH 90x170x40), which held the agar network block.
- Matrix plate (in-house production), held the different probe types.
- 10-channel syringe pump SP200 (*World Precision Instruments Inc., Sarasota, USA*), pushed the perfusate through the probes into the network.
- 8 syringe pumps Aladdin2-220 (*World Precision Instruments Inc., Sarasota, USA*), withdrew a mixture of glucose and perfusate out of the network.
- 1 syringe pump PHD 4400 programmable (*Harvard Apparatus Inc., Holliston, USA*), same function.

- 9 250 μ gastight syringes, Type 1725RN (*Hamilton Bonaduz AG, Bonaduz, Switzerland*), spanned into the withdrawing syringe pumps.
- 9 1ml PRIMO disposable syringes (*CODAN pvb Medical GmbH, Lensahn, Germany*), spanned into the 10-channel syringe pump.
- 3 cOFM V1.0 probes (*in-house production*)
- 3 cOFM V2.0 probes (*Biegler Medizinelektronik GmbH, Mauerbach, Austria*)
- 3 cOFM V3.0 probes (*in-house production*)
- Vials (*Eppendorf AG, Hamburg, Germany*), to store the withdrawn samples.
- Pipettes and syringes (*Eppendorf AG, Hamburg, Germany*), for the glucose measurements.
- Super GL compact Glucose Analyser (*Dr. Mueller Geraetebau GmbH, Freital, Germany*)
- Temperature Sensor with Logger 177-T3 (*Testo GmbH, Vienna, Austria*)
- Heating plate CT2200/E (*Rommelsbacher Elektrohausgeraete GmbH, Dinkelsbuehl, Germany*), to create the agar network.
- Electronic analytical balance ALC110.4 (*Sartorius Group - Acculab, Goettingen, Germany*)

2. Chemicals.

- Agarose Standard for DNA and RNA electrophoresis (*Carl Roth GmbH, Karlsruhe, Germany*)
- Glucose Solution 10% (*Fresenius-Kabi GmbH, Graz, Austria*)
- ddH₂O
- Cyanolit 214.F (Cianoacrylate)
- Calibration solution for the Super GL Analyzer
- Reagent solution for the Super GL Analyzer
- Acetone
- Ethanol

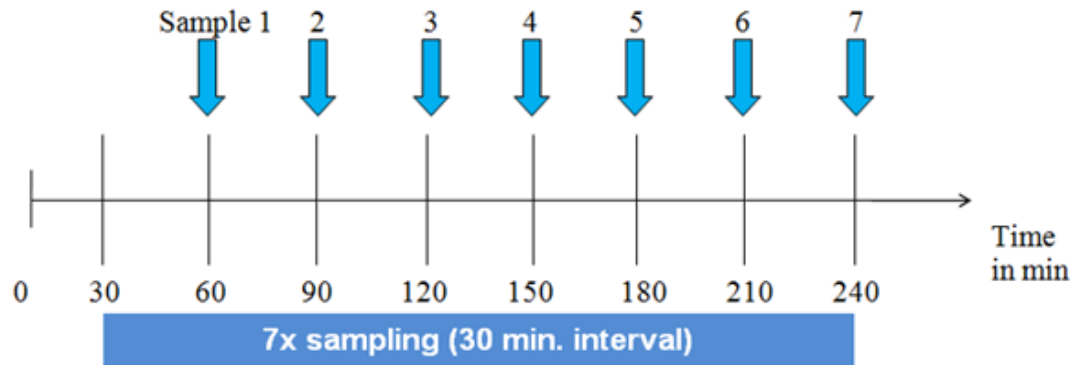


Figure 2.19.: Time line for the in-vitro sampling.

2.4.2. Main studies

In the main studies, Version 1.0, Version 2.0 and the improved test system Version 3.1 were used. The specific aims of the main studies were to compare the exchange performance of glucose molecules between the different probe types and to assess the mean fluid flow through the types.

Samples

The perfusate was ddH₂O. The withdrawn liquid was therefore a glucose solution.

Matrix plate and measurement setup

The matrix plate was adapted to hold the improved test system V3.1. All probe type bodies were bonded to the matrix plate using Cyanoacrylate, and filled with ddH₂O before the perfusion started. In contrast to the feasibility studies, the connections of the probes to the syringes were realized in one piece during manufacturing. This decision was taken to minimize intersections between different tubing modules, where small gas bubbles can easily clog the fluidic pathway. The measurements were made in a time period of 4 hours, with sampling at 30 minutes each, see Fig. 2.19. At each sampling step, the temperature of the gel was measured. All other setup properties were equal to those in the feasibility studies.

Agar diffusion model

Instead of a 1%, a more realistic 0.6% agar gel network (Chen et al., 2004) with a glucose concentration of 2.5% was used. To do so, 3g agarose was mixed with 125 ml of a 10% glucose solution.

Measurement of glucose concentrations

The feasibility studies showed, that the concentration values of the first peak outranged the measurable glucose concentrations of the analyzer. Therefore, the withdrawn samples of measurement point 1 were 1:2-diluted. All other settings were equal to the feasibility studies.

For all probes, concentration-time-plots were created. A linear regression was made, and mean and SD were calculated omitting the primary peak for every probe type. The mean concentrations of the probe types were compared by using Mean and SD.

Flow rate estimation

Mean flow rates were estimated for every single probe by using the method presented in the feasibility studies, see equation (2.7). Herefore, empty and filled vials were weighted, the difference was divided by the sampling time ($t=30$ min). Flow-time-plots were created.

Required Materials

1. Materials and devices.

- Metallic laboratory dish (WxLxH 90x170x40)
- Matrix plate (*in-house production*)
- 10-channel syringe pump SP200 (*World Precision Instruments Inc., Sarasota, USA*)
- 9 syringe pumps Aladdin2-220 (*World Precision Instruments Inc., Sarasota, USA*)
- 9 250 μ L gastight syringes, Type 1725RN (*Hamilton Bonaduz AG, Bonaduz, Switzerland*)
- 9 1ml PRIMO disposable syringes (*CODAN pvb Medical GmbH, Lensahn, Germany*)
- 3 cOFM V1.0 probes (*in-house production*)
- 3 cOFM V2.0 probes (*Biegler Medizinelektronik GmbH, Mauerbach, Austria*)

- 3 cOFM V3.1 probes (*in-house production*)
- Vials (*Eppendorf AG, Hamburg, Germany*)
- Pipettes and syringes (*Eppendorf AG, Hamburg, Germany*)
- Super GL compact Glucose Analyser (*Dr. Mueller Geraetebau GmbH, Freital, Germany*)
- Temperature Sensor 177-T3 with Logger (*Testo GmbH, Vienna, Austria*)
- Heating plate CT2200/E (*Rommelsbacher Elektrohausgeraete GmbH, Dinkelsbuehl, Germany*)
- Electronic analytical balance ALC110.4 (*Sartorius Group - Acculab, Goettingen, Germany*)

2. Chemicals.

- Agarose Standard for DNA and RNA electrophoresis (*Carl Roth GmbH, Karlsruhe, Germany*)
- Glucose Solution 10% (*Fresenius-Kabi GmbH, Graz, Austria*)
- ddH₂O, Acetone, Ethanol
- Cyanolit 214.F (Cyanoacrylate)
- Calibration solution for the Super GL Analyzer
- Reagent solution for the Super GL Analyzer

2.5. Performance Comparison In-Vivo

2.5.1. Objective

The aim of these measurements was a comparative study between the cOFM probe V1.0 and the redesigned prototype V2.0. As parameter of comparison, the relative recovery (RR) of deuterium (heavy water) has been chosen. This substance is a heavier isotope of hydrogen and contains a proton and a neutron. It is distributed homogeneously in the animal body after the so-called equilibration period (often about 12 hours after injection) and diffuses freely through the BBB ([Speakman, 1997](#)). Moreover, the study should give an information about the handling and the functionality of the miniaturized probe under real, in-vivo study conditions.

2.5.2. Animals

8 subjects were divided into 2 groups:

- Group 1:
 - 4 Subjects (Sprague-Dawley rats, male, 300g - 400g; Charles River, Germany)
 - Probe type: cOFM V1.0

- Group 2:
 - 4 Subjects (Sprague-Dawley rats, male, 300g - 400g; Charles River, Germany)
 - Probe type: cOFM V2.0
 - * Subgroup 2.1: Incision closed by cyanoacrylate adhesive
 - * Subgroup 2.2: Incision closed by suture material

The probes were implanted in the frontal lobe, the exchange area was 2 mm below the brain surface.

The staff at the animal care facility (Institute for Biomedical Research, Medical University Graz) provided appropriate animal care. Implantation and sampling was done by a specially trained surgeon, Guenther Rautner. Measurements of the deuterium concentrations were provided by Joanneum Research RESOURCES.

2.5.3. Implantation

The following protocol is based on the implantation of the cOFM probes V2.0. The cOFM probe V1.0 were implanted likewise.

The rats were anesthetized in an incubation box using a mix of Isoflurane and oxygen. To avoid pain and stress for the animals, 1.5 ml/kg FMD (Fentanyl, Midazolam, Domitor) was injected subcutaneously (s.c.).

The heads of the rats were shaved to prepare them for surgery. Next, the head was fixed in a stereotactic frame. A 15 mm midline incision was made to expose the skull. A 0.8 mm hole for probe insertion was drilled into the skull 2 mm lateral to the bregma, see Fig. 2.20(a).

The probe was slowly inserted into the left frontal lobe, and attached to the skull by two fixation screws and dental cement, see Fig. 2.20(b) and Fig. 2.20(c).

In the last step of the implantation procedure, the scalp was dragged over the new probes and closed. The scalp of the animals in subgroup 2.1 was closed by using cyanoacrylate adhesive, see Fig. 2.20(d). The scalps of animals in subgroup 2.2 were sutured, see Fig. 2.20(e).

The animals received Rimadyl (painkiller) and Cefotaxim (antibiotic) for three days after surgery and were kept in individual housing for one day (Fig. 2.21). The animals got a resting period of 14 days to re-establish the BBB.

Required materials

1. Devices.

- Isoflurane Vaporizer anesthesia unit (*Rothacher and Partner, Bern, Switzerland*)
- Electronic analytical balance ALC110.4 (*Sartorius Group - Acculab, Goettingen, Germany*)
- Stereotactic frame system (*David Kopf Instruments*)
- OP lamp macrospot 1500
- Drilling machine NG2/S, FBS 12/E (*Proxxon*)
- Dental drill (*Fine Science Tool Microdrill Burr d=0.8mm*)
- Bone screws (*Fine Science Tool Bone Screw 1.17x4.7*)
- Screwdriver
- Dental cement (*iCEM Self Adhesive; Heraeus (D)*)

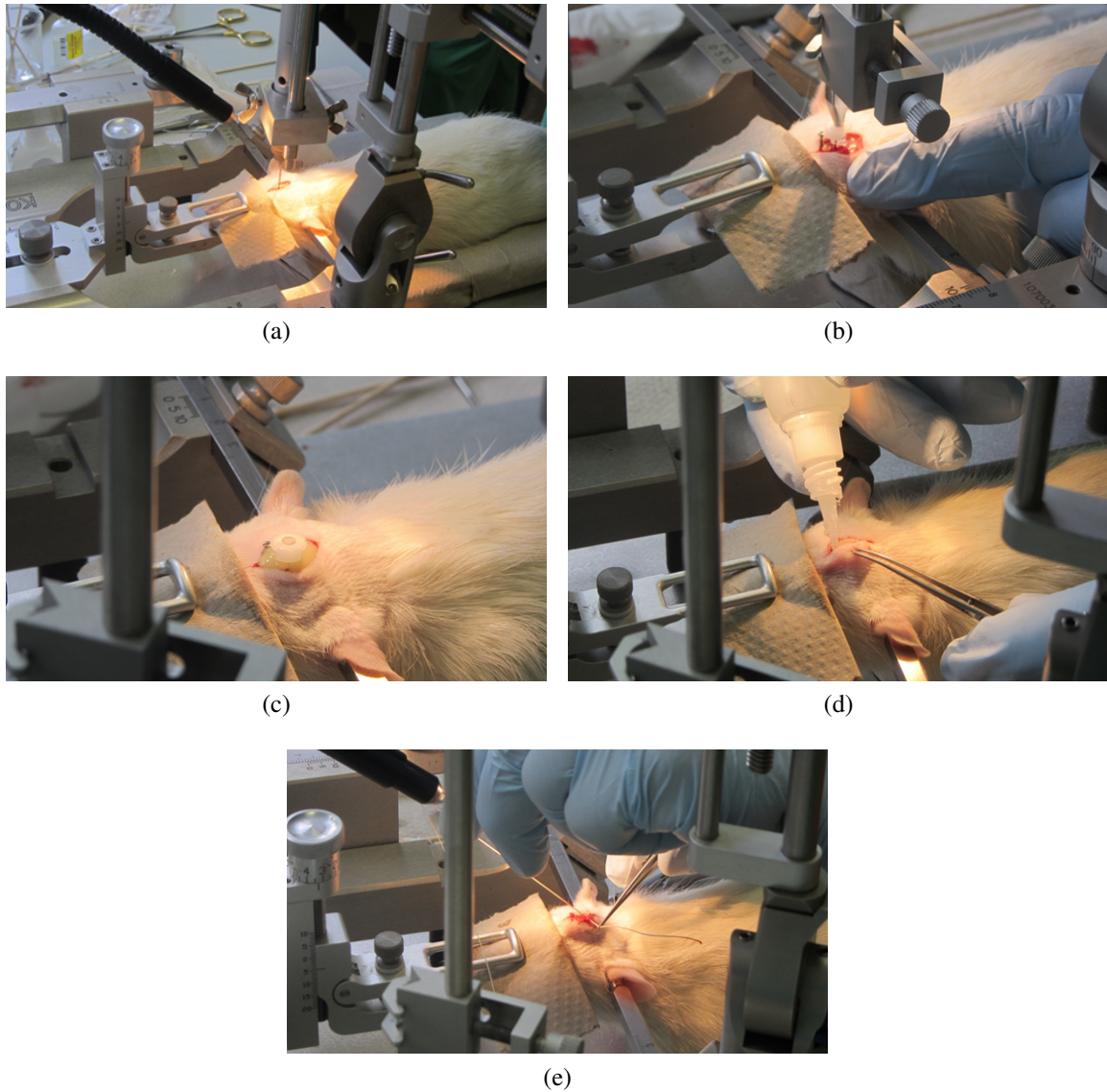


Figure 2.20.: Implanting the cOFM probe V2.0: (a) drilling a 0.8 mm hole into the skull; (b) insertion of the cOFM probe V2.0; (c) attached cOFM probe; (d) closing the scalp using cyanoacrylate; (e) suturing the open scalp.

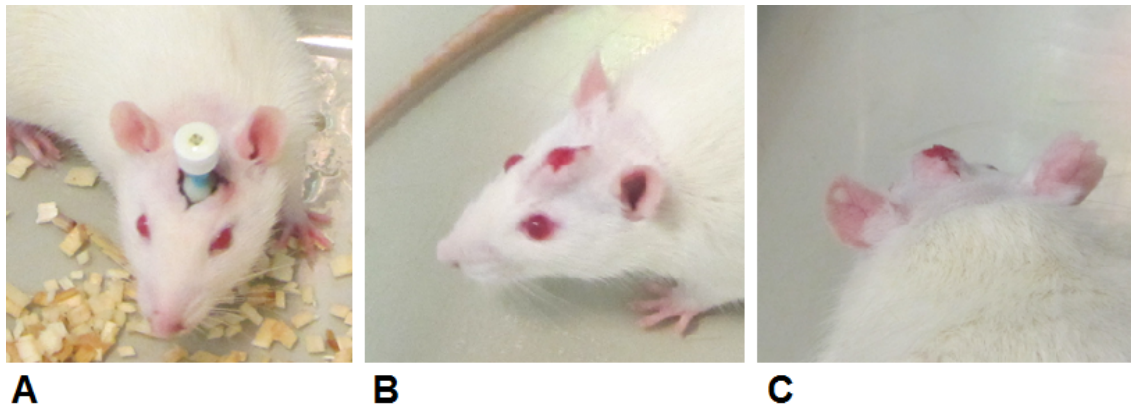


Figure 2.21.: Implanted cOFM probes: (A) rat with cOFM probe V1.0. Due to the dimensions of the state-of-art probe, the scalp was not closed; (B) rats with cOFM probe V2.0 and glued scalp incision; (C) sutured scalp incision.

- Ultraviolet lamp
- 4 cOFM probes V1.0 (*in-house production*)
- 4 cOFM probes V2.0 (*BIEGLER Medizinelektronik*)
- Syringes, cannulas, tweezers and scalpel (blades Nr. 10)
- Sterile sewing set
- Sterile and single-use swabs
- Razor
- Cyanoacrylate adhesive

2. Drugs and Chemicals.

- Isoflurane (volatile anaestheticum)
- Fentanyl (analgesic)
- Midazolam (Benzodiazepin, sedative)
- Domitor (Medotimidin, sedative)
- Anexate (Flumazenil - Antagonist to Benzodiazepin)
- Antisedan (Atipamezol - Antagonist to Medotomidin)
- Carprofen - Rimadyl (Analgesic)
- Cefotaxim - Clarofan (Antibioticum)
- Eye ointment
- Ethanol

2.5.4. Marker Injection

12h before the sampling started, deuterium was injected i.p. (intraperitoneal) into the rats. During the deuterium equilibration period, animals were kept in housing, food and water were provided *ad libidum*. The injection volume IV in ml was calculated using the following formula (Speakman, 1997):

$$IV = \frac{0.65BW DIE}{IE}, \quad (2.8)$$

where BW is the body weight in g, DIE is the desired initial enrichment (500 ppm) and IE is the injection enrichment (500000 ppm, 50% deuterium).

2.5.5. Sampling and deuterium measurement

The cOFM probe channels were rinsed and filled with perfusate. The Run-In phase was 20 minutes long, the first sample was discarded. 5 samples per animal were taken with a 60 minutes interval (Fig. 2.22, Fig. 2.23). Empty and filled vials were weighted to estimate flow rates, and were freeze-dried and stored at 80°C. Assuming a homogeneous distribution of deuterium in the body of the rat, blood plasma, extracted from the rats tail tip, can be used as reference for the RR calculation. During sampling, the rats were anesthetized using a mixture of oxygen and Isoflurane.

Deuterium enrichments in the sample and in the blood plasma were measured at JOANNEUM RESEARCH Resources using Isotope-ratio mass spectrometry (IRMS), which provides a high accuracy in measuring small amounts of isotopes in water samples.

2.5.6. Quantitative analysis

The mean flow rates through the different probe types were estimated using the method presented in the in-vitro studies. The RR in % were calculated using the following formula:

$$RR = \frac{c_{sample}}{c_{blood}} 100\%, \quad (2.9)$$

where c_{sample} is the concentration of deuterium (ppm) in the cOFM sample and c_{blood} is the mean concentration in the blood plasma of a subject. The RR were plotted in a RR vs. time

plot for each probe type. Mean RR from V1.0 and V2.0 were compared to each other.

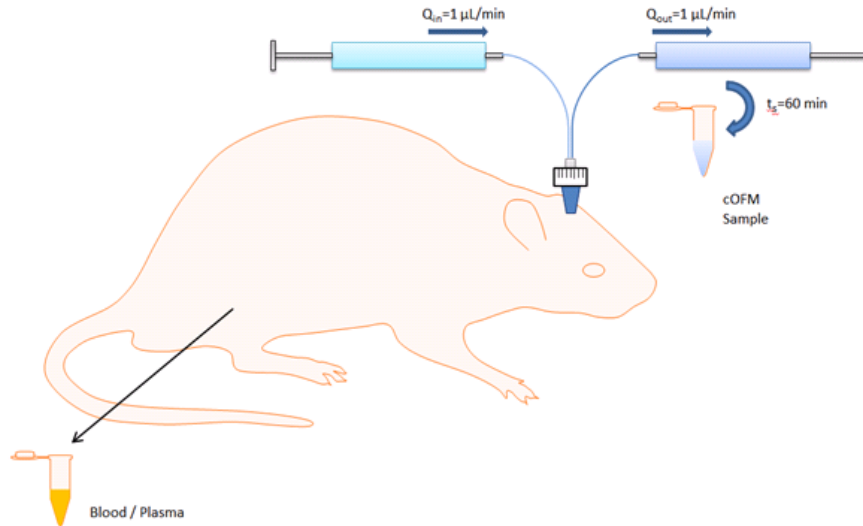


Figure 2.22.: In vivo setup. The probes were implanted in the frontal lobe of the rats. After re-establishment of the BBB (14 days), deuterium was injected 12 hours before the measurement started. After the equilibration period, the healing dummies were replaced by the probe inserts, and the sampling started. Blood plasma was extracted from the rats tail tip and used as reference for the RR calculation.

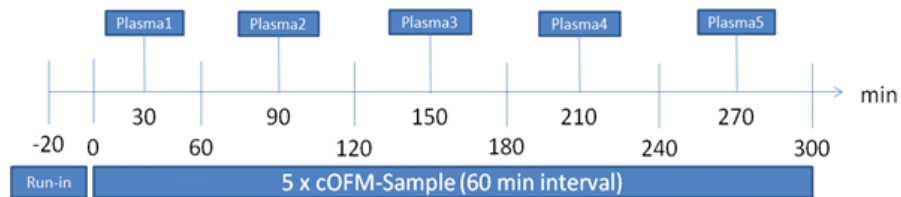


Figure 2.23.: In vivo timeline.

3. Results

3.1. Rotational Rheometry

The **feasibility studies** yielded the results given in Fig. 3.1. For both liquids, lower temperatures resulted in increased viscosity values. In addition, the liquid with the higher protein content (200 g/l) was more viscous than the perfusate. Increased shear rates did not change significantly the viscosity values, both liquids showed hence a Newtonian behavior between 0 and 100 1/s. Figure 3.2 shows the results of the **main studies** using CSF and ddH₂O at 38°C between shear rates of 46.4 and 1000 1/s. CSF had a higher viscosity than water at the same temperature. Results of the linear regression for ddH₂O are presented in Fig. 3.3. The interception point (1.0125 mPa s) nearly equals the mean viscosity of CSF (1.0158 mPa s), and the gradient, the SDs and the determination coefficient are very small. Hence both liquids showed hence a Newtonian behavior.

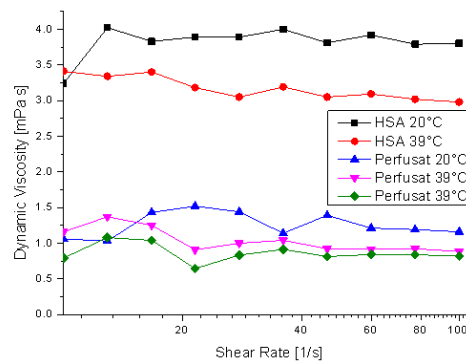


Figure 3.1.: Dynamic viscosity values of perfusate and HSA (200 g/l) at different temperatures for shear rates between 0 and 100 1/s. Lower temperatures resulted in increased viscosity values, the liquid with the higher protein content was more viscous than the perfusate. Hence both liquids showed a Newtonian behavior between 0 and 100 1/s.

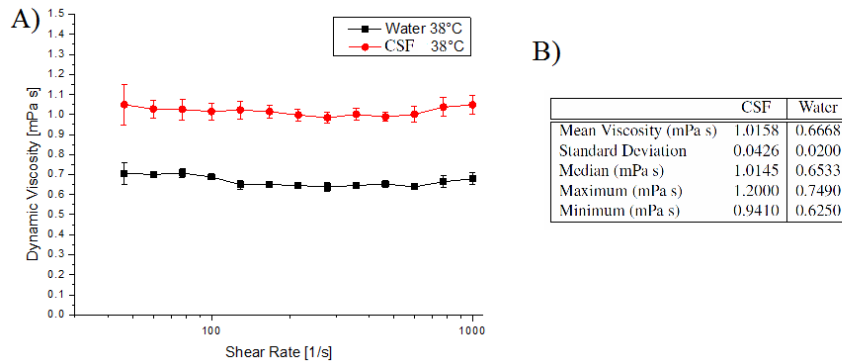


Figure 3.2.: Results from the rheometric main studies: A) dynamic viscosity vs. shear rate for ddH₂O and CSF. CSF had a higher viscosity than water at the same temperature; B) Mean, SD, Median, Maximum and Minimum of the viscosity values for both liquids.

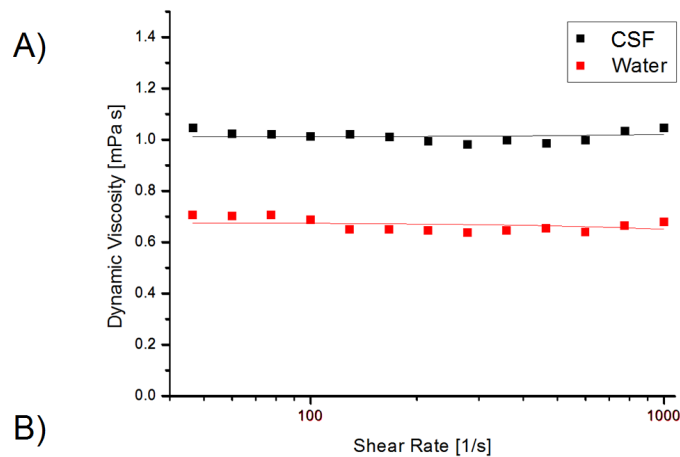


Figure 3.3.: Results from the linear regression analysis: A) linear regression of CSF and ddH₂O. Both liquids showed a Newtonian behavior; B) linear regression parameters for CSF.

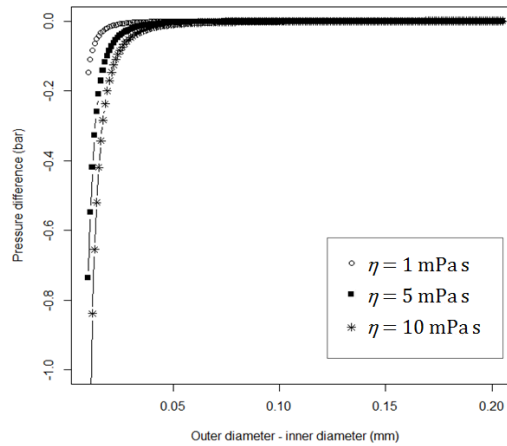


Figure 3.4.: Theoretical flow estimation for three idealized fluids (viscosities: 1 mPa s, 5 mPa s, 10 mPa s). An annular channel geometry with fixed inner diameter (0.12 mm), varying outer diameter (between 0.12 and 0.32 mm) and channel length of 30 mm has been chosen. The outer diameter (OD) should be at least 0.05 mm bigger than the inner diameter to prevent high pressure differences. Furthermore, the OD should be increased when the viscosity is higher.

3.2. Miniaturization in Theory

The theoretical flow for three idealized, incompressible fluids (viscosities: 1 mPa s, 5 mPa s, 10 mPa s) was estimated for an annular geometry ($r = 0.06$ mm, R between 0.06 mm and 0.16 mm) and a channel length of 30 mm. The annular channel in the miniaturized cOFM test systems has the same diameters, but is only about 4 mm long. The estimation lead to the results given in Fig. 3.4.

The outer diameter (OD) should be at least 0.05 mm bigger than the inner diameter (ID) to prevent high pressure differences, which lead to outgassing of soluted gas molecules and hence to unwanted occurrence of gas bubbles. Furthermore, the OD should be increased when dealing with more viscous liquids.

Measurement	c_{water} in g/l	c_{Naf} in g/l
1	2.10	2.12
2	2.11	2.12
3	2.13	2.16
4	2.12	2.13
5	2.13	2.15
Mean concentration	2.12	2.14

Table 3.1.: Measured glucose concentrations in a glucose solution mixed with ddH₂O and Naf. The addition of Naf increased the measured glucose concentration by 0.02 g/l. Compared to the results from the feasibility and main studies, the influence of Naf on the measurements is minimal.

3.3. Performance Comparison In-Vitro

3.3.1. Feasibility studies

Influence of Naf on the glucose concentration measurements.

Table 3.1 presents the measured glucose concentrations of the solution with ddH₂O (left) and Naf (right). The expected glucose concentration was 2.12 g/l. It was found that the addition of Naf increased the measured glucose concentration by 0.02 g/l, which is 0.11 mmol/l. The measured concentration values in the feasibility and main studies ranged between 1.4 and 60 mmol/l. The influence of Naf on the measurements is therefore minimal.

Flow rate estimation of the 10-channel syringe pump.

Table 3.2 shows the measured and calculated weights in g of the syringes and the test vial before and after a perfusion time $T_p = 60$ min.

60 mg water was withdrawn by the pulling syringe in 60 min. Thus, its mean withdrawal rate was 1 $\mu\text{l}/\text{min}$; 62 mg was pushed out of the pushing syringe, thus the 10-channel syringe pump had a mean pump rate of 1.02 $\mu\text{l}/\text{min}$, slightly higher than expected.

Glucose concentration measurements.

All probe types V1.0 could be used to measure the RR of glucose molecules over 6 hours. Perfusions through V1.0b and V1.0c started 30 min. after V1.0a due to clogging of the microchannels induced by gas bubbles. Out of three V2.0 prototypes, only V2.0a worked

	$T_p=0$ min.	$T_p=60$ min., calculated	$T_p=60$ min., measured	Difference
Pushing Syringe	4.131g	4.071g	4.073g	-0.062g
Pulling Syringe	15.215g	15.275g	15.275g	+0.060g
Test vial	2.300g	2.300g	2.303g	+0.003g

Table 3.2.: Flow rate estimation using the weights of the test vial, pushing and pulling syringe. Weights were measured at $T_p=0$ min. and $T_p=60$ min, and calculated for $T_p=60$ min.

as expected. The microchannels of V2.0b and V2.0c were occluded due to crippling of the small PI inflow tubing and gas bubbles. Test system V3.0b was the only system which could be used. It was possible to establish a constant fluid flow through V3.0a, but no glucose could be measured. V3.0c was clogged before the perfusion started. Figure 3.5 shows the results of the measurements.

The results show a high variability between the different probes. In addition, the first peaks could not be measured because the concentrations were higher than the measurement range of the glucose analyzer. The frequent occurrence of gas bubbles and the handling problems with V2.0 yield a limited significance of the results, hence the glucose concentration measurements were repeated.

3.3.2. Main studies

Flow Rates

Mean flow rates were estimated by weighting empty and filled vials. The results are shown in the Fig. 3.6. The mean flow rates were slightly lower than $1.0 \mu\text{l}/\text{min}$, variations are mainly due to small gas bubbles.

cOFM Version V1.0

Single curves of the measured glucose concentrations using probe type V1.0 are shown in Fig. 3.7. The first peaks with high glucose concentrations occurred as expected (22 to 58 mmol/l). The measured concentrations of samples 2-7 varied between 1.4 and 22.1 mmol/l. The mean glucose concentration, omitting the first peak, is 11.24 mmol/l (SD = 6.68). A linear regression yielded a slowly falling gradient (-0.02259) and a very high determination coefficient (0.78471).

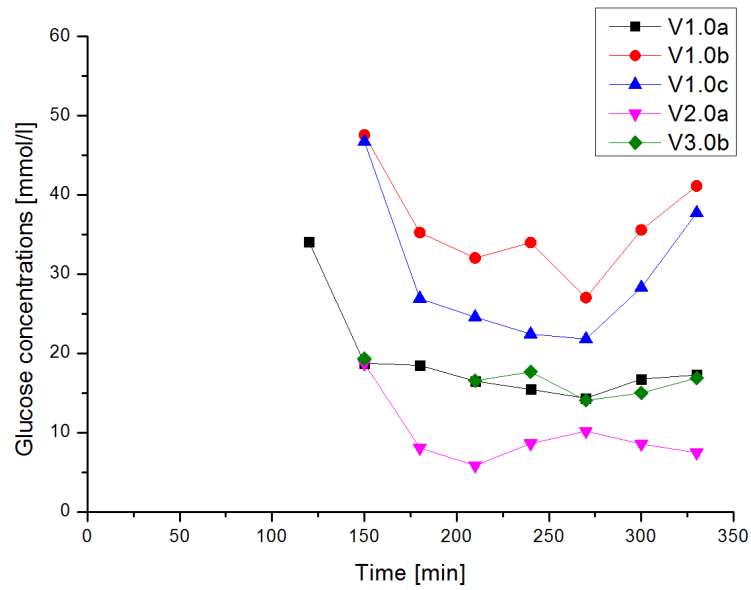


Figure 3.5.: Glucose concentrations measured in the feasibility studies. There is a high variability in the measured concentration values between the different probes. In addition, the peaks of the first samples outranged the measurement range of the analyzer.

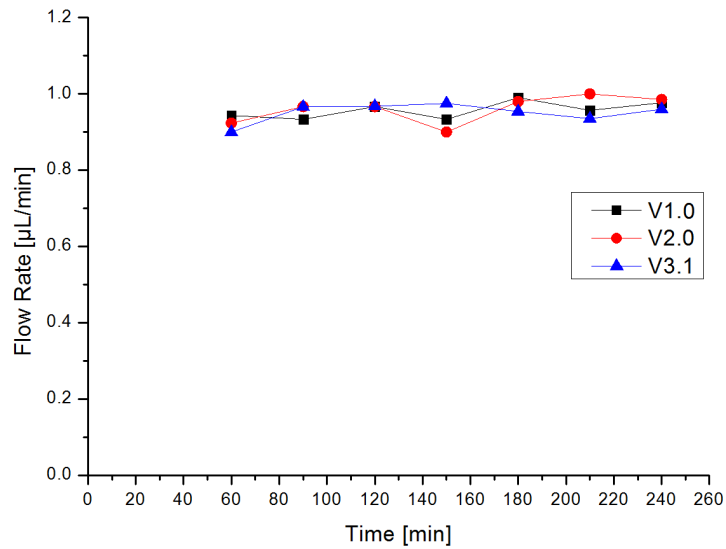


Figure 3.6.: In-vitro main studies. Mean flow rates, slightly lower than $1.0 \mu\text{l}/\text{min}$.

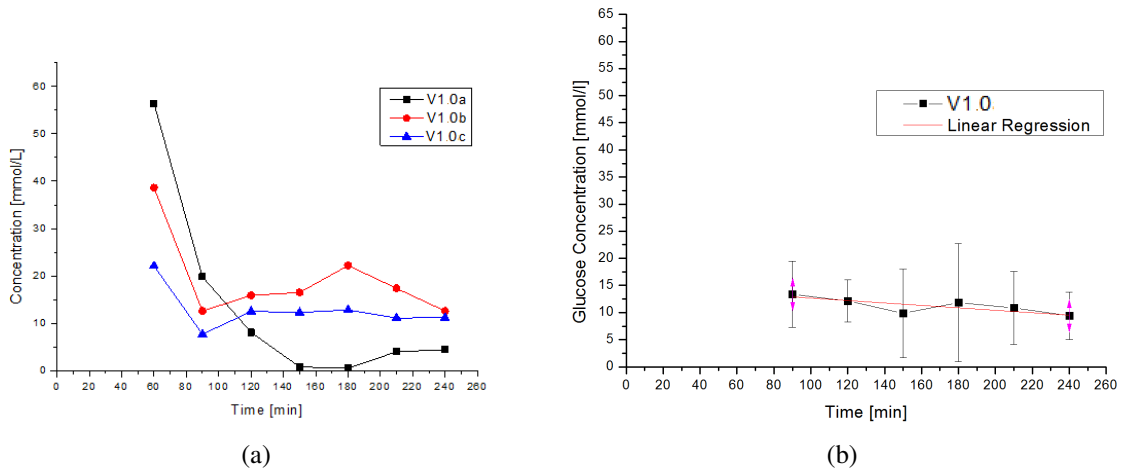


Figure 3.7.: Results from the in-vitro main studies, cOFM probe type V1.0: (a) single curves of the measured glucose concentrations using probe type V1.0. The first peaks with high glucose concentrations varied between 22 to 58 mmol/l, the measured concentrations of the samples 2-7 varied 1.4 and 22.1 mmol/l; (b) Means, SD and linear regression of the measured concentration curves using probe type V1.0, omitting the first peak. The mean concentration is 11.24 mmol/l, the gradient of the linear regression is slowly falling, the determination coefficient is very high.

cOFM Version V2.0

The measured glucose concentrations using the prototypes V2.0 are presented in Fig. 3.8. The first peak did not occur. The measured concentrations of samples 1-7 varied between 8.5 and 30.0 mmol/l. The mean glucose concentration is 13.85 mmol/l (SD = 5.53). In contrast to probe type V1.0, the linear regression produced a slowly increasing gradient (0.00117) and a small determination coefficient (-0.19943).

cOFM Version V3.1

Single curves of the test systems V3.1 are shown in Fig. 3.9. The first peaks with high glucose concentrations did occur and varied between 30 and 60 mmol/l. Samples 2-7 had a glucose concentration between 1.4 and 26.1 mmol/l. The mean glucose concentration, omitting the first peak, is 9.62 mmol/l (SD = 5.53). A linear regression produced a slowly decreasing gradient (-0.02243) and a determination coefficient of 0.56958.

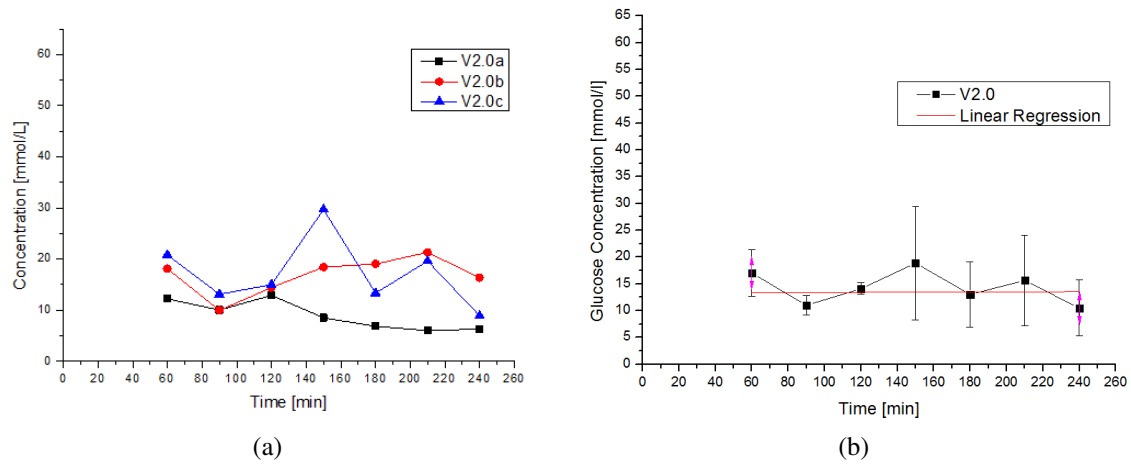


Figure 3.8.: Results from the in-vitro main studies, cOFM probe type V2.0: (a) single curves of the measured glucose concentrations using probe type V2.0. The measured concentrations of samples 1-7 varied between 8.5 and 30.0 mmol/l; (b) Means, SD and linear regression of the measured concentration curves using probe type V2.0. The mean concentration is 13.85 mmol/l, the gradient of the linear regression is slowly increasing, the determination coefficient is small.

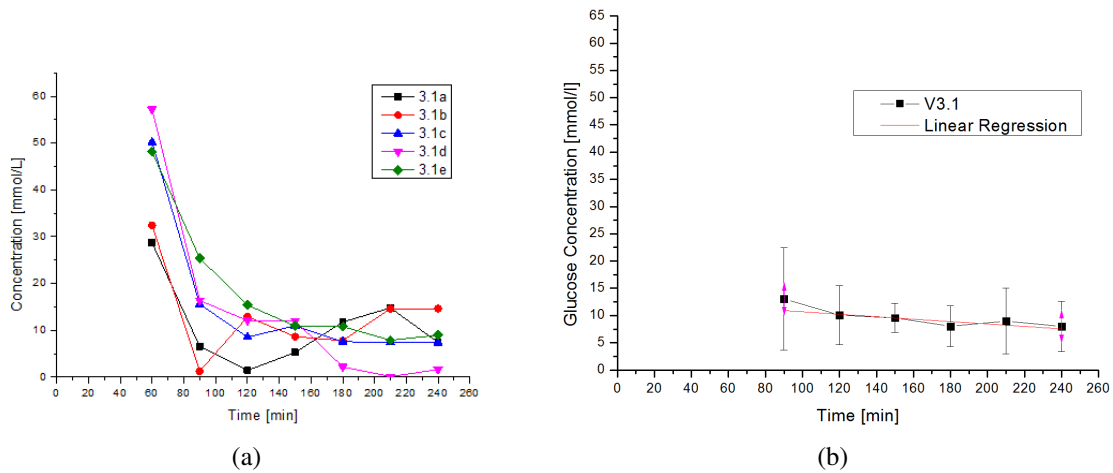


Figure 3.9.: Results from the in-vitro main studies, cOFM probe type V3.1: (a) single curves of the measured glucose concentrations using probe type V3.1. The measured concentrations of samples 1-7 varied between 1.4 and 26.1 mmol/l; (b) Means, SD and linear regression of the measured concentration curves using probe type V3.1. The mean concentration is 9.62 mmol/l, the gradient of the linear regression is slowly decreasing, the determination coefficient is 0.56958.

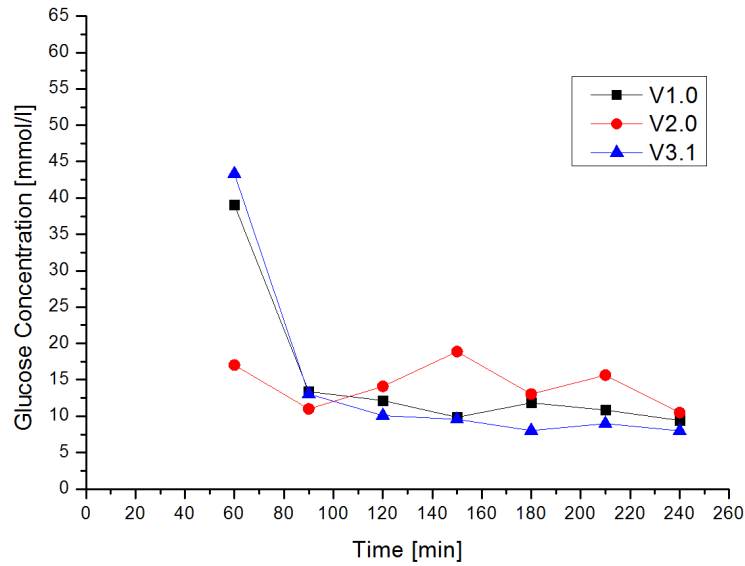


Figure 3.10.: Combined results from the in-vitro main studies. The curves of V1.0 and V2.0 lie in the same range. The glucose concentrations measured using V3.1 were only slightly smaller compared to V1.0 and V2.0.

Comparison

Figure 3.10 shows a comparison of the mean concentration curves of the three probe types, an overview of the results from the in-vitro studies is given in Table 3.3. The mean glucose concentrations were calculated by omitting the first peak. Using V1.0 ($\Delta A = 0.22\text{mm}^2$), a mean glucose concentration of 11.24 mmol/l could be measured. The mean concentration of V2.0 ($\Delta A = 0.12\text{mm}^2$) was even higher, 13.85 mmol/l. The concentration curves of V1.0 and V2.0 are in the same range. The glucose concentrations measured using V3.1 ($\Delta A = 0.01\text{mm}^2$) were only slightly smaller compared to V1.0 and V2.0. The mean concentration was 9.62 mmol/l.

The miniaturization from V1.0 to V2.0 did hence not lead to a decline in the exchange performance of glucose molecules. The exchange performance of V3.1 was only slightly smaller.

Probe type	ΔA in mm^2	Measured concentration range in mmol/l	Mean concentration in mmol/l	SD in %
V1.0	0.22	1.4 – 22.1	11.24	6.68
V2.0	0.12	8.5 – 30.0	13.85	5.53
V3.1	0.01	1.4 – 26.1	9.62	5.53

Table 3.3.: Combined results from the in-vitro main studies.

Probe type	Subject	ΔA in mm^2	Measured concentration range in ppm	Reference concentration in ppm
V1.0	S1	0.22	39.35 – 41.16	132.28
V1.0	S2	0.22	37.22 – 42.20	135.76
V1.0	S3	0.22	42.39 – 44.12	129.98
V1.0	S4	0.22	35.09 – 38.90	137.61
V2.0	S1	0.12	33.98 – 45.33	141.19
V2.0	S2	0.12	36.25 – 37.90	123.42
V2.0	S3	0.12	39.46 – 42.90	122.51

Table 3.4.: In-vivo studies: measured deuterium enrichments in cOFM and blood samples.

3.4. Performance Comparison In-Vivo

A comparison of the mean flow rates between V1.0 and V2.0 is shown in Fig. 3.11. They were slightly lower than $1.0 \mu\text{l}/\text{min}$. The measured deuterium concentration ranges in cOFM samples for each subject are shown in Table 3.4.

The RR at each time point for each sample was calculated using formula (2.9). The results for probe types V1.0 and V2.0 are shown in Fig. 3.12 and Fig. 3.13, respectively. The RR ranged between about 25 and 35% for each probe type and subject.

The mean RR of deuterium were 30.3% using probe type V1.0, and 30.6% using the smaller probe type V2.0, see Fig. 3.14. Hence, there is no difference in the RR of deuterium when miniaturizing the channel dimensions.

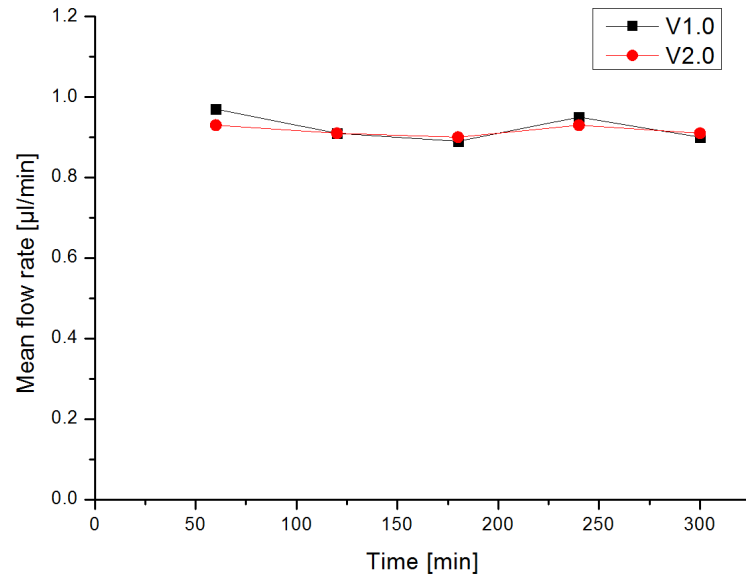


Figure 3.11.: In-vivo flow rates of V1.0 and V2.0, slightly lower than 1.0 $\mu\text{l}/\text{min}$.

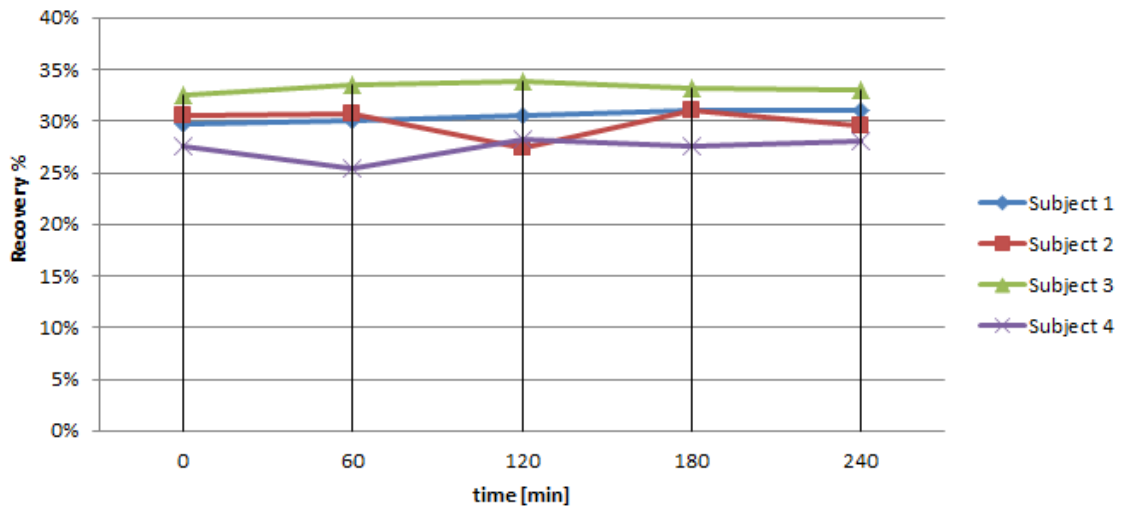


Figure 3.12.: In-vivo deuterium RR using probe type V1.0. The RR ranged between 25 and 35% at each time point.

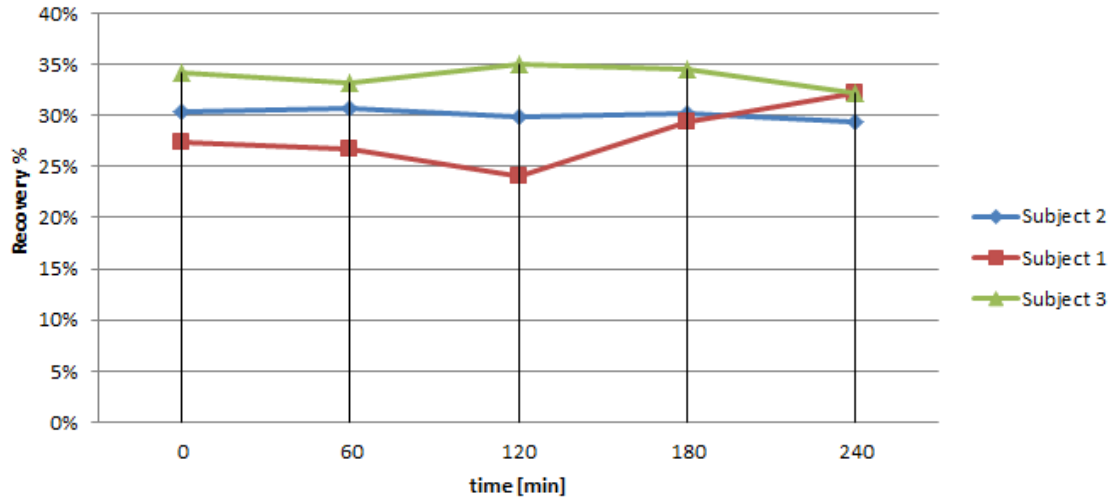


Figure 3.13.: In-vivo deuterium RR using probe type V2.0. The RR ranged between 25 and 35% at each time point.

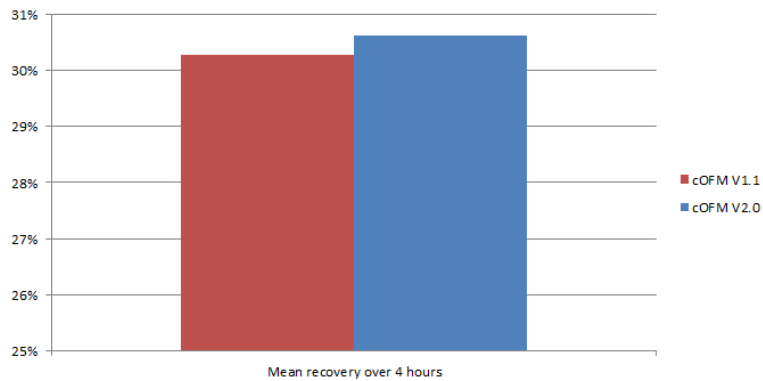


Figure 3.14.: Comparison of the mean deuterium RR between V1.0 and V2.0. The mean RR of deuterium were 30.3% using probe type V1.0, and 30.6% using the smaller probe type V2.0. There is hence no difference in the RR of deuterium when miniaturizing the channel dimensions.

4. Discussion

4.1. Rheological Characterization

The fluids of interest (ISF, CSF, perfusate and mixtures) were characterized by evaluating their composition and their viscosity. The influence of different protein concentrations on the surface tension is discussed below.

The *composition of the perfusate and the sample*, which are in contact with the microchannels of the cOFM probe, is generally multi-phase (see chapter 2.2). The perfusate matches the basic composition of the ISF to minimize the influence on the chemical and physiological environment of the BBB. It is hence a mixture of water and substances like glucose and NaCl (Table 2.1, McNay and Sherwin, 2004). In contrast to the perfusate, the withdrawn sample contains also other substances found in the ISF, like different proteins or the analyte of interest. Due to the disruption of cells during implantation, a low amount of substances of the CSF and the ICF is sampled. In addition, a specific amount of particles like blood clots or skull splinters are taken up. Furthermore, small gas bubbles can occur in the microchannels.

In the *rheometry* feasibility studies (Section 2.2.2), a standard cOFM perfusate and a protein solution (200 g/l) were compared. The results were presented in Fig. 3.1, and lead to the conclusion that a higher protein content and a lower temperature leads to higher viscosity values. Even solutions with a high protein concentration behave like a Newtonian liquid between shear rates of 0 and 100 1/s. In the main studies (Fig. 3.2), CSF and water were compared at the same temperature. Due to its higher protein content, CSF is slightly more viscous than water and behaves like a Newtonian substance between shear rates of 40 and 1000 1/s. In cOFM, a diluted CSF-like sample is withdrawn. It is therefore more viscous than water, but less viscous than pure CSF. These experimental findings are consistent with the studies by Brydon et al., 1995 and Bloomfield et al., 1998. The temperature at the implanted probe tip is higher than in the sample syringe. The viscosity is hence lower at the tip.

The influence of proteins on the *surface tension* and the contact angle of the CSF was studied in a paper by [Brydon et al., 1995](#). They used a dynamic contact angle analyzer, which is based on the Wilhelmy plate method (see Fig. 4.1). The liquid of interest is placed into a container. A test material, in this case a glass strip, is lowered into the liquid and then withdrawn by automatically adjusting the positioning height of the container. The surface tension is calculated by the change in applied force to pull the material out of the liquid. The results presented in this paper are shown in Fig. 4.2. Surface tension values fell from 70 mN/m (distilled water) to about 60 mN/m for CSF with a protein concentration of 0.05 g/l. Afterwards, surface tension remained nearly constant with a mean surface tension of 44.8 mN/m. [Gonzalez-Tello et al., 2009](#) performed a study evaluating the surface tensions of whey concentrate solutions with different protein concentrations. They used the De Nuoy Ring method, which is similar to the Wilhelmy plate method, but uses a ring instead of a plate. They measured a surface tension of 72 mN/m for solutions without proteins, which fell to 42.5 mN/m by increasing the protein content, and remained constant at about 46 mN/m afterwards. The effect of different protein concentrations on the surface tension is much higher than the effect of a change in temperature.

The withdrawn sample is therefore a water-like, Newtonian liquid with a slightly enhanced viscosity. Its surface tension is about 50 mN/m, and is therefore more wettable than distilled water. The liquid often includes small gas bubbles, and is therefore more compliant. Occasionally, large macromolecules and particles like blood clots occur and influence the flow behavior.

4.2. cOFM Probes

The microchannels of the cOFM probes are made of PTFE, PTFE-coated PI tubings or PTFE-like materials (FEP), see Section 2.3.1. These polymeric materials are very hydrophobic, the adsorption of water-soluble analytes is hence minimized. Such materials are biocompatible and have in addition a low friction coefficient, which affects positively the flow through the channels, especially if gas bubbles occur. Rough surfaces yield a variety of different dynamic contact angles and make the flow non-uniform. PI tubings for the probe tips have been chosen because they are very stiff and therefore easy to handle. In addition, PI tubings can be manufactured with very small diameters and walls. PI tubings with OD = 0.12 mm are the smallest tubings available on the market.

The current **cOFM probe V1.0** (Section 2.3.2) has the disadvantage of having a large guide

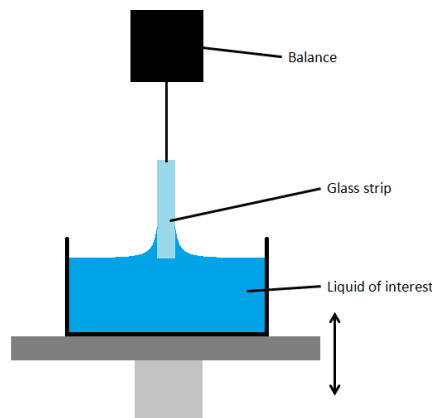


Figure 4.1.: The Wilhelmy plate method to determine the surface tension of a test liquid. The liquid of interest is placed into a container. A test material, in this case a glass strip, is lowered into the liquid and then withdrawn by automatically adjusting the positioning height of the container. The surface tension is calculated by the change in applied force to pull the material out of the liquid.

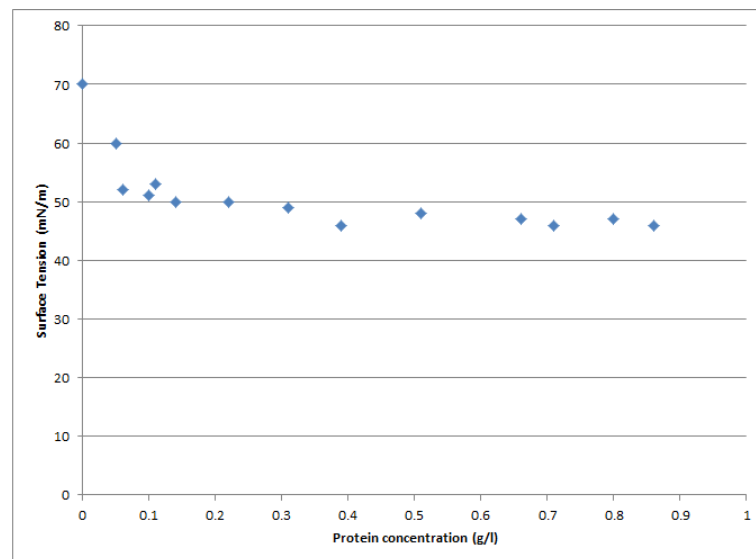


Figure 4.2.: Surface tension of liquids with different protein concentration measured with the Wilhelmy plate method, modified from [Brydon et al., 1995](#). Surface tension values fell from 70 mN/m (distilled water) to about 60 mN/m for CSF with a protein concentration of 0.05 g/l. Afterwards, surface tension remained nearly constant with a mean surface tension of 44.8 mN/m.

cannula (OD = 0.8 mm) and a large probe body. The aim was to miniaturize the OD of the guide cannula to minimize implantation trauma.

The **prototype V2.0** (Section 2.3.3) has a smaller guide cannula and a smaller probe body. In contrast to V1.0, the smaller probe body lead to the possibility to impose and close the scalps over the probes. The probability of loosing them during the healing phase is hence minimized and the animals could kept pairwise from day 2 after implantation. Compared to V1.0, which had a straight channel geometry, V2.0 has two 90° angles in the outflow pathway. Here, sedimentation effects of large macromolecules and particles can occur due to inertial effects. Nevertheless, such effects are kept minimal due to laminar flow characteristic. In addition, the outflow path contains 2 interfaces between different channel geometries: annular outflow path, rectangular path and circular path. Large gas bubbles are able to clogg the fluidic network at these interfaces. This effect occurred in the in-vitro feasibility studies, where large gas bubbles expanded due to compliancy from the outflow PTFE pathway inside the probe body. While V1.0 has a concentric design, the design of V2.0 is directed. This way, rotational motions during implantation, which could cause further tissue traumas, are minimized. The handling of the miniaturized cOFM probe V2.0 showed significant difficulties in-vitro and in-vivo.

The **test systems** (Section 2.3.4) were built to simulate cOFM systems with the smallest tubing diameter commercially available. The first test system V3.0 was used in the in-vitro feasibility studies. Its miniaturized probe tip was inserted into the guide cannula of a V1.0 probe. This yielded the opportunity to use a healing dummy in the experiments, but lead to the disadvantage that the miniaturized probe tip was not fully surrounded by agarose gel during sampling. In contrast, the probe tip of test system V3.1 was fully surrounded by agarose gel. The system was inserted into the gel without a healing dummy, which caused no problems during sampling.

The lowest size for miniaturized tubing diameters was estimated by calculating the pressure difference needed to withdraw a homogeneous, incompressible fluid through a small, annular, 30 mm long tubing (Section 2.3.5). The results showed, that the outer diameter of the annular channel should be at least 0.05 mm larger than the inner diameter, which was set to 0.12 mm (Fig. 3.4). This constraint is satisfied in the miniaturized test systems, where the outer diameter of the channel is 0.06 mm larger than the inner diameter. This estimation is however idealized. Firstly, the outflow channel is longer than 30 mm and has several different channel geometries. However, the annular geometry is by far the smallest one in the fluidic network and builds up the largest hydraulic resistance. Secondly, the fluid

is not homogeneous and incompressible, but multiphase and compressible due to small gas bubbles.

4.3. In-Vitro Performance

In the **feasibility studies** (Section 2.4.1), the major problems were the frequent occurrence of gas bubbles and the difficult handling of the miniaturized prototypes. Due to the perfusion system setup, which included several channel interfaces to enlarge the connection tubings from probes to syringes, the fluidic systems were often clogged by gas bubbles. For the main studies, the connection tubings were realized in one piece during manufacturing to minimize channel interfaces, which had a positive effect.

The handling of the miniaturized prototypes V2.0 resulted to be another problem. The difficulty was to successfully insert the small PI inflow tubing into the guide cannula without crippling it at edges. This is challenging, because the parts of the systems are very small, and the small PI inflow tubing has to be inserted into the guide cannula before the probe insert can be put into the probe body. Crippling generally lead to a sealing of the fluidic system during the in-vitro feasibility studies. Based on this problem, a new improved design was developed.

The measured glucose concentrations showed a high variability (Fig. 3.5) and outranged the measurement range of the analyzer at the first samples. Hence the decision to repeat the experiments.

The **main studies** (Section 2.4.2) included an estimation of the mean flow rates and the measurement of the glucose concentrations. The mean flow rates over 1 hour was estimated by using the weighting method, which yielded the result that the rates are slightly smaller than $1 \mu\text{l}/\text{min}$ (Fig. 3.6). The glucose concentration measurements lead to the results presented in Section 3.3.2. The primary peak was estimated by using a dilution series. All values after the first peak ranged between almost 0 and 30 mmol/l, the mean concentrations ranged between 9.62 and 13.85 mmol/l (Table 3.3). The concentration curve of V2.0 lacks of the initial peak (Fig. 3.8) This can be explained by the fact that V2.0 had smaller connecting tubings than the other probe types. Therefore, the peak occurred earlier and was very likely missed during the Run-In phase. Using the prototype V2.0, it was possible to measure higher concentrations than using V1.0. The values of V3.1 were not significantly smaller than those measured with the other probe types. Therefore, smaller tubing diameters at the probe tips have no influence on the exchange performance of glucose molecules.

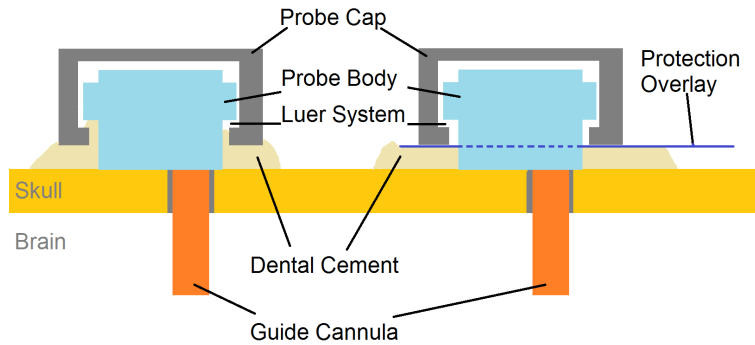


Figure 4.3.: Protection overlay for cOFM probe type V2.0. Due to the small probe body height, the dental cement fills very easily into the luer system and locks it when hardened out. This makes it challenging to remove the probe cap. The protection overlay protects the luer system by being placed under the probe during implantation.

It should be mentioned, that glucose molecules are small compared to macromolecules found in the ISF and are in addition water-soluble. Furthermore, the in-vitro model is idealized. The gel consists of an agar network, distilled water and glucose molecules, but lacks macromolecules and particles, which could influence the fluid flow.

4.4. In-Vivo Performance

In-vivo (2.5), the performances of V1.0 and V2.0 have been compared by evaluating the differences in RR of deuterium.

A challenge was encountered during the implantation of probe type V2.0. Due to the small probe body height, the dental cement flows easily into the luer system and locks it after curing. This makes it difficult to remove the probe cap. To overcome this problem, a protection overlay (Fig. 4.3) was manufactured, which protects the luer system by being placed under the probe during implantation.

The mean flow rates through both probe types, estimated using the weighting method, were slightly smaller than $1 \mu\text{l}/\text{min}$ (Fig. 3.11).

To estimate the RR, the deuterium enrichments in the samples and in the blood plasma (reference) were used. The results, presented in Section 3.4, lead to the conclusion that there

is no difference in the RR of deuterium between V1.0 (30.3%) and V2.0 (30.6%). During sampling, no problems in the fluid flow occurred due to macromolecules or particles. Small gas bubbles were withdrawn steadily and did not clog the system.

4.5. Conclusion

The current cOFM probe type V1.0 was miniaturized by decreasing probe body height and guide cannula diameters. Starting from a guide cannula OD of 0.8 mm (V1.0), the tubing was miniaturized to 0.5 mm (prototype V2.0). The results showed no differences in the Relative Recovery of glucose (in-vitro) and deuterium (in-vivo). Test systems with even smaller guide cannula diameters (OD = 0.25 mm) were evaluated in-vitro with the same results. To enhance the handling capability, a new prototype was designed.

4.5.1. Handling optimization

To account for the challenging insertion of the probe insert of V2.0, the new prototype design (V2.1) features a *connecting piece*, a *longer probe insert* and a *steeper cone*. The connecting piece is attached to the probe body after removing the healing dummy using the luer system, and increases hence the probe body height. This way, the probe insert has first to be slid into the probe before the small inflow PI tubing reaches the guide cannula. Furthermore, the cone is steeper than in V2.0. These enhancements minimize the probability to cripple the inflow PI tubings at edges. In addition and in contrast to V2.0, the new prototype has *distinguishable inflow and outflow tubings*, so that both pathways are defined and not mixed up during sampling. The small PI inflow tubings will furthermore be protected by a small, removable tubing to prevent crippling during transport. A schematic of the new prototype design is shown in Fig. 4.4. The probe bodies of the new prototypes will be milled out of PEEK instead of PMMA, all other materials will not be changed. The implantation procedure equals to V2.0. Due to the fact, that the connecting piece is attached after removing the healing dummy, the probe body height during the BBB re-establishment remains as small as V2.0. The fluidic pathway of V2.1 equals to V2.0 too.

4.5.2. Outlook

In future, the prototypes V2.1 will be serially produced by using the injection molding technique. There will be 2 variants of the probe type: one with a guide cannula with OD

= 0.53 mm, which will be used for pre-clinical studies with rats, the other with a guide cannula with OD = 0.25 mm, which will be used in mice. The probe types V2.1, especially those with minimized channel diameters, will further be compared to V1.0 by evaluating the influence and RR of macromolecules.

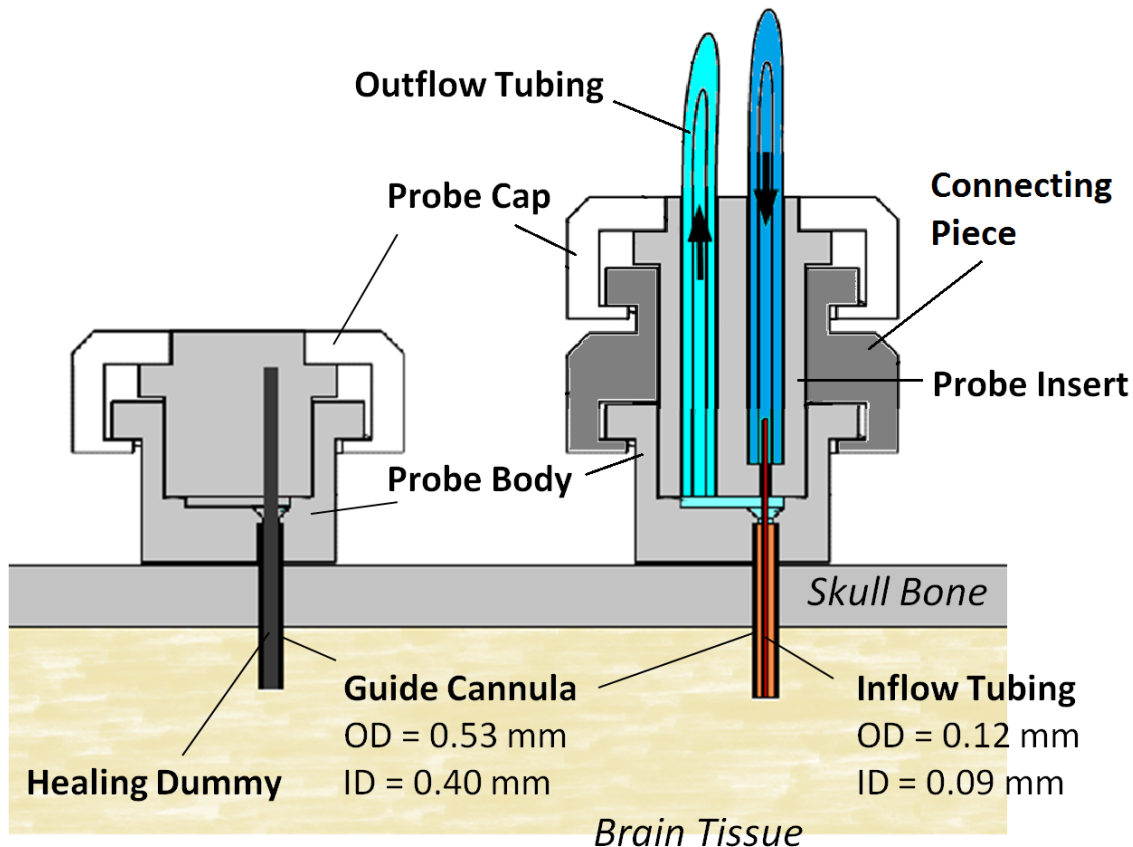


Figure 4.4.: Design of the new prototype V2.1 for rats. It features a connecting piece to increase the probe body height, a steeper cone and distinguishable inflow and outflow tubings. During the BBB re-establishment phase (left), the probe body height remains as small as V2.0. For sampling (right), the healing dummy will be replaced and the connecting piece will be attached. This way, the insertion of the probe insert is facilitated and the crippling probability of the small PI inflow tubing is minimized.

Bibliography

- N. J. Abbott, L. Roennbaeck, and E. Hansson. Astrocyte-endothelial interactions at the blood-brain barrier. *Nature Reviews - Neuroscience*, 7:41–53, 2006.
- K. Aktories, U. Foerstermann, F. B. Hofmann, K. Starke. *Allgemeine und spezielle Pharmakologie und Toxikologie*. Elsevier GmbH, Muenchen, 2009.
- T. Bayraktar, and S. B. Pidugu. Characterization of liquid flows in microfluidic systems. *International Journal of Heat and Mass Transfer*, 40:815–824, 2006.
- M. Bodenlenz, L. A. Schaupp, T. Druml, R. Sommer, A. Wutte, H. C. Schaller, F. Sinner, P. Wach, and T. R. Pieber. Measurement of interstitial insulin in human adipose and muscle tissue under moderate hyperinsulinemia by means of direct interstitial access. *American Journal of Physiology - Endocrinology and Metabolism*, 289:296-300, 2005.
- M. Bodenlenz, C. Hoefferer, C. Magnes, R. Schaller-Ammann, L. A. Schaupp, F. Feichtner, M. Ratzner, K. Pickl, F. Sinner, A. Wutte, S. Korsatko, G. Koehler, F. J. Legat, E. M. Benfeldt, A. M. Wright, D. Neddermann, T. Jung, and T. R. Pieber. Dermal PK/PD of a lipophilic topical drug in psoriatic patients by continuous intradermal membrane-free sampling. *European Journal of Pharmaceutics and Biopharmaceutics*, 81:635-641, 2012.
- I. Brasnjevic, H. W.M. Steinbusch, C. Schmitz, P. Martinez-Martinez. Delivery of peptide and protein drugs over the blood-brain barrier. *Progress in Neurobiology*, 87:212–251, 2009.
- H. Bruus. *Theoretical Microfluidics*. Oxford University Press, Oxford, New York, 2008.
- I. G. Bloomfield, I. H. Johnston, and L. E. Bilston. Effects of proteins, blood cells and glucose on the viscosity of cerebrospinal fluid. *Pediatric Neurosurgery*, 28:246-251, 1998.
- L. Bocquet, and E. Charlaix. Nanofluidics, from bulk to interfaces. *Chemical Society Reviews*, 39:1073–1095, 2010.
- H. K. Brydon, R. Hayward, W. Harkness, and R. Bayston. Physical properties of cerebrospinal fluid of relevance to shunt function. 1: The effect of protein upon CSF viscosity. *British Journal of Neurosurgery*, 9:639–644, 1995.

- H. K. Brydon, R. Hayward, W. Harkness, and R. Bayston. Physical properties of cerebrospinal fluid of relevance to shunt function. 2: The effect of protein upon CSF surface tension and contact angle. *British Journal of Neurosurgery*, 9:645–651, 1995.
- V. I. Chefer, A. C. Thompson, A. Zapata, and T. S. Shippenberg. Overview of Brain Microdialysis. *Current Protocols in Neuroscience*, 47:7.1.1–7.1.28, 2009.
- Z. J. Chen, G. T. Gillies, W. C. Broaddus, S. S. Prabhu, H. Fillmore, R. M. Mitchell, F. D. Corwin, and P. P. Fatouros. A realistic brain tissue phantom for intraparenchymal infusion studies. *Journal of Neurosurgery*, 101:314–322, 2004.
- A. S. Darvesh, R. T. Carroll, W. J. Geldenhuys, G. A. Gudelsky, J. Klein, C. K. Meshul, and C. J. Van der Schyf. In vivo brain microdialysis: advances in neuropsychopharmacology and drug discovery. *Expert Opinion on Drug Discovery*, 6:109–127, 2011.
- M. Ellmerer, L. A. Schaupp, G. Sendlhofer, A. Wutte, G. A. Brunner, Z. Trajanoski, F. Skrabal, P. Wach, and T. R. Pieber. Lactate metabolism of subcutaneous adipose tissue studied by open flow microperfusion. *The Journal of Clinical Endocrinology & Metabolism*, 83:4394–4401, 1998.
- P. Gonzalez-Tello, F. Camacho, E. M. Guadix, G. Luzon, and P. A. Gonzalez. Density, viscosity and surface tension of whey protein concentrate solutions. *Journal of Food Process Engineering*, 32:235–247, 2009.
- A. Guenther, M. T. Kreutzer. Multi-phase flow. In V. Hessel, A. Renken, J. C. Schouten, J. Yoshida, editors, *Micro Process Engineering: A Comprehensive Handbook*, pages 3–40, Weinheim, 2009. WILEY-VCH Verlag GmbH & Co. KGaA.
- S. Ha, E. Wintermantel, G. Maier. Biokompatible Polymere. In E. Wintermantel, S. Ha, editors, *Medizintechnik - Life Science Engineering*, pages 219–276, Berlin, Heidelberg, New York 2009. Springer-Verlag.
- M. Hammarlund-Udenaes, M. Fridn, S. Syvaenen, and Gupta. On the rate and extent of drug delivery to the brain. *Pharmaceutical Research*, 25:8, 2008.
- D. T. Ikeoka, C. Pachler, J. K. Mader, G. Bock, A. L. Neves, E. Svehlikova, F. Feichtner, G. Koehler, C. J. Wrighton, T. R. Pieber, and M. Ellmerer. Lipid-heparin infusion suppresses the IL-10 response to trauma in subcutaneous adipose tissue in humans. *Obesity (Silver Spring)*, 19:715–721, 2011.
- D. Janasek, J. Franzke, and A. Manz. Scaling and the design of miniaturized chemical-analysis systems. *Nature*, 442:374–380, 2006.
- T. J. Kroath. *Aufbau und Evaluierung eines OFM-Systems im zentralen Nervensystem der Ratte*. Master Thesis, Graz University of Technology, 2011.

- E. Lauga, M. P. Brenner, and H. A. Stone,. Microfluidics: The no-slip boundary condition. In C. Tropea, A. Yarin, J. F. Foss, editors, *Springer Handbook of Experimental Fluid Mechanics*, pages 1219–1240, Berlin, Heidelberg, New York 2007. Springer-Verlag.
- E. C. McNay, and R. S. Sherwin. From artificial cerebro-spinal fluid (aCSF) to artificial extracellular fluid (aECF): microdialysis perfusate composition effects on in vivo brain ECF glucose measurements. *Journal of Neuroscience Methods*, 132:35–43, 2004.
- T. G. Mezger. *The Rheology Handbook: For Users of Rotational and Oscillatory Rheometers*. Vincentz Network GmbH & Co. KG., Hannover, 2006.
- N. T. Nguyen and S. T. Wereley. *Fundamentals and Applications of Microfluidics*. Artech House Inc., Norwood, 2006.
- J. Olesen, A. Gustavssonb, M. Svensson, H. U. Wittchen, and B. Joensson. The economic cost of brain disorders in Europe. *European Journal of Neurology*, 19:155–162, 2012.
- W. M. Pardridge. The blood-brain barrier and neurotherapeutics. *NeuroRx*, 2:1–2, 2005.
- J. Park and R. S. Lakes. *Biomaterials - An Introduction*. Springer Science+Business Media, LLC., New York, 2007.
- T. Pieber, T. Birngruber, M. Bodenlenz, C. Hoefflerer, S. Mautner, K. Tiffner, F. Sinner. Open flow microperfusion: an alternative method to microdialysis?. In M. Mueller, editor, *Microdialysis in Drug Development*, pages 283–302, Vienna, 2013. Springer-Verlag. CAAPS Advances in the Pharmaceutical Science Series.
- C. Rivet, H. Lee, A. Hirsch, S. Hamilton, and H. Lu. Microfluidics for medical diagnostics and biosensors. *Chemical Engineering Science*, 66:1490–1507, 2011.
- K. V. Sharp, R. J. Adrian, J. G. Santiago, J. I. Molho,. Liquid flows in microchannels. In M. Gad-el-Hak, editor, *MEMS: Introduction and Fundamentals (The MEMS Handbook, Second Edition)*, pages 10-1–10-45, Boca Raton, 2006. CRC Press.
- F. Skrabal, Z. Trajanoski, H. Kontscheider, P. Kotantko and P. Wach. Portable system for on-line continuous ex vivo monitoring of subcutaneous tissue glucose using open tissue perfusion. *Medical & Biological Engineering & Computing*, 22:116–118, 1995.
- J. R Speakman. *Doubly Labelled Water. Theory and Practice*. Chapman and Hall, London, 1997.
- T. M. Squires, and S. R. Quake. Microfluidics: fluid physics at the nanoliter scale. *Reviews of Modern Physics*, 77:977–1026, 2005.
- L. Weng, S. Liang, L. Zhang, X. Zhang, and J. Xu. Transport of glucose and poly(ethylene glycol)s in agarose gels studied by the refractive index method. *Macromolecules*, 38: 5236–5242, 2005.

G. M. Whitesides. The origins and the future of microfluidics. *Nature*, 442:368–373, 2006.

J. O Wilkes. *Fluid Mechanics for Chemical Engineers with Microfluidics and CFD*. Prentice Hall, Upper Saddle River, 2005.

L. Y. Yeo, H. C. Chang, P. P. Chang, and J. R. Friend. Microfluidic devices for bioapplications. *Small*, 7:12–48, 2011

List of Figures

1.1. Transport mechanisms over the Blood-Brain Barrier	2
1.2. Schematic of an OFM sampling system	4
1.3. cOFM technology compared to other sizes scales.	6
1.4. Surface tension, contact angle and capillary effect.	7
1.5. Taylor dispersion.	9
1.6. Master Thesis workflow.	11
2.1. Working principle of the cOFM	14
2.2. Fluids of interest.	16
2.3. Rotational rheometry.	18
2.4. Rheometer.	19
2.5. Important polymer properties for cOFM probes.	22
2.6. The cOFM probe V1.0	24
2.7. Different parts of the cOFM probe V1.0	25
2.8. Schematic of a fixed cOFM probe.	26
2.9. The cOFM probe V2.0	29
2.10. The different parts the cOFM probe V2.0.	30
2.11. Schematic and image of the test system 3.0.	32
2.12. Schematic and image of the test system 3.1.	34
2.13. Probe tip comparison	36
2.14. Fluidic system for the flow rate estimation of the 10-channel syringe pump.	39
2.15. In-vitro perfusion system	40
2.16. Measurement setup of the in-vitro feasibility studies.	41
2.17. Time line for the in-vitro sampling.	41
2.18. Glucose measurement setup.	42
2.19. Time line for the in-vitro sampling.	44
2.20. Implanting the cOFM probe V2.0.	49
2.21. Implanted cOFM probes.	50
2.22. In vivo setup.	52
2.23. In vivo timeline.	52
3.1. Dynamic viscosity values of perfusate and HSA	53
3.2. Dynamic viscosity vs. shear rate for ddH ₂ O and CSF.	54
3.3. Linear regression of CSF and ddH ₂ O.	54
3.4. Theoretical flow estimation.	55

3.5. In-vitro feasibility studies: Measured glucose concentrations.	58
3.6. In-vitro main studies: Mean flow rates.	58
3.7. Results from the in-vitro main studies, cOFM probe type V1.0.	59
3.8. Results from the in-vitro main studies, cOFM probe type V2.0.	60
3.9. Results from the in-vitro main studies, cOFM probe type V3.1.	60
3.10. Combined results from the in-vitro main studies.	61
3.11. In-vivo flow rates.	63
3.12. In-vivo deuterium RR using probe type V1.0.	63
3.13. In-vivo deuterium RR using probe type V2.0.	64
3.14. Comparison of the mean deuterium RR between V1.0 and V2.0.	64
4.1. The Wilhelmy plate method.	67
4.2. Surface tension of liquids with different protein concentration	67
4.3. Protection overlay for cOFM probe type V2.0.	70
4.4. Design of the new prototype V2.1	72

List of Tables

2.1. Exemplar composition of a cOFM perfusate.	16
2.2. Probe tip comparison.	36
3.1. Influence of Naf on glucose concentration measurements	56
3.2. Flow rate estimation of the 10-channel syringe pump.	57
3.3. Combined results from the in-vitro main studies.	62
3.4. Measured deuterium concentrations.	62

Appendix

A. General material properties

The following datasheets were retrieved from <http://www.accudynetest.com> (2012) unless stated otherwise.

A.1. PTFE

Material properties of PTFE

Chemical properties

	Minimum value	Maximum value	Unit	Remarks	Sources
Solidification shrinkage	3.5	6	%		Idemat 2003
Water absorption			%		

Electrical properties

	Minimum value	Maximum value	Unit	Remarks	Sources
Breakdown potential	50	80	kV/mm		Idemat 2003
Dielectric loss factor			%		
Electrochemical potential			V		
Resistivity	1.00E+022	1.00E+022	Ohm.mm ² /m		Idemat 2003

Mechanical properties

	Minimum value	Maximum value	Unit	Remarks	Sources
Bending strength	5	6	MPa		Idemat 2003
Compressive strength	7	8	MPa		Idemat 2003
Creep strength			MPa		
Density	2150	2200	kg/m ³		Idemat 2003
Elongation	350	550	%		Idemat 2003
Fatigue failure			MPa		
Friction coefficient	0.05	0.08			Idemat 2003
Impact strength	1.6	1.6	J/cm		Idemat 2003
Shear modulus	110	350	MPa		Idemat 2003
Tensile strength	25	36	MPa		Idemat 2003
Thickness			MPa		
Yield strength			MPa		
Young's modulus	410	750	MPa		Idemat 2003

Source: Matbase - the independent online material selection resource

http://www.matbase.com/materials/natural-and-synthetic-polymers/engineering-polymers/material_properties_of_ptfe.html (retrieved: 21.02.2013)

Surface Energy Data for PTFE: Polytetrafluoroethylene, CAS # 9002-84-0

Source ^(a)	Mst. Type ^(b)	Data ^(c)	Comments ^(d)
Fox, 1950 ⁽⁹⁾	Critical ST	$\gamma_c = 18.5 \text{ mJ/m}^2$; 20°C	Test liquids not known.
Ellison, 1954 ⁽⁸⁾	Critical ST	$\gamma_c = 18 \text{ mJ/m}^2$; 20°C	Various test liquids.
Fowkes, 1964 ⁽⁷³⁾	Critical ST	$\gamma_c = 19.5 \text{ mJ/m}^2$; no temp cited	Test liquids not known.
Hamilton, 1972 ⁽⁷⁴⁾	Critical ST	$\gamma_c = 18 \text{ mJ/m}^2$; no temp cited	Test liquids not known.
Wu, 1982 ⁽⁴⁶⁾	Critical ST	$\gamma_c = 19 \text{ mJ/m}^2$; 20°C	Test liquids not known.
Markgraf, 2005 ⁽⁶²⁾	Critical ST	$\gamma_c = 19\text{-}20 \text{ mJ/m}^2$; no temp cited	Test liquids not known.
Fox, 1950 ⁽⁹⁾	Contact angle	$\theta_w^Y = 108^\circ$; 20°C	Samples pressed against plate glass at 150°C, boiled in nitric-sulfuric acid, and triple rinsed in distilled water.
Owens, 1969 ⁽¹⁵⁵⁾	Contact angle	$\theta_w^Y = 108^\circ$; no temp cited	
Dann, 1970 ⁽⁹⁴⁾	Contact angle	$\theta_w^A = 112^\circ$; 25°C	Sessile drop method; surface cleaned with detergent and rinsed with distilled water.
Hu, 1970 ⁽²³³⁾	Contact angle	$\theta_w^A = 98^\circ$; no temp cited	
Kaelble, 1971 ⁽¹⁰⁴⁾	Contact angle	$\theta_w^Y = 117^\circ$; 22°C	Sessile drop method; surface cleaned with detergent and rinsed with distilled water.
Collins, 1973 ⁽⁶⁹⁾	Contact angle	$\theta_w^A = 109^\circ$; no temp cited	By sessile drops on tiltable stage.
El Shimi, 1974 ⁽¹⁵⁶⁾	Contact angle	$\theta_w^Y = 112^\circ$; no temp cited	
Tamai, 1977 ⁽¹⁵⁹⁾	Contact angle	$\theta_w^Y = 114^\circ$; no temp cited	
Moshonov, 1980 ⁽¹¹⁸⁾	Contact angle	$\theta_w^Y = 104^\circ$; no temp cited	Measured 60 secs. after application of water droplet; surface cleaned with isopropanol at 60°C and rinsed with methanol.
Penn, 1980 ⁽¹⁵⁷⁾	Contact angle	$\theta_w^Y = 112^\circ$; no temp cited	
Omenyi, 1981 ⁽¹⁷⁸⁾	Contact angle	$\theta_w^A = 104^\circ$; 20°C	
Wu, 1982 ⁽²⁷⁾	Contact angle	$\theta_w^A = 109^\circ$, $\theta_w^R = 106^\circ$ $d\theta_w = 3^\circ$; 20°C	
Busscher, 1983 ⁽¹⁵⁸⁾	Contact angle	$\theta_w^Y = 116^\circ$; no temp cited	
Strobel, 1985 ⁽⁶⁸⁾	Contact angle	$\theta_w^A = 121^\circ$; no temp cited	Commercial grade film, supplied by 3M Company.
Guiseppe, 1986 ⁽⁷⁷⁾	Contact angle	$\theta_w^Y = 112^\circ$; no temp cited	
Janczuk, 1989 ⁽¹⁰⁶⁾	Contact angle	$\theta_w^Y = 111^\circ$; 20°C	Polished, then triple boiled in HCl solution and rinsed with distilled water.
Sperati, 1989 ⁽²²²⁾	Contact angle	$\theta_w^A = 116^\circ$, $\theta_w^R = 92^\circ$ $d\theta_w = 24^\circ$; no temp cited	
Egitto, 1990 ⁽⁶⁵⁾	Contact angle	$\theta_w^Y = 116^\circ$; no temp cited	
Yasuda, 1994 ⁽¹⁶⁰⁾	Contact angle	$\theta_w^Y = 100^\circ$; no temp cited	
Owen, 1996 ⁽¹³⁶⁾	Contact angle	$\theta_w^A = 108^\circ$; no temp cited	
Brewis, 1998 ⁽¹⁵³⁾	Contact angle	$\theta_w^A = 106^\circ$, $\theta_w^R = 90^\circ$ $d\theta_w = 16^\circ$; no temp cited	
Cho, 2000 ⁽⁹⁹⁾	Contact angle	$\theta_w^Y = 100^\circ$; no temp cited	Measured by sessile drop method.
Grundke, 2000 ⁽²⁵⁶⁾	Contact angle	$\theta_w^Y = 104^\circ$; no temp cited	Measured by ADSA.
Starov, 2000 ⁽²⁸²⁾	Contact angle	$\theta_w^Y = 105^\circ$; no temp cited	PTFE film, cleaned with alcohol and water, soaked in 50°C

Owens, 1969 ⁽¹⁵⁵⁾	Contact angle	$\gamma_s = 19.1 \text{ mJ/m}^2$ ($\gamma_s^d = 18.6$, $\gamma_s^p = 0.5$); no temp cited	sulfochromic acid, rinsed with distilled water, and dried with pure nitrogen. Test liquids: water and diiodomethane, by geometric mean equation.
Dann, 1970 ⁽⁹⁴⁾	Contact angle	$\gamma_s^d = 21 \text{ mJ/m}^2$; 25°C	Various test liquids (extrapolated value).
Kaelble, 1971 ⁽¹⁰⁴⁾	Contact angle	$\gamma_s = 18.0 \text{ mJ/m}^2$ ($\gamma_s^d = 16.9$, $\gamma_s^p = 1.1$); 22°C	From contact angles with various test liquids.
Wu, 1971 ⁽²⁹⁾	Contact angle	$\gamma_s = 22.5 \text{ mJ/m}^2$ ($\gamma_s^d = 20.5$, $\gamma_s^p = 2.0$); 20°C	Test liquids: water and diiodomethane, by harmonic mean equation.
Kitazaki, 1972 ⁽¹⁹¹⁾	Contact angle	$\gamma_s = 21.5 \text{ mJ/m}^2$ ($\gamma_s^d = 19.4$, $\gamma_s^p = 2.1$); no temp cited	Various test liquids; original results split polar component into hydrogen- and non-hydrogen bonding parameters.
Wu, 1979 ⁽⁴⁵⁾	Contact angle	$\gamma_c = 22.6 \text{ mJ/m}^2$; 20°C	Test liquids not known; calculated by the equation of state method.
Busscher, 1981 ⁽⁷²⁾	Contact angle	$\gamma_s = 22.1 \text{ mJ/m}^2$ ($\gamma_s^d = 22.1$, $\gamma_s^p = 0.0$); no temp cited	Test liquids: water and propanol.
Omenyi, 1981 ⁽¹⁷⁸⁾	Contact angle	$\gamma_s = 20.0 \text{ mJ/m}^2$; 20°C	Test liquids not known.
Janczuk, 1989 ⁽¹⁰⁶⁾	Contact angle	$\gamma_s = 21.8 \text{ mJ/m}^2$ ($\gamma_s^d = 21.7$; $\gamma_s^p = 0.05$); no temp cited	Various test liquids, by geometric mean equation.
Janczuk, 1989 ⁽¹⁰⁸⁾	Contact angle	$\gamma_s = 25.0 \text{ mJ/m}^2$ ($\gamma_s^d = 25.0$; $\gamma_s^p = 0.0$); no temp cited	Various test liquids, by harmonic-geometric mean equation.
Janczuk, 1989 ⁽¹⁰⁸⁾	Contact angle	$\gamma_s = 25.8 \text{ mJ/m}^2$ ($\gamma_s^d = 25.8$; $\gamma_s^p = 0.0$); no temp cited	Various test liquids, by harmonic mean equation.
Janczuk, 1990 ⁽¹⁰⁵⁾	Contact angle	$\gamma_s = 20.6 \text{ mJ/m}^2$; no temp cited	Test liquids: water and diiodomethane.
Janczuk, 1990 ⁽¹⁰⁵⁾	Contact angle	$\gamma_s = 21.4 \text{ mJ/m}^2$; no temp cited	Averaged over 28 test liquids.
Spelt, 1992 ⁽⁸⁸⁾	Contact angle	$\gamma_c = 20.0 \text{ mJ/m}^2$; 23°C	Test liquids not known; calculated by the equation of state method.
Morra, 1999 ⁽¹³⁴⁾	Contact angle	$\gamma_s = 20.1 \text{ mJ/m}^2$ ($\gamma_s^{LW} = 20.1$, $\gamma_s^{AB} = 0.0$, $\gamma_s^+ = 0.0$, $\gamma_s^- = 0.0$); no temp cited	Test liquids not known; acid-base analysis based on reference values for water of $\gamma^+ = 48.5 \text{ mJ/m}^2$ and $\gamma^- = 11.2 \text{ mJ/m}^2$.
Chang, 2000 ⁽¹⁶²⁾	Contact angle	$\gamma_s = 17.0 \text{ mJ/m}^2$; no temp cited	
Grundke, 2000 ⁽²⁵⁶⁾	Contact angle	$\gamma_s = 20.1 \text{ mJ/m}^2$; no temp cited	
Della Volpe, 2000 ⁽¹⁶³⁾	Contact angle	$\gamma_s = 22.2 \text{ mJ/m}^2$; no temp cited	Re-calculated from data produced by Janczuk, 1990 ⁽¹⁰⁵⁾ .
Schoff, 2003 ⁽²⁶³⁾	Contact angle	$\gamma_s = 21.5 \text{ mJ/m}^2$ ($\gamma_s^{LW} = 19.6$, $\gamma_s^{AB} = 1.9$, $\gamma_s^+ = 0.3$, $\gamma_s^- = 3.2$); no temp cited	Test liquids not known; acid-base analysis.
Detre, 1967 ⁽⁴⁰⁾	From polymer melt	$\gamma_s = 21.5 \text{ mJ/m}^2$; 20°C	Direct measurement of polymer melt extrapolated to 20°C; molecular formula $C_{21}F_{44}$; $M_n = 1088$.
Detre, 1969 ⁽²⁴⁶⁾	From polymer melt	$\gamma_s = 19.3 \text{ mJ/m}^2$; 20°C	Direct measurement of polymer melt extrapolated to 20°C; $M_n = 1038$.
Wu, 1971 ⁽²⁹⁾	From polymer melt	$\gamma_s = 26.5 \text{ mJ/m}^2$; 20°C	Direct measurement of polymer melt extrapolated to 20°C.
Wu, 1974 ⁽⁴⁷⁾	From polymer melt	$\gamma_s = 25.7 \text{ mJ/m}^2$; 20°C	Direct measurement of polymer melt extrapolated to 20°C; Infinite molecular weight.
Wu, 1974 ⁽⁴⁷⁾	From polymer melt	$\gamma_s = 23.9 \text{ mJ/m}^2$ ($\gamma_s^d = 21.8$, $\gamma_s^p = 2.1$); 20°C	Direct measurement of polymer melt extrapolated to 20°C; polarity calculated from interfacial tension with PE by

Good, 1960 ⁽³¹⁾	Calculated	$\gamma_s = 27.8 \text{ mJ/m}^2$; 20°C	harmonic mean. Infinite molecular weight.
Good, 1960 ⁽³¹⁾	Calculated	$\gamma_s = 21.0 \text{ mJ/m}^2$; 20°C	Calculated from low-molecular weight liquid homologs.
Good, 1964 ⁽¹⁶⁾	Calculated	$\gamma_s = 24.0 \text{ mJ/m}^2$; 20°C	Estimated from molecular constants, using $u = 0$ debye.
Lee, 1968 ⁽¹³¹⁾	Calculated	$\gamma_s = 17 \text{ mJ/m}^2$; no temp cited	Estimated from molecular constants, using $u = 1.2$ debyes.
Wu, 1968 ⁽¹⁸²⁾	Calculated	$\gamma_s = 21 \text{ mJ/m}^2$; 20°C	Calculated from glass temperature of 223K.
Sewell, 1971 ⁽¹⁹³⁾	Calculated	$\gamma_s = 15.8 \text{ mJ/m}^2$; no temp cited	Calculated from molecular constitution.
Sewell, 1971 ⁽¹⁹³⁾	Calculated	$\gamma_s = 14.7 \text{ mJ/m}^2$; no temp cited	Calculated from parachor and cohesive energy.
Wu, 1974 ⁽⁴⁷⁾	Calculated	$\gamma_s = 25.8 \text{ mJ/m}^2$; 20°C	Calculated by least squares from cohesive energy and molar volume.
Wu, 1974 ⁽⁴⁷⁾	Calculated	$\gamma_s = 25.9 \text{ mJ/m}^2$; 20°C	Calculated from free volume theory and molecular weight.
Van Krevelen, 1976 ⁽⁸⁵⁾	Calculated	$\gamma_s = 26 \text{ mJ/m}^2$; no temp cited	Calculated from free volume theory and molecular weight.
Wu, 1979 ⁽⁴⁵⁾	Calculated	$\gamma_s = 23.9 \text{ mJ/m}^2$; 20°C	Calculated from parachor parameter.
Vargha-Butler, 1985 ⁽¹⁸⁰⁾	Calculated	$\gamma_s = 20.0 \text{ mJ/m}^2$; 23°C	Calculated from liquid homologs. Infinite molecular weight.
Owen, 1996 ⁽¹³⁶⁾	Calculated	$\gamma_s = 25.6 \text{ mJ/m}^2$; no temp cited	Calculated from sedimentation volume.
Grundke, 2000 ⁽²⁵⁶⁾	Calculated	$\theta_w^Y = 104^\circ$; no temp cited	Direct measurement of liquid surface tension extrapolated to infinite molecular weight.
Grundke, 2000 ⁽²⁵⁶⁾	Other	$\gamma_s = 20.4 \text{ mJ/m}^2$; no temp cited	Calculated from capillary penetration into packed polymer powder.
			Determined by capillary penetration into packed polymer powder.

A.2. PI

Material properties of PI

Chemical properties

	Minimum value	Maximum value	Unit	Remarks	Sources
Solidification shrinkage	1	1	%		Idemat 2003
Water absorption	0.24	0.3	%		Idemat 2003

Electrical properties

	Minimum value	Maximum value	Unit	Remarks	Sources
Breakdown potential	22	22	kV/mm		Idemat 2003
Dielectric loss factor			%		
Electrochemical potential			V		
Resistivity	1.00E+021	1.00E+021	Ohm.mm ² /m		Idemat 2003

Mechanical properties

	Minimum value	Maximum value	Unit	Remarks	Sources
Bending strength	100	130	MPa		Idemat 2003
Compressive strength	165	165	MPa		Idemat 2003
Creep strength			MPa		
Density	1400	1430	kg/m ³		Idemat 2003
Elongation	5	7	%		Idemat 2003
Fatigue failure	20	20	MPa		Idemat 2003
Friction coefficient	0.29	0.29			Idemat 2003
Impact strength	2.5	5	J/cm		Idemat 2003
Shear modulus			MPa		
Tensile strength	85	90	MPa		Idemat 2003
Thickness			MPa		
Yield strength	73	73	MPa		Idemat 2003
Young's modulus	3100	3100	MPa		Idemat 2003

Source: Matbase - the independent online material selection resource

http://www.matbase.com/materials/natural-and-synthetic-polymers/engineering-polymers/material_properties_of_pi.html (retrieved: 21.02.2013)

Polyimid-Schläuche

Allgemeines

Produkte auf der Basis von Polyimid bieten Eigenschaften, die weit über denjenigen von üblichen Thermoplasten liegen:

- Wärmebeständigkeit: Dauertemperatur 230°C, kurzzeitig bis 350°C.
- Strahlenvernetztes, thermostabilisiertes Polymer mit ausgezeichneten mechanischen Eigenschaften.
- Beständig gegen Strahlung, Lösemittel, Säuren, Öl und Tiefsttemperaturen (Kryogene).
- Abmessungen im Mikrobereich

Unsere Polyimid-Schläuche unterscheiden sich von vergleichbaren Produkten durch folgende Eigenschaften:

- Um 40% höhere Elastizität im Vergleich zu Wettbewerbsprodukten, was eine optimale Dehnung und plastische Verformbarkeit ergibt.
- Die einmalige Verbindung von Duktilität, Stärke und Steifheit ergeben grössere Zähigkeit und Beständigkeit als andere Polyimid-Schläuche. Dies zeigt sich besonders bei zyklischen Belastungen. Wiederholtes Biegen, Drücken und Ziehen beeinträchtigen nicht die strukturelle Integrität der Schläuche.
- Das verwendete Beschichtungsverfahren verhindert ein Ablösen von einzelnen Schichten, wie das bei minderwertigeren Schläuchen der Fall sein kann.

Für medizinische wie für elektrische Anwendungen geeignet.

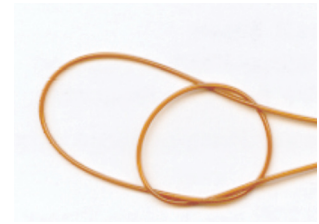
Abmessungen

Innendurchmesser von 0,0025 – 0,1440" bzw. 0,0635 – 3,658 mm

Wandstärken von 0,00025 – 0,008" bzw. 0,00635 – 0,203 mm

Materialeigenschaften von Standard Polyimid-Schläuchen

Durchschlagsfestigkeit:	6'000 Volt/mil (1 Mil = 0,0254 mm)
Bruchfestigkeit:	30'000 PSI (1 PSI = 6,89 kPa)
Bruchdehnung:	152 %
Betriebstemperatur:	230°C
Schmelztemperatur:	300°C
Zerstörung bei:	450°C
Reibungskoeffizient:	0,268
Gammastrahlenbeständigkeit:	gut (37 kGY während 8 Std.), kGY = Kilogray
Feuchtigkeitsaufnahme:	0,841 % (24 Std.)
Wärmeleitfähigkeit:	0,205 W/(K.m)
Farben:	bernsteinfarben (Standard), dunkelrot, grün, schwarz, crème



Mit Drahtgeflecht verstärkte Polyimid-Schläuche

Metallische Drähte oder nicht metallische Fasern sind im Schlauch als Geflecht zur Verstärkung eingebettet.

Erhöhte Knick- und Quetschbeständigkeit, Drehungsübertragung sowie Stossfestigkeit.

Innendurchmesser von 0.003" – 0,010" (0,076 – 0,254 mm)

Längen von 1- 7 feet (0,305 – 2,135 m)

Mit Drahtgeflecht verstärkte Polyimid-Schläuche

Metallische Drähte oder nicht metallische Fasern sind im Schlauch als Geflecht zur Verstärkung eingebettet.

Erhöhte Knick- und Quetschbeständigkeit, Drehungsübertragung sowie Stossfestigkeit.

Innendurchmesser von 0.003" – 0,010" (0,076 – 0,254 mm).

Längen von 1- 7 feet (0,305 – 2,135 m)

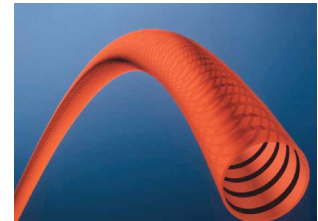
**Mit Spiraldraht verstärkte Polyimid-Schläuche**

Metallische Drähte oder nicht metallische Fasern sind spiralförmig zur Verstärkung im Schlauch eingebettet.

Erhöhte Knick- und Quetschbeständigkeit, Drehungsübertragung sowie Stossfestigkeit.

Innendurchmesser von 0.0113" – 0,072" (0,289 – 1,829 mm).

Längen von 1- 7 feet (0,305 – 2,135 m)

**Low Friction Polyimid-Schläuche**

Niedriger Reibungskoeffizient wie PTFE und Materialeigenschaften wie Polyimid.

Geeignet als Medizinalschlauch oder als Drahtüberzug.

Beständig gegen Gammastrahlen.

Polyimid-Schläuche mit eingebettetem Leiter

Die innovative Idee: Bei Polyimid-Schläuchen mit minimalsten Durchmessern dient ein in die Wand eingebetteter Leiter als elektrischer Zugang und als mechanische Verstärkung zugleich. Der vorzugsweise isolierte Leiter kann längs, spiralförmig oder als Geflecht eingebettet werden.

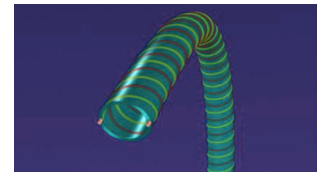
Leiterabmessungen von AWG 41 bis AWG 49.

Es können elektrische Leiter und metallische oder nicht metallische Verstärkungen mit einander kombiniert werden.

Mit diesen Schläuchen ist eine Verkleinerung der Abmessung von Apparaten möglich.

Anwendbar für Thermoleitungen und Sensoren.

Grosse Auswahl an Leitermaterialien.

**Polyimid-Schläuche mit Kontrastmitteleigenschaften**

Material auf Basis von Polyimid mit Kontrastmitteleigenschaften zwecks

Sichtbarkeit beim Röntgen und in der Fluoroskopie.

Kostengünstige Variante zu metallischen Schläuchen.

Wärmeleitfähige Polyimid-Schläuche

Polyimid-Schläuche aus speziell zusammengesetztem Material zur Verbesserung der Wärmeleitfähigkeit, ohne dabei die elektrischen Isoliereigenschaften zu reduzieren.

75 % höhere Wärmeleitfähigkeit als Standard Polyimid.

Durchschlagsfestigkeit über 3 kV pro Zoll.

Polyimid-Schläuche mit PTFE-Gleitschicht

Eigenschaften

Diese Polyimidschläuche können innen und/oder aussen mit einer Gleitschicht aus PTFE versehen. Diese reduziert die Reibung, sodass ein Einführen des Polyimidschlauches in ein Gerät oder eines Leiters in den Schlauch sehr erleichtert wird. Man verbindet damit die Vorteile von Polyimid mit den Eigenschaften von PTFE

- beständig gegen Gammastrahlen

Technische Daten	Polyimid	PTFE	Polyimidschlauch mit Gleitschicht
Feuchtigkeitsaufnahme	0,84%	0%	0,23%
Betriebstemperatur	230°C	260°C	230°C
Durchschlagsfestigkeit (trocken)	248 kV/mm	59 kV/mm	130 kV/mm
Zugfestigkeit	306 N/mm ²	27,6 N/mm ²	159 N/mm ²
Dehnung	80%	250%	65%
Elastizitätsmodul	1972 N/mm ²	407 N/mm ²	1600 N/mm ²
Reibungskoeffizient dynamisch	0,27	0,09	0,13
Reibungskoeffizient statisch	0,15	0,04	0,07
Klebkraft mit Cyanoacrylat-Kleber (Reisstest)	11,0 N/mm ²	1,0 N/mm ²	5,86 N/mm ²
biokompatibel	ja	ja	ja

Diese Angaben sind Richtwerte. Diese Werte müssen vom Anwender überprüft werden.

Polyimid-Mikro-Schläuche

Anwendung

Produkt	Beschreibung	allgemein	Medizinische Anwendung
Standard Polyimid Schlauch	ausschliesslich aus Polyimid aufgebauter, dünnwandiger Mikroschlauch	Isolierschlauch, invasiver Katheterschlauch	Angioplastie, Stent-Platzierung, Herzkatheter
Polymer- Polyimid Verbund-Schlauch	aus Polyimid -Polymer- Verbund aufgebauter, dünnwandiger Mikroschlauch	Invasiver Katheterschlauch	Angioplastie, Stent-Platzierung, Herzkatheter
Draht verstärkter Polyimid Schlauch	aus verschiedenen Drähten und Polymid aufgebauter Mikroschlauch	Invasiver Katheterschlauch	Angioplastie, Stent-Platzierung, Herzkatheter

Abmessungen

Innendurchmesser [mm]	AWG Grösse	French Size	Wanddicke [mm]	Toleranz Innendurchmesser [mm]	Toleranz Innendurchmesser [mm]	Drahtverstärkung
0,0711 - 0,0787	41-40	1F	0,013	+/- 0,005	+/- 0,0063	nein
0,089 - 0,127	39-36	1F	0,013-0,003	+/- 0,005	+/- 0,0063	nein
0,142 - 0,180	35-33	1F	0,013-0,04	+/- 0,005	+/- 0,0063	nein
0,203 - 0,254	32-30	1F	0,013-0,08	+/- .00025	+/- 0,0063	ja
0,287 - 0,511	29-24	1-3F	0,013-0,013	+/- 0,007	+/- 50% der Wand	ja
0,574 - 0,813	23-20	2-4F	0,013-0,018	+/- 0,007	+/- 50% der Wand	ja
0,912 - 1,45	19-15	3-5F	0,03-0,018	+/- 0,013	+/- 50% der Wand	ja
1,63 - 1,83	14-13	5-6F	0,04-0,018	+/- 0,018	+/- 50% der Wand	ja
2,05 - 2,31	12-11	7F	0,08-0,018	+/- 0,018	+/- 50% der Wand	ja

Surface Energy Data for Polyimide, CAS # 25038-81-7

Source ^(a)	Mst. Type ^(b)	Data ^(c)	Comments ^(d)
Kogoma, 1987 ⁽⁶⁶⁾ Egitto, 1990 ⁽⁶⁵⁾ Thomas, 1991 ⁽²⁴²⁾	Contact angle Contact angle Contact angle	$\theta_W^Y = 73^\circ$; no temp cited $\theta_W^Y = 70^\circ$; no temp cited $\theta_W^A = 70^\circ$, $\theta_W^R = 47^\circ$, $d\theta_W = 23^\circ$; no temp cited	Kapton film. PMDA-ODA polyimide.
Matienzo, 1992 ⁽²⁴³⁾ Matienzo, 1992 ⁽²⁴³⁾ Matienzo, 1992 ⁽²⁴³⁾ Inagaki, 1994 ⁽¹¹⁵⁾ Lee, 1996 ⁽²⁴⁴⁾	Contact angle Contact angle Contact angle Contact angle Contact angle	$\theta_W^Y = 70^\circ$; no temp cited $\theta_W^Y = 70^\circ$; no temp cited $\theta_W^Y = 71^\circ$; no temp cited $\theta_W^A = 74.7^\circ$; 20°C $\theta_W^A = 85^\circ$, $\theta_W^R = 38^\circ$, $d\theta_W = 47^\circ$; no temp cited	Kapton-H (PMDA-ODA) film. Upilex-S (BPDA-PDA) film. Upilex-R (BPDA-ODA) film. Kapton H film. PMDA-ODA polyimide.
Lee, 1996 ⁽²⁴⁴⁾	Contact angle	$\theta_W^A = 79^\circ$, $\theta_W^R = 41^\circ$, $d\theta_W = 38^\circ$; no temp cited	BPDA-PDA polyimide.
Lee, 1996 ⁽²⁴⁴⁾	Contact angle	$\theta_W^A = 87^\circ$, $\theta_W^R = 67^\circ$, $d\theta_W = 20^\circ$; no temp cited	6FDA-ODA (fluorinated) polyimide.
Gotoh, 2000 ⁽¹⁰⁰⁾	Contact angle	$\theta_W^A = 76.9^\circ$, $\theta_W^R = 39.5^\circ$, $d\theta_W = 37.4^\circ$; no temp cited	Measured by sessile drop method; Kapton 100H.
Gotoh, 2004 ⁽⁹²⁾	Contact angle	$\theta_W^A = 76.4^\circ$; $\theta_W^R = 38.2^\circ$, $d\theta_W = 38.2^\circ$; no temp cited	Measured by Wilhelmy plate method; Kapton 100H.
Cho, 2005 ⁽²²⁶⁾ Wu, 1989 ⁽²⁷³⁾ Inagaki, 1994 ⁽¹¹⁵⁾	Contact angle Contact angle Contact angle	$\theta_W^Y = 75^\circ$; no temp cited $\gamma_s = 41.0 \text{ mJ/m}^2$ ($\gamma_s^d = 26.3$, $\gamma_s^p = 14.7$); $\gamma_s = 37 \text{ mJ/m}^2$; 20°C	Measured by sessile drop method. Test liquids not known. Kapton H film. Test liquids: water, diiodomethane, glycerol, formamide, and tricresyl phosphate. Kapton H film.
Gotoh, 2004 ⁽⁹²⁾	Contact angle	$\gamma_s = 44.0 \text{ mJ/m}^2$ ($\gamma_s^{LW} = 42.5$, $\gamma_s^{AB} = 1.5$, $\gamma_s^+ = 0.1$, $\gamma_s^- = 6.0$); no temp cited	Test liquids: water, diiodomethane, and ethylene glycol, by sessile drop method; acid-base analysis. Kapton 100H.
Cho, 2005 ⁽²²⁶⁾	Contact angle	$\gamma_s = 53 \text{ mJ/m}^2$ ($\gamma_s^d = 50$, $\gamma_s^p = 3$); no temp cited	Test liquids: water and formamide.
Vetelino, 1997 ⁽⁸¹⁾ Vetelino, 1997 ⁽⁸¹⁾	Calculated Calculated	$\theta_W^A = 85^\circ$, $\theta_W^R = 67^\circ$, $d\theta_W = 18^\circ$; no temp cited $\theta_W^A = 75^\circ$, $\theta_W^R = 46^\circ$, $d\theta_W = 29^\circ$; no temp cited	OCG 285 polyimide; calculated from surface acoustic waves. DuPont 5878 polyimide; calculated from surface acoustic waves.

A.3. PEEK

Material properties of PEEK

Chemical properties

	Minimum value	Maximum value	Unit	Remarks	Sources
Solidification shrinkage			%		
Water absorption	0.5	0.5	%		Idemat 2003

Electrical properties

	Minimum value	Maximum value	Unit	Remarks	Sources
Breakdown potential	190000	190000	kV/mm		Idemat 2003
Dielectric loss factor			%		
Electrochemical potential			V		
Resistivity			Ohm.mm ² /m		

Mechanical properties

	Minimum value	Maximum value	Unit	Remarks	Sources
Bending strength			MPa		
Compressive strength			MPa		
Creep strength			MPa		
Density	1320	1320	kg/m ³		Idemat 2003
Elongation	50	50	%		Idemat 2003
Fatigue failure			MPa		
Friction coefficient					
Impact strength			J/cm		
Shear modulus			MPa		
Tensile strength	92	92	MPa		Idemat 2003
Thickness			MPa		
Yield strength			MPa		
Young's modulus	3850	3850	MPa		Idemat 2003

Source: Matbase - the independent online material selection resource

http://www.matbase.com/materials/natural-and-synthetic-polymers/engineering-polymers/material_properties_of_peek.html (retrieved: 21.02.2013)

Surface Energy Data for PEEK: Poly(ether ether ketone), CAS # 29658-26-2

Source ^(a)	Mst. Type ^(b)	Data ^(c)	Comments ^(d)
Matienzo, 1992 ⁽²⁴³⁾	Contact angle	$\theta_w^Y = 91^\circ$; no temp cited	Stabar film.
Bee, 1993 ⁽²¹⁴⁾	Contact angle	$\theta_w^A = 85^\circ$, $\theta_w^R = 55^\circ$, $d\theta_w = 30^\circ$; no temp cited	
Marchand-Brynaert, 2000 ⁽⁹⁷⁾	Contact angle	$\theta_w^Y = 88^\circ$; no temp cited	No details available.
Surface-tension.de, 2007 ⁽¹¹⁰⁾	Unknown	$\gamma_s = 42.1 \text{ mJ/m}^2$ ($\gamma_s^d = 36.2$, $\gamma_s^p = 5.9$); 20°C	

©2009 Diversified Enterprises

A.4. PMMA

Material properties of PMMA

Chemical properties

	Minimum value	Maximum value	Unit	Remarks	Sources
Solidification shrinkage	0.3	0.8	%		Idemat 2003
Water absorption	0.3	0.4	%		Idemat 2003

Electrical properties

	Minimum value	Maximum value	Unit	Remarks	Sources
Breakdown potential	16	30	kV/mm		Idemat 2003
Dielectric loss factor	0.04	0.06	%		Idemat 2003
Electrochemical potential			V		
Resistivity	1.00E+019		Ohm.mm ² /m		

Mechanical properties

	Minimum value	Maximum value	Unit	Remarks	Sources
Bending strength	120	148	MPa		Idemat 2003
Compressive strength	83	124	MPa		Idemat 2003
Creep strength			MPa		
Density	1170	1200	kg/m ³		Idemat 2003
Elongation	2	10	%		Idemat 2003
Fatigue failure	11	12	MPa		Idemat 2003
Friction coefficient	0.54	0.54			Idemat 2003
Impact strength	0.16	0.27	J/cm		Idemat 2003
Shear modulus	1700	1700	MPa		Idemat 2003
Tensile strength	48	76	MPa		Idemat 2003
Thickness			MPa		
Yield strength			MPa		
Young's modulus	1800	3100	MPa		Idemat 2003

Source: Matbase - the independent online material selection resource

http://www.matbase.com/materials/natural-and-synthetic-polymers/engineering-polymers/material_properties_of_pmma.html (retrieved: 21.02.2013)

Surface Energy Data for PMMA: Poly(methylmethacrylate), CAS # 9011-14-7

Source ^(a)	Mst. Type ^(b)	Data ^(c)	Comments ^(d)
Jarvis, 1964 ⁽¹⁵⁾	Critical ST	$\gamma_c = 39 \text{ mJ/m}^2$; 25°C	Various test liquids.
Lee, 1968 ⁽¹³¹⁾	Critical ST	$\gamma_c = 38 \text{ mJ/m}^2$; no temp cited	Test liquids: water, glycerol, formamide, alcohols, and long-chain polyglycols.
Dann, 1970 ⁽⁹⁴⁾	Critical ST	$\gamma_c = 30.5 \text{ mJ/m}^2$; 25°C	Ethylene glycol/2-ethoxyethanol mixes, based on advancing contact angles.
Dann, 1970 ⁽⁹⁴⁾	Critical ST	$\gamma_c = 39 \text{ mJ/m}^2$; 25°C	Ethylene glycol/2-ethoxyethanol mixes, based on retreating contact angles.
Dann, 1970 ⁽⁹⁴⁾	Critical ST	$\gamma_c = 31.5 \text{ mJ/m}^2$; 25°C	Polyglycol blends, based on advancing contact angles.
Dann, 1970 ⁽⁹⁴⁾	Critical ST	$\gamma_c = 37 \text{ mJ/m}^2$; 25°C	Polyglycol blends, based on retreating contact angles.
Dann, 1970 ⁽⁹⁴⁾	Critical ST	$\gamma_c = 30 \text{ mJ/m}^2$; 25°C	Formamide/2-ethoxyethanol mixes, based on advancing contact angles.
Dann, 1970 ⁽⁹⁴⁾	Critical ST	$\gamma_c = 41 \text{ mJ/m}^2$; 25°C	Formamide/2-ethoxyethanol mixes, based on retreating contact angles.
Dann, 1970 ⁽⁹⁴⁾	Critical ST	$\gamma_c = 45 \text{ mJ/m}^2$; 25°C	Per ASTM D-2578, using formamide/2-ethoxyethanol mixes.
Jarvis, 1964 ⁽¹⁵⁾	Contact angle	$\theta_W^A = 94^\circ$; 25°C, 15-30% RH	Polymer surface prepared by solvent evaporation.
Jarvis, 1964 ⁽¹⁵⁾	Contact angle	$\theta_W^A = 80^\circ$; 25°C, 15-30% RH	Smooth surface prepared by pressing polymer powder against stainless steel at 150°C.
Dann, 1970 ⁽⁹⁴⁾	Contact angle	$\theta_W^A = 74^\circ$; 25°C	Sessile drop method; surface cleaned with detergent and rinsed with distilled water.
Wu, 1971 ⁽²⁹⁾	Contact angle	$\theta_W^Y = 80^\circ$; 20°C	
Panzer, 1973 ⁽²⁵⁰⁾	Contact angle	$\theta_W^A = 71^\circ$; no temp cited	
Omenyi, 1980 ⁽²⁶⁶⁾	Contact angle	$\theta_W^Y = 73^\circ$; no temp cited	
Winters, 1985 ⁽¹⁸⁴⁾	Contact angle	$\theta_W^Y = 73^\circ$; no temp cited	
Janczuk, 1989 ⁽¹⁰⁶⁾	Contact angle	$\theta_W^Y = 73.8^\circ$; 20°C	Unspecified cleaning method (per Good); ultrasonically rinsed with distilled water.
van Oss, 1990 ⁽²⁾	Contact angle	$\theta_W^Y = 60^\circ$; 20°C	
van Oss, 1990 ⁽²⁾	Contact angle	$\theta_W^Y = 72^\circ$; 20°C	
Jonsson, 1992 ⁽¹¹²⁾	Contact angle	$\theta_W^Y = 62^\circ$; no temp cited	Cleaned by sonification in a 70/30 ethanol/water solution and rinsed with distilled water.
Van Oss, 1992 ⁽²³⁶⁾	Contact angle	$\theta_W^A = 59.3^\circ$; no temp cited	
McNally, 1993 ⁽⁵⁾	Contact angle	$\theta_W^A = 75^\circ$, $\theta_W^R = 58^\circ$, $d\theta_W = 17^\circ$; 25°C	
Fukuzawa, 1994 ⁽¹¹³⁾	Contact angle	$\theta_W^Y = 71.3^\circ$; no temp cited	Contact angle measured after stabilizing for 15 secs.
Etzler, 2000 ⁽²⁵⁰⁾	Contact angle	$\theta_W^A = 77.9^\circ$; 20°C	Measured by Wilhelmy plate method.
McCafferty, 2000 ⁽²¹⁷⁾	Contact angle	$\theta_W^Y = 64.3^\circ$; no temp cited	Surface cleaned with light methanol wipe.
Della Volpe, 2002 ⁽¹⁴¹⁾	Contact angle	$\theta_W^A = 70.1^\circ$, $\theta_W^R = 50.3^\circ$, $d\theta_W = 19.8^\circ$; no temp cited	
Cho, 2005 ⁽²²⁶⁾	Contact angle	$\theta_W^Y = 61^\circ$; no temp cited	Measured by sessile drop method.

Della Volpe, 2006 ⁽¹³⁷⁾	Contact angle	$\theta_W^Y = 69.9^\circ$; no temp cited	Wilhelmy plate method; surface cleaned in trichloroethylene; droplet size 3 μ l.
Della Volpe, 2006 ⁽¹³⁷⁾	Contact angle	$\theta_W^Y = 66.8^\circ$; no temp cited	Wilhelmy plate method; surface cleaned in trichloroethylene; droplet size 5 μ l.
Della Volpe, 2006 ⁽¹³⁷⁾	Contact angle	$\theta_W^Y = 64.4^\circ$; no temp cited	Vibrationally induced equilibrium method; surface cleaned in trichloroethylene; droplet size 3 μ l.
Della Volpe, 2006 ⁽¹³⁷⁾	Contact angle	$\theta_W^Y = 62.3^\circ$; no temp cited	Vibrationally induced equilibrium method; surface cleaned in trichloroethylene; droplet size 5 μ l.
Johansson, 2006 ⁽¹¹³⁾	Contact angle	$\theta_W^A = 67^\circ$; no temp cited	Ultrasonically cleaned in isopropanol and rinsed with ethanol.
Dann, 1970 ⁽⁹⁴⁾	Contact angle	$\gamma_s^d = 41$ mJ/m ² ; 25°C	Various test liquids.
Wu, 1971 ⁽²⁹⁾	Contact angle	$\gamma_s = 40.2$ mJ/m ² ($\gamma_s^d = 35.8$; $\gamma_s^p = 4.4$); 20°C	Test liquids: water and diiodomethane, by geometric mean equation.
Wu, 1971 ⁽²⁹⁾	Contact angle	$\gamma_s = 41.2$ mJ/m ² ($\gamma_s^d = 30.9$; $\gamma_s^p = 10.3$); 20°C	Test liquids: water and diiodomethane, by harmonic mean equation.
Kitazaki, 1972 ⁽¹⁹¹⁾	Contact angle	$\gamma_s = 43.2$ mJ/m ² ($\gamma_s^d = 42.4$, $\gamma_s^p = 0.8$); no temp cited	Various test liquids; original results split polar component into hydrogen- and non-hydrogen bonding parameters.
Wu, 1979 ⁽⁴⁵⁾	Contact angle	$\gamma_c = 42.5$ mJ/m ² ; 20°C	Test liquids not known; calculated by the equation of state method.
Busscher, 1981 ⁽⁷²⁾	Contact angle	$\gamma_s = 44.3$ mJ/m ² ($\gamma_s^d = 33.7$, $\gamma_s^p = 10.6$); no temp cited	Test liquids: water and propanol.
Chaudhury, 1984 ⁽²¹⁾	Contact angle	$\gamma_s = 40.6$ mJ/m ² ($\gamma_s^{LW} = 40.6$, $\gamma_s^{AB} = 0.0$, $\gamma_s^+ = 0.0$, $\gamma_s^- = 12.0$); 20°C	Test liquids: water, alpha-bromonaphthalene, diiodomethane, formamide, and glycerin; acid-base analysis.
van Oss, 1987 ⁽²⁴⁾	Contact angle	$\gamma_s = 40.0$ mJ/m ² ($\gamma_s^{LW} = 40.0$, $\gamma_s^{AB} = 0.0$, $\gamma_s^+ = 0.0$, $\gamma_s^- = 14.6$); 20°C	Test liquids: water, alpha-bromonaphthalene, diiodomethane, formamide, and glycerin; acid-base analysis.
Janczuk, 1988 ⁽¹⁰⁷⁾	Contact angle	$\gamma_s = 44.9$ mJ/m ² ($\gamma_s^d = 39.0$; $\gamma_s^p = 6.0$); no temp cited	Various test liquids, by geometric mean equation.
Janczuk, 1989 ⁽¹⁰⁸⁾	Contact angle	$\gamma_s = 45.0$ mJ/m ² ($\gamma_s^d = 38.3$; $\gamma_s^p = 6.8$); no temp cited	Various test liquids, by harmonic-geometric mean equation.
Janczuk, 1989 ⁽¹⁰⁸⁾	Contact angle	$\gamma_s = 46.7$ mJ/m ² ($\gamma_s^d = 34.6$; $\gamma_s^p = 12.1$); no temp cited	Various test liquids, by harmonic mean equation.
van Oss, 1990 ⁽²⁾	Contact angle	$\gamma_s = 43.2$ mJ/m ² ($\gamma_s^{LW} = 43.2$, $\gamma_s^{AB} = 0.0$, $\gamma_s^+ = 0.0$, $\gamma_s^- = 22.4$); 20°C	Test liquids water, alpha-bromonaphthalene, diiodomethane, formamide, and glycerin; acid-base analysis.
van Oss, 1990 ⁽²⁾	Contact angle	$\gamma_s = 41.4$ mJ/m ² ($\gamma_s^{LW} = 41.4$, $\gamma_s^{AB} = 0.0$, $\gamma_s^+ = 0.0$, $\gamma_s^- = 12.2$); 20°C	Test liquids: water, alpha-bromonaphthalene, diiodomethane, formamide, and glycerin; acid-base analysis.
Janczuk, 1990 ⁽¹⁰⁵⁾	Contact angle	$\gamma_s = 43.2$ mJ/m ² ; no temp cited	Test liquids: water and diiodomethane.
Janczuk, 1990 ⁽¹⁰⁵⁾	Contact angle	$\gamma_s = 41.5$ mJ/m ² ; no temp cited	Averaged over 28 test liquids.
Berger, 1991 ⁽¹⁴⁵⁾	Contact angle	$\gamma_s = 43.9$ mJ/m ² ($\gamma_s^d = 37.2$; $\gamma_s^p = 6.7$); no temp cited	Various test liquids, by geometric mean equation; surface cleaned with acetone.
Berger, 1991 ⁽¹⁴⁵⁾	Contact angle	$\gamma_s = 41.7$ mJ/m ² ($\gamma_s^d = 37.6$; $\gamma_s^p = 4.1$); no temp cited	Various test liquids, by geometric mean equation; surface cleaned with dichloromethane.
Berger, 1991 ⁽¹⁴⁵⁾	Contact angle	$\gamma_s = 42.9$ mJ/m ² ($\gamma_s^d = 38.6$; $\gamma_s^p = 4.3$);	Various test liquids, by geometric mean equation; surface

Ruckenstein, 1993 ⁽⁶⁾	Contact angle	no temp cited $\gamma_s = 51.2 \text{ mJ/m}^2$ ($\gamma_s^d = 39.4$; $\gamma_s^p = 11.8$); no temp cited	cleaned with detergent. Octane droplets and air bubbles submersed in water; geometric mean equation
Fukuzawa, 1994 ⁽¹¹³⁾	Contact angle	$\gamma_s = 41.1 \text{ mJ/m}^2$ ($\gamma_s^{LW} = 40.2$, $\gamma_s^{AB} = 0.9$, $\gamma_s^+ = 0.02$, $\gamma_s^- = 12.2$); no temp cited	Test liquids: water, formamide, and diiodomethane; acid-base analysis, calculated per Good and van Oss ⁽⁸⁶⁾ . Contact angles measured after stabilizing for 15 secs.
Fukuzawa, 1994 ⁽¹¹³⁾	Contact angle	$\gamma_s = 48.8 \text{ mJ/m}^2$; no temp cited	Test liquids: water, formamide, and diiodomethane; acid-base analysis calculated by arithmetic and geometric means.
Hwang, 1995 ⁽²⁵⁷⁾	Contact angle	$\gamma_s = 38.5 \text{ mJ/m}^2$; no temp cited	Test liquids not known.
Lloyd, 1995 ⁽²¹⁸⁾	Contact angle	$\gamma_s^{LW} = 35.0$, $\gamma_s^+ = 0.0$, $\gamma_s^- = 12.2$; no temp cited	Test liquids not known; acid-base analysis.
Lee, 1999 ⁽¹¹⁶⁾	Contact angle	$\gamma_s = 43.2 \text{ mJ/m}^2$ ($\gamma_s^{LW} = 43.2$, $\gamma_s^{AB} = 0.0$, $\gamma_s^+ = 0.0$, $\gamma_s^- = 8.8$); 20°C	Test liquids: water, alpha-bromonaphthalene, diiodomethane, formamide, and glycerin; acid-base analysis, based on reference values for water of $\gamma^+ = 34.2 \text{ mJ/m}^2$ and $\gamma = 19 \text{ mJ/m}^2$.
Morra, 1999 ⁽¹³⁴⁾	Contact angle	$\gamma_s = 37.7 \text{ mJ/m}^2$ ($\gamma_s^{LW} = 37.4$, $\gamma_s^{AB} = 0.3$, $\gamma_s^+ = 0.01$, $\gamma_s^- = 2.2$); no temp cited	Test liquids not known; acid-base analysis based on reference values for water of $\gamma^+ = 48.5 \text{ mJ/m}^2$ and $\gamma = 11.2 \text{ mJ/m}^2$.
Etzler, 2000 ⁽⁴⁷¹⁾	Contact angle	$\gamma_s = 40.5 \text{ mJ/m}^2$ ($\gamma_s^{LW} = 40.5$, $\gamma_s^{AB} = 0.0$, $\gamma_s^+ = 0.0$, $\gamma_s^- = 6.8$); 20°C	Various test liquids; acid-base analysis, by Good-van Oss method. Commercial sample, unknown plasticizer content.
Kwok, 2000 ⁽¹⁶⁶⁾	Contact angle	$\gamma_c = 38.3 \text{ mJ/m}^2$; no temp cited	Re-calculated by equation of state method from data produced by Kwok, 1998 ⁽¹⁷⁰⁾ .
Kwok, 2000 ⁽¹⁶⁶⁾	Contact angle	$\gamma_c = 38.2 \text{ mJ/m}^2$; no temp cited	Re-calculated by alternate equation of state method from data produced by Kwok, 1998 ⁽¹⁷⁰⁾ .
McCafferty, 2000 ⁽²¹⁷⁾	Contact angle	$\gamma_s = 48.9 \text{ mJ/m}^2$ ($\gamma_s^{LW} = 46.5$, $\gamma_s^{AB} = 2.4$, $\gamma_s^+ = 0.08$, $\gamma_s^- = 18.1$); no temp cited	Test liquids: water, diiodomethane, formamide, glycerin, and ethylene glycol; acid-base analysis. Cleaned with methanol wipe.
Della Volpe, 2002 ⁽¹⁴¹⁾	Contact angle	$\gamma_s = 42.3 \text{ mJ/m}^2$ ($\gamma_s^{LW} = 41.6$, $\gamma_s^{AB} = 0.7$, $\gamma_s^+ = 0.0$, $\gamma_s^- = 5.3$); no temp cited	Various test liquids; acid-base analysis based on reference values for water of $\gamma^+ = 48.5 \text{ mJ/m}^2$ and $\gamma = 11.2 \text{ mJ/m}^2$; from advancing contact angles.
Della Volpe, 2002 ⁽¹⁴¹⁾	Contact angle	$\gamma_s = 45.2 \text{ mJ/m}^2$ ($\gamma_s^{LW} = 43.1$, $\gamma_s^{AB} = 2.1$, $\gamma_s^+ = 0.1$, $\gamma_s^- = 7.6$); no temp cited	Various test liquids; acid-base analysis based on reference values for water of $\gamma^+ = 48.5 \text{ mJ/m}^2$ and $\gamma = 11.2 \text{ mJ/m}^2$; from equilibrium (average of advancing and receding) contact angles.
^(c) Cho, 2005 ⁽²²⁶⁾	Contact angle	$\gamma_s = 42 \text{ mJ/m}^2$ ($\gamma_s^d = 20$, $\gamma_s^p = 22$); no temp cited	Test liquids: water and formamide.
Wu, 1970 ⁽³⁵⁾	From polymer melt	$\gamma_s = 41.1 \text{ mJ/m}^2$ ($\gamma_s^d = 29.6$; $\gamma_s^p = 11.5$); 20°C	Measurement by pendant drop of polymer melt extrapolated to 20°C; polarity calculated from interfacial tension with PE by harmonic mean. $M_v = 3000$.
Wu, 1971 ⁽²⁹⁾	From polymer melt	$\gamma_s = 41.1 \text{ mJ/m}^2$ ($\gamma_s^d = 29.0$, $\gamma_s^p = 12.1$); 20°C	Measurement by pendant drop of polymer melt extrapolated to 20°C; polarity calculated from interfacial tension with PE by geometric mean equation.
Wu, 1979 ⁽⁴⁵⁾	From polymer melt	$\gamma_s = 41.4 \text{ mJ/m}^2$; 20°C	Direct measurement of polymer melt extrapolated to 20°C.
Wu, 1968 ⁽¹⁸²⁾	Calculated	$\gamma_s = 36 \text{ mJ/m}^2$; 20°C	Calculated from molecular constitution.
Wu, 1970 ⁽³⁵⁾	Calculated	$\gamma_s = 41.1 \text{ mJ/m}^2$; 20°C	Calculated from parachor and molecular weight.

Sewell, 1971 ⁽¹⁹³⁾	Calculated	$\gamma_s = 35.1 \text{ mJ/m}^2$; no temp cited	Calculated by least squares from cohesive energy and molar volume.
Van Krevelen, 1976 ⁽⁸⁵⁾	Calculated	$\gamma_s = 42 \text{ mJ/m}^2$; no temp cited	Calculated from parachor parameter.
Omenyi, 1980 ⁽²⁶⁶⁾	Calculated	$\theta_w^y = 74.6^\circ$; 20°C	Calculated from critical velocities of PMMA powder in salol, naphthalene, and biphenyl.
Omenyi, 1980 ⁽²⁶⁶⁾	Calculated	$\gamma_s = 38.6 \text{ mJ/m}^2$; 20°C	Calculated from critical velocities of PMMA powder in salol, naphthalene, and biphenyl.
Wu, 1982 ⁽⁵⁰⁾	Calculated	$\theta_w = 68^\circ$; 20°C	Calculated from the theory of fractional polarity by geometric mean equation.
Wu, 1982 ⁽⁵⁰⁾	Calculated	$\theta_w = 78^\circ$; 20°C	Calculated from the theory of fractional polarity by harmonic mean equation.
Wu, 1982 ⁽¹⁸⁾	Calculated	$\gamma_s = 36.9 \text{ mJ/m}^2$; 20°C	Calculated from cohesive energy density and solubility parameters.
Pritykin, 1986 ⁽¹⁹⁹⁾	Calculated	$\gamma_s = 35.5 \text{ mJ/m}^2$; no temp cited	Calculated from cohesion parameters and monomer refractometric characteristics, equation 1.
Pritykin, 1986 ⁽¹⁹⁹⁾	Calculated	$\gamma_s = 36.6 \text{ mJ/m}^2$; no temp cited	Calculated from cohesion parameters and monomer refractometric characteristics, equation 2.
Van Ness, 1992 ⁽¹⁸⁶⁾	Calculated	$\gamma_s = 37.7 \text{ mJ/m}^2$; 20°C	Calculated molten surface tension value, extrapolated to 20°C .
^(d) Mangipudi, 1996 ⁽²⁶⁹⁾	Other	$\gamma_s = 53 \text{ mJ/m}^2$; no temp cited	Measured by contact deformation per Johnson-Kendall-Roberts method.

A.5. FEP

DuPont FEP

FLUOROCARBON FILM

Properties Bulletin

Description

DuPont FEP film is a transparent, thermoplastic film that can be heat sealed, thermoformed, vacuum formed, heat bonded, welded, metalized, laminated—combined with dozens of other materials, and can also be used as an excellent hot-melt adhesive.

This wide variety of fabrication possibilities combines with the following important properties to offer a unique balance of capabilities not available in any other plastic film.

Chemical Compatibility

- DuPont FEP film is chemically inert and resistant to virtually all chemicals, except molten alkali metals, gaseous fluorine, and certain complex halogenated compounds such as chlorine trifluoride at elevated temperatures and pressures.
- Low permeability to liquids, gases, moisture, and organic vapors

Electrical Reliability

- Superior reliability and retention of properties over large areas of film
- High dielectric strength, over 6500 V/mil for 1 mil film (260 kV/mm for 0.025 mm film)
- No electrical tracking, non-wetting, and non-charring
- Very low power factor and dielectric constant, only slight change over wide ranges of temperature and frequency

Wide Thermal Range

- Continuous service temperature -240 to 205°C (-400 to 400°F)
- Melting range 250 to 280°C (500 to 540°F)
- Heat sealable

Mechanical Toughness

- Superior anti-stick and low frictional properties
- High resistance to impact and tearing
- Useful physical properties at cryogenic temperatures

Long Time Weatherability*

- Inert to outdoor exposure; no measurable change after 20 years in Florida
- High transmittance of ultraviolet and all but far infrared radiation

Reliability

- DuPont FEP film contains no plasticizers or other foreign materials
- Conventional equipment and techniques can be used for processing: basic composition and properties will not be influenced
- Rigid quality control by DuPont ensures uniform gauge, void-free film

The convenience of FEP fluoropolymer in easy-to-use film facilitates the design and fabrication of this low-friction thermoplastic for all sorts of high-performance jobs. It is transparent and can be heat sealed, thermoformed, welded, and heat bonded.

Superior anti-stick properties make it an ideal release film for many applications. A cementable type with an invisible surface treatment is available for bonding to one or both sides with adhesives. This versatility is augmented by the superior properties of a true melt-processible fluorocarbon and by the wide choice of product dimensions available from DuPont.

*Type C film is not recommended for outdoor use



The miracles of science™

Table 1 – Types and Gauges of DuPont FEP Fluorocarbon Film

Gauge	50	100	175	200	300	500	750	1000	2000
Thickness, mil	0.5	1	1.75	2	3	5	7.5	10	20
Thickness, μm	12.5	25	44	50	75	125	190	250	500
Approx. area factor, ft^2/lb	180	90	51	45	30	18	12	9	4.5
Approx. area factor, m^2/kg	36	18	10.3	9	6.4	2.5	2	1.2	0.6
Availability									
Type A - FEP, general-purpose	X	X	X	X	X	X	X	X	X
Type C - FEP, one side cementable	—	X	X	X	X	X	—	—	—
Type C-20 - FEP, both sides cementable	—	X	—	X	—	X	—	—	—

Note: Each roll of DuPont film is clearly identified as to resin type, film thickness, and film type.

FEP	500	C
Resin type	Film thickness, 500 gauge, 5 mil	Film type, cementable one side

Property Values of DuPont FEP Fluorocarbon Film

Property	Test Method	Typical Value ^a	
		SI Units	English Units
Mechanical			
Tensile Strength at Break	ASTM D-882	21 N/mm ²	3000 psi
Elongation at Break	ASTM D-882	300%	
Yield Point	ASTM D-882	12 MPa	1700 psi
Elastic Modulus	ASTM D-882	480 MPa	70,000 psi
Impact Strength	DuPont pneumatic impact tester	7.7 X 10 ³ J/m	144 ft-lb/in
Folding Endurance (MIT)	ASTM D-2176	10,000 cycles	
Tear Strength—Initial (Graves)	ASTM D-1004	2.65 N	270 g force
Tear Strength—Propagating (Elmendorf)	ASTM D-1922	1.23 N	125 g
Bursting Strength (Mullen)	ASTM D-774	76 kPa	11 psi
Thermal			
Melt Point	ASTM D-3418 (DTA)	260–280°C	500–536°F
Zero Strength Temperature	b	255°C	490°F
Coefficient of Thermal Conductivity	Cenco-Fitch	0.195 W/m×K	1.35 Btu×in/h×ft ² ×°F
Specific Heat	—	1172 J/kg×K	0.28 Btu/lb×°F
Heat Deflection Temperature at 0.46 N/mm ² (66 psi) at 1.82 N/mm ² (264 psi)	ASTM D-648 Tensile Bars	70°C 51°C	158°F 124°F
Dimensional Stability	30 min at 150°C (302°F)	MD = 0.72% expansion TD = 2.2% shrinkage	
Flammability Classification ^e	ANSI/UL 94	VTM-0	
Oxygen Index	ASTM D-2863	95%	

^aFor 0.025 mm (1 mil) film at 25°C (77°F) unless otherwise specified.

^bTemperature at which a film supports a load of 0.14 N/mm² (20 psi) for 5 sec.

^cThis classification rating is not intended to reflect hazards presented by this or any other material under actual fire conditions.

^dSamples melted in arc did not track.

^eTo convert to $\text{cm}^3/100 \text{ in}^2 \times 24 \text{ h} \times \text{atm}$, multiply by 0.0645.

Property Values of DuPont FEP Fluorocarbon Film (continued)

Property	Test Method	Typical Value ^a	
		SI Units	English Units
Electrical			
Dielectric Strength, short-time in air at 23°C (73°F), 6.35 mm (1/4 in) diameter electrode, 0.79 mm (1/32 in) radius 60 Hz, 500 V/s rate of rise: 0.025 mm (1 mil) film 5 mm (20 mil) film	ASTM D-149 Method A	260 kV/mm 70 kV/mm	6500 V/mil 1800 V/mil
Dielectric Constant, 25°C (77°F), 100 Hz to 1 MHz –40 to 225°C (–40 to 437°F), 1000 Hz	ASTM D-150	2.0 2.02–1.93	
Dissipation Factor, 25°C (77°F), 100 Hz to 1 MHz –40 to 225°C (–40 to 437°F), 1000 Hz –40 to 240°C (–40 to 464°F), 1 MHz	ASTM D-150	0.0002–0.0007 0.0002 0.0005	
Volume Resistivity, –40 to 240°C (–40 to 464°F)	ASTM D-257	>1 X 10 ¹⁸ ohm.cm	
Surface Resistivity, –40 to 240°C (–40 to 464°C)	ASTM D-257	>1 X 10 ¹⁶ ohm/sq	
Surface Arc Resistance	ASTM D-495	>165 sec ^d	
Insulation Resistance at 100°C (212°F) at 150°C (302°F) at 200°C (392°F)	Based upon 0.2 MF wound capacitor sections, using single layer, Teflon [®] 50A Film	350,000 Mohm×μF 250,000 Mohm×μF 65,000 Mohm×μF	
Chemical			
Moisture Absorption	—	< 0.01%	
Weatherability	Continuous exposure in Florida	No adverse effects after 20 yr	
Permeability, Gas:	ASTM D-1434	cm ³ /m ² ×24 h×atm ^e	
Carbon Dioxide		25.9 X 10 ³	
Hydrogen		34.1 X 10 ³	
Nitrogen		5.0 X 10 ³	
Oxygen		11.6 X 10 ³	
Permeability, Vapors:	ASTM E-96	g/m ² ×d	g/100 in ² ×24 h
Acetic Acid		6.3	0.41
Acetone		14.7	0.95
Benzene		9.9	0.64
Carbon Tetrachloride		4.8	0.31
Ethyl Alcohol		10.7	0.69
Hexane		8.7	0.56
Water	7.0	0.40	

^aFor 0.025 mm (1 mil) film at 25°C (77°F) unless otherwise specified.

^bTemperature at which a film supports a load of 0.14 N/mm² (20 psi) for 5 sec.

^cThis classification rating is not intended to reflect hazards presented by this or any other material under actual fire conditions.

^dSamples melted in arc did not track.

^eTo convert to cm³/100 in²×24 h×atm, multiply by 0.0645.

DuPont FEP fluoropolymer is chemically inert and solvent-resistant to virtually all chemicals except molten alkali metals, gaseous fluorine, and certain complex halogenated compounds such as chlorine trifluoride at elevated temperatures and pressures.

Property Values of DuPont FEP Fluorocarbon Film (continued)

Property	Test Method	Typical Value ^a	
		SI Units	English Units
Miscellaneous			
Density	ASTM D-1505	2150 kg/m ³	134 lb/ft ³
Coefficient of Friction, Kinetic (Film-to-Steel)	ASTM D-1894	0.1–0.3	
Refractive Index	ASTM D-542	1.341–1.347	
Solar Transmission	ASTM E-424	96%	

For more information call (302) 479-7731

www.teflon.com

DuPont Fluoroproducts
P.O. Box 80713
Wilmington, DE 19880-0713

Europe

DuPont de Nemours Int'l SA
 DuPont Fluoroproducts
 2, chemin du Pavillon
 P.O. Box 50
 CH-1218 Le Grand-Saconnex
 Geneva, Switzerland

Japan

DuPont Kabushiki Katsha
 Arco Tower
 8-1, Shimomeguro 1-chome
 Meguro-ku, Tokyo 153
 Japan
 81-3-5434-6139

Asia Pacific

DuPont China Holding Co. Ltd.
 Bldg. 11, 399 Keyuan Road
 Zhangjiang Hi-Tech Park
 Pudong New District
 Shanghai, 201203, China
 Tel: +86 400 88 51 888

Canada

DuPont Canada, Inc.
 DuPont Fluoroproducts
 P.O. Box 2200, Streetsville
 7070 Mississauga Road
 Mississauga, Ontario, Canada
 L5M 2H3
 (800) 207-0756

South America

DuPont do Brasil S/A
 Fluoropolymers
 Alameda Itapecuru, 506
 06454-080 - Alphaville
 P.O. Box 263
 Barueri, Sao Paulo, Brazil
 0800-171715
 Produtos.Brazil@bra.dupont.com

www.teflon.com

Copyright © 2010 DuPont or its affiliates. All rights reserved. The DuPont Oval Logo, DuPont™, The miracles of science™, and Teflon®, are registered trademarks or trademarks of E. I. du Pont de Nemours and Company or its affiliates.

NO PART OF THIS MATERIAL MAY BE REPRODUCED, STORED IN A RETRIEVAL SYSTEM OR TRANSMITTED IN ANY FORM OR BY ANY MEANS ELECTRONIC, MECHANICAL, PHOTOCOPYING, RECORDING OR OTHERWISE WITHOUT THE PRIOR WRITTEN PERMISSION OF DUPONT.

The data listed herein fall within the normal range of product properties but they should not be used to establish specification limits nor used alone as the basis of design. The DuPont Company assumes no obligation or liability for any advice furnished by it or for results obtained with respect to these products. All such advice is provided gratis and Buyer assumes sole responsibility for results obtained in reliance thereon. DuPont warrants that the material itself does not infringe any United States patent but no license is implied nor is any further patent warranty made.

CAUTION: Do not use in medical applications involving permanent implantation in the human body or contact with internal body fluids or tissues. For other medical applications, see "DuPont Medical Caution Statement," H-50102.



Surface Energy Data for FEP: Fluorinated ethylene propylene, CAS # 25067-11-2

Source ^(a)	Mst. Type ^(b)	Data ^(c)	Comments ^(d)
Sperati, 1989 ⁽²²²⁾	Critical ST	$\gamma_c = 17.8-18.6 \text{ mJ/m}^2$; no temp cited	Test liquids not known.
Markgraf, 2005 ⁽⁶²⁾	Critical ST	$\gamma_c = 18-22 \text{ mJ/m}^2$; no temp cited	Test liquids not known.
Petke, 1969 ⁽²³⁴⁾	Contact angle	$\theta_w^A = 108^\circ$; no temp cited	
Dwight, 1974 ⁽⁵²⁾	Contact angle	$\theta_w^A = 109^\circ$, $\theta_w^R = 93^\circ$, $d\theta_w = 16^\circ$; no temp cited	
Westerdahl, 1974 ⁽⁶³⁾	Contact angle	$\theta_w^Y = 103^\circ$, no temp cited	Commercial grade film, thickness 5 mils.
Triolo, 1983 ⁽¹⁸⁹⁾	Contact angle	$\theta_w^R = 96^\circ$; no temp cited	Data estimated from graph. Fully hydrated sample immersed in water; interface with advancing, submerged octane bubble.
Egitto, 1990 ⁽⁶⁵⁾	Contact angle	$\theta_w^Y = 110^\circ$, no temp cited	
Li, 1992 ⁽¹⁷⁶⁾	Contact angle	$\theta_w^Y = 111.6^\circ$; 20°C	
Pettit, 1992 ⁽³⁰⁵⁾	Contact angle	$\theta_w^Y = 103^\circ$; no temp cited	
Bee, 1993 ⁽²¹⁴⁾	Contact angle	$\theta_w^A = 115^\circ$, $\theta_w^R = 100^\circ$, $d\theta_w = 15^\circ$; no temp cited	
Good, 1998 ⁽¹⁵¹⁾	Contact angle	$\theta_w^A = 118.6^\circ$, $\theta_w^R = 105.2^\circ$, $d\theta_w = 13.4^\circ$; no temp cited	Surface rinsed with unspecified light hydrocarbon.
Angu, 2000 ⁽²²⁰⁾	Contact angle	$\theta_w^Y = 101.5^\circ$; no temp cited	Underwater captive bubble method, measured on concave tubular surface; technique A.
Angu, 2000 ⁽²²⁰⁾	Contact angle	$\theta_w^Y = 107.3^\circ$; no temp cited	Underwater captive bubble method, measured on concave tubular surface; technique B.
Ebnesajjad, 2006 ⁽²⁸⁰⁾	Contact angle	$\theta_w^Y = 101^\circ$, no temp cited	FEP-coated wire.
Chaudhury, 1984 ⁽²¹⁾	Contact angle	$\gamma_s = 17.9 \text{ mJ/m}^2$ ($\gamma_s^{LW} = 17.9$, $\gamma_s^{AB} = 0.0$, $\gamma_s^+ = 0.0$, $\gamma_s^- = 0.0$); 20°C	Test liquids: water, alpha-bromonaphthalene, diiodomethane, formamide, and glycerin; acid-base analysis.
Li, 1992 ⁽¹⁷⁶⁾	Contact angle	$\gamma_c = 15.9 \text{ mJ/m}^2$; 20°C	Test liquids not known; from advancing contact angles by equation of state method.
Kwok, 2000 ⁽¹⁶⁶⁾	Contact angle	$\gamma_c = 18.0 \text{ mJ/m}^2$; no temp cited	Re-calculated by equation of state method from data produced by Kwok, 1995 ⁽¹⁶⁷⁾ .
Kwok, 2000 ⁽¹⁶⁶⁾	Contact angle	$\gamma_c = 17.8 \text{ mJ/m}^2$; no temp cited	Re-calculated by alternate equation of state method from data produced by Kwok, 1995 ⁽¹⁶⁷⁾ .
Ebnesajjad, 2006 ⁽²⁸⁰⁾	Contact angle	$\gamma_s = 16.9 \text{ mJ/m}^2$ ($\gamma_s^d = 14.3$, $\gamma_s^p = 2.6$); no temp cited	Test liquids: water, diiodomethane, and xylene; FEP-coated wire, by geometric mean equation.
Ebnesajjad, 2006 ⁽²⁸⁰⁾	Contact angle	$\gamma_s = 22.7 \text{ mJ/m}^2$ ($\gamma_s^d = 17.3$, $\gamma_s^p = 5.4$); no temp cited	Test liquids: water, diiodomethane, and xylene; FEP-coated wire, by harmonic mean equation.
Andrews, 1973 ⁽⁵¹⁾	Unknown	$\gamma_s = 20.0 \text{ mJ/m}^2$ ($\gamma_s^d = 19.6$, $\gamma_s^p = 0.4$); no temp cited	Test details unknown; probably by contact angle.
Wu, 1982 ⁽⁴⁹⁾	Unknown	$\gamma_s = 18.8 \text{ mJ/m}^2$; 20°C	Measurement method not cited; PE molded under nitrogen.

B. SOP Rheometer

SOP „Rotational Viscosity Measurements using the Rheometer Physics MCR 301”

1. Purpose

This document describes the booting and settings of the Rheometer Physics MCR 301 by Anton Paar, and leads through a simple rotational viscosity measurement of a fluid.'

The document was created during viscosity measurements for a diploma thesis. The tests were done at 04/04/2012, 26/04/2012 and 12/06/2012 at the Institute of Biomechanics (TUG) under the supervision of Michael Unterberger MSc.

2. Responsibilities

It's obligatory to follow this SOP to provide constant quality of measurement.

3. Required Materials

- Rheometry Working Station:
 - o Rheometer Physics MCR 301 by Anton Paar
 - o Compressor by Jun-Air
 - o Heating/cooling unit by Anton Paar
 - o PC by DELL (Microsoft Windows XP) with Software RheoPlus
- Liquid Sample
 - o Human Albumin Solution 200g/L and Perfusate with Glucose and 0.3% HSA
 - o Liquor, Water, Oil
- ddH₂O, Alcohol and Cleaning Sheets
- Small syringe



Fig. 1: Rheometer and PC

4. Setting up and starting the Rheometer



Fig.2. Before starting the measurements, make sure that both air exits of the compressor are connected with the rheometer.

4.1 Starting the compressor

- Compressed air is used to supply the air bearing of the rheometer.
- Press the green button to start the compressor (Fig. 3).
- Keep the two exits of the blue filter boxes (at the back of the compressor) shut until a certain pressure is reached and no air streams out anymore (Fig. 4).
- Set the operating pressure (Fig.3, right gauge) to 5 bar. To do so, pull out the button and rotate it.
- The boiler pressure (Fig. 3, left gauge) should not be less than 5 bar during the measurements. After pumping, the boiler pressure is at 8 bar. It decreases to 5 bar after ca. 3 minutes.



Fig. 3: Frontal view of the compressor



Fig. 5: Opened heating / cooling system.

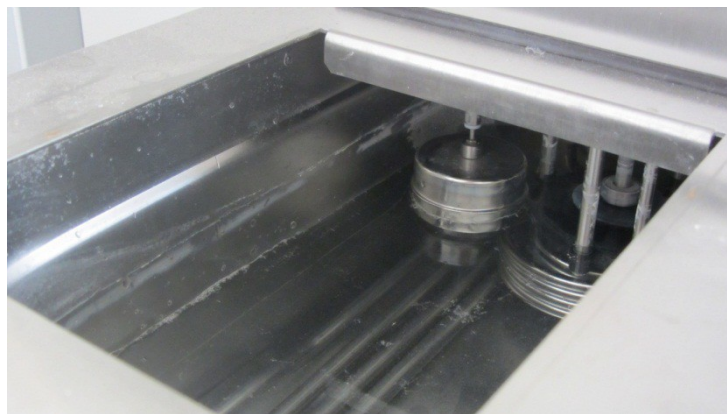


Fig. 6: Fill in deionized water.



Fig. 7: After starting the system.

4.4 Starting the rheometer

- Switch on the rheometer (Fig. 8)
- Wait for the instrument to boot, which takes about 1 minute. The instrument is ready when the display shows "Status: O.K." in the last line.
- Connect the device with the PC over LAN by pressing the "Online"-button on the rheometer (Fig.9).
- In RheoPlus, click on the "Device"-Button
- *If the rheometer isn't detected automatically, open the Control Panel in RheoPlus, and click "Detect".*
- Fix the cap of the rheometer using a screw (Fig. 10 A, B).
- Click on "Initialize"
- During initialization, the measuring head will move to the top position to check the gap sensor. The rotor will perform several revolutions at high speed to check the position sensor.
- Set the temperature (Meas.-Cell), the heating system of the cap starts to work

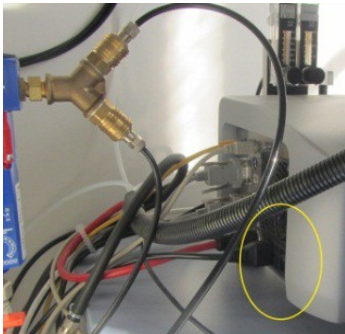


Fig. 8



Fig. 9



Fig. 10 (← A; ↑ B)

4.5 Measuring system

- We use a parallel plate system with a diameter of 43 mm (PP43/GC, Fig. 11)
- Mount the device by locking it into the ring system of the cap. To do so, push up the sleeve and insert the upper end of the measuring system to the coupling. (Fig. 12)
 - The markings of the measuring system and the coupling system must be aligned.
- The sensor of the rheometer recognizes the measurement system, further adjustments are done automatically.

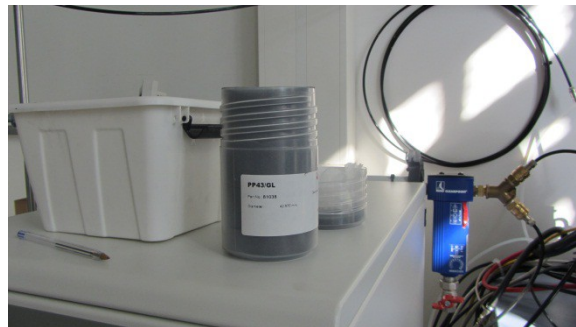


Fig. 11



Fig. 12

- In RheoPlus (Fig. 13), click on “Set Zero Gap” to bring the cap to zero position. The measurement system is being set to zero position, and the normal forces are set to 0 N at the minimum position.
- Set the position manually. In our experiment, we used a measuring position of 0.5 mm and a lift position of 45 mm.
- Click on “Continue” when asked.

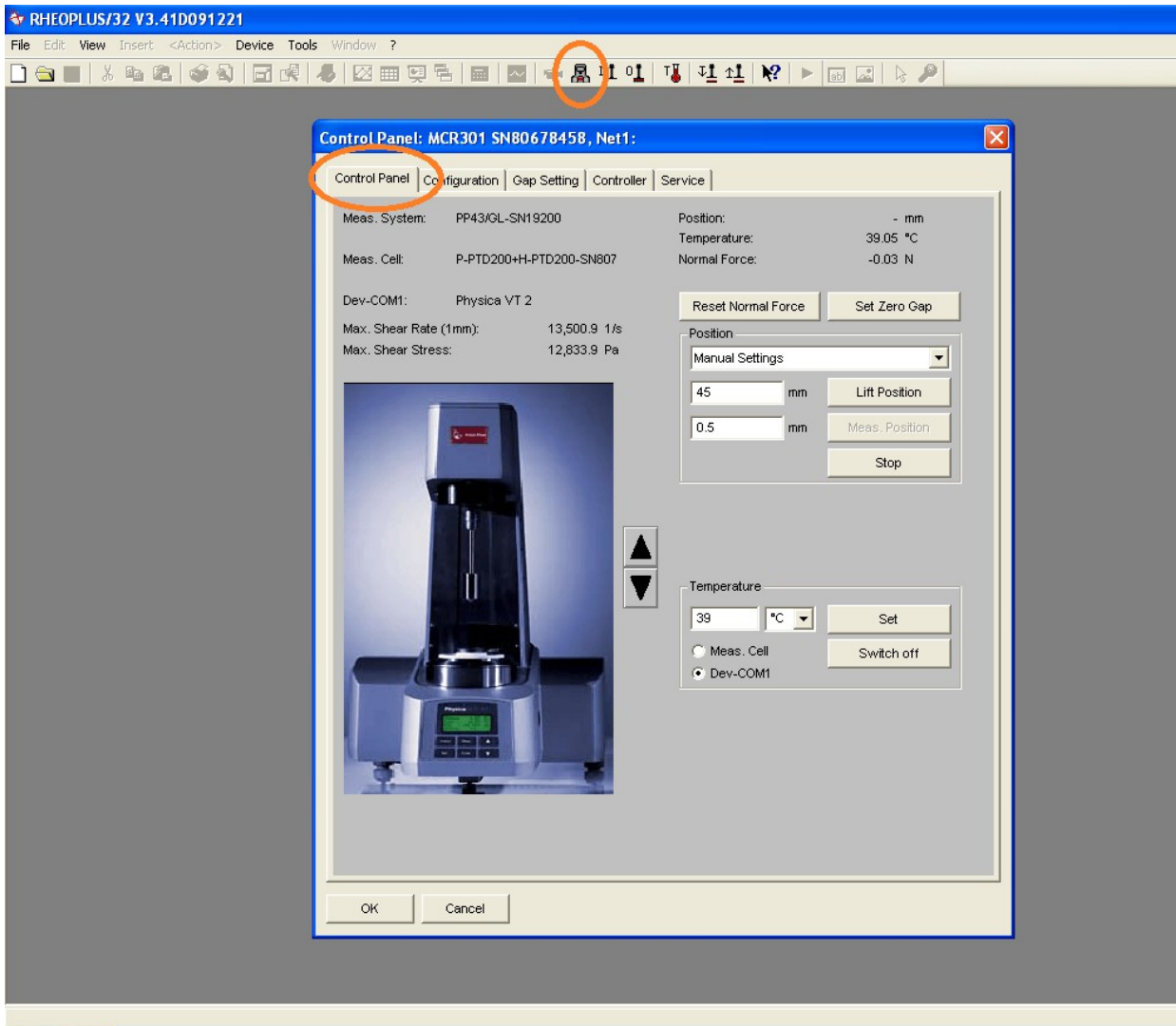


Fig. 13

4.6 Calibration

- In the service panel of RheoPlus (Fig. 14), go to Meas.-System and click on “Start”.
- Switch off the compressor (when it is not pumping). Make sure that the boiler pressure does not decrease below 5 bar. If the calibration is taking too long (> ca. 3 min) and the boiler pressure sinks under 5 bar, have a break and let the compressor pump again.
- Don't touch or shake the system.
- After finishing, click “Save”.

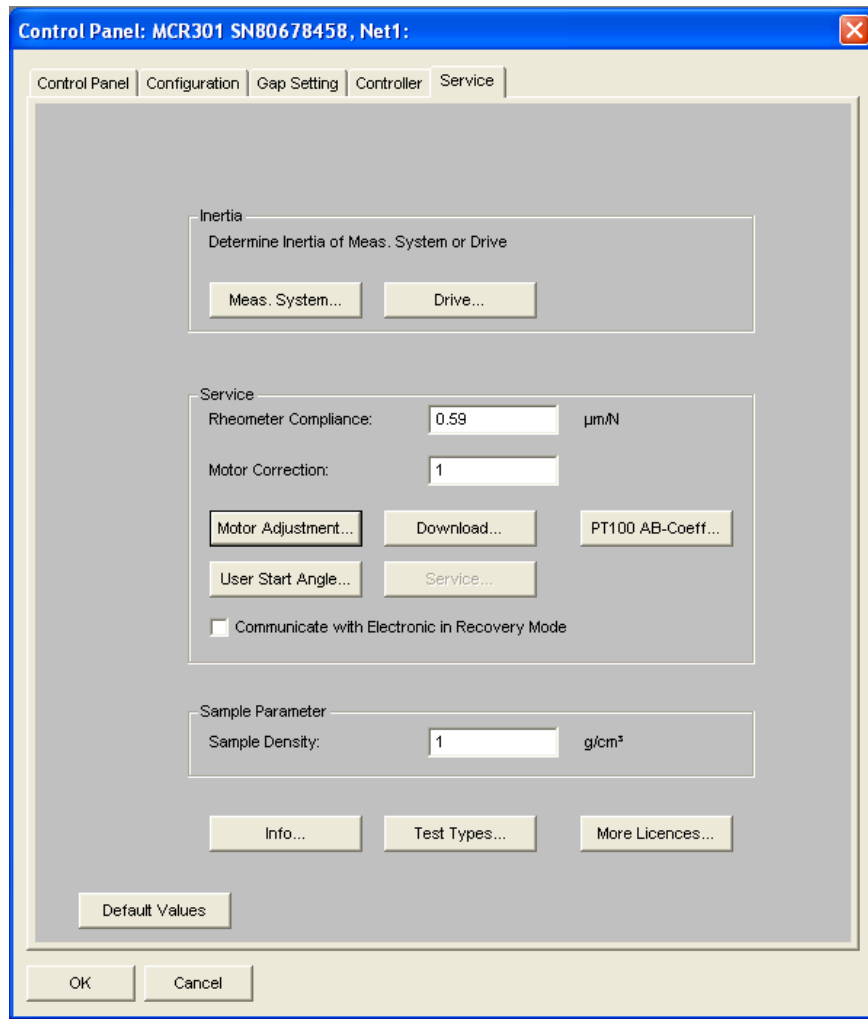


Fig. 14

4.6 Motor Adjustment (once a month for frequently used rheometers)

- Click on the button in the service panel, make sure the compressor is switched off.

4.7 Cleaning

- Lift the cap to 45 mm (Button “Lift position” in the control panel)
- When using biological samples, first disinfect the plates, and then clean them 10 times with distilled water.
- Note: The plates (Fig. 15) are very robust.
- After cleaning, set the cap to measuring position.
- Click “OK” in the control panel.
- “Save?”: Yes



Fig. 15

5. Create a work sheet

- Go to RheoPlus, and create a new worksheet. You can choose between several protocols. Here we choose the “const. shear rate”, and modify the protocol.
- Several windows are opened (i.e. Fig. 16). The axes can be set by clicking twice. As parameters, we use mPa s and 1/s.
- In the workbook assistant:
 - You can change the setups for the rheometer (i.e. if you like to change the temperature)
 - You can edit the shear rate (or the measuring profile)
 - You can start the test
- One of the windows is called “Measurement 1” (i.e. Fig. 17)
 - You see the settings for the measuring system and the two heating systems (the heater/cooler described afore and the heater of the cap.)
 - To change the values, click twice. A new window opens, you can set it to “active” and set the values.
 - In Fig. 18, you see the settings for the rotational test. In addition, we set the temperature for the cap (PT...).
 - We choose the shear rate as rotational parameter. As profile, we choose Ramp Log+point/Dekade.
- Info: Measure point duration:
 - If we choose a variable measure point duration for different velocities, the means of the velocities are calculated differently.
 - If we choose no time-setting (fixed measuring point duration), we get better and safer results, but it could be that it takes longer than 3 min (Compressor!)
- At the end, we check the profile. Next, fill out infos for the measurements.

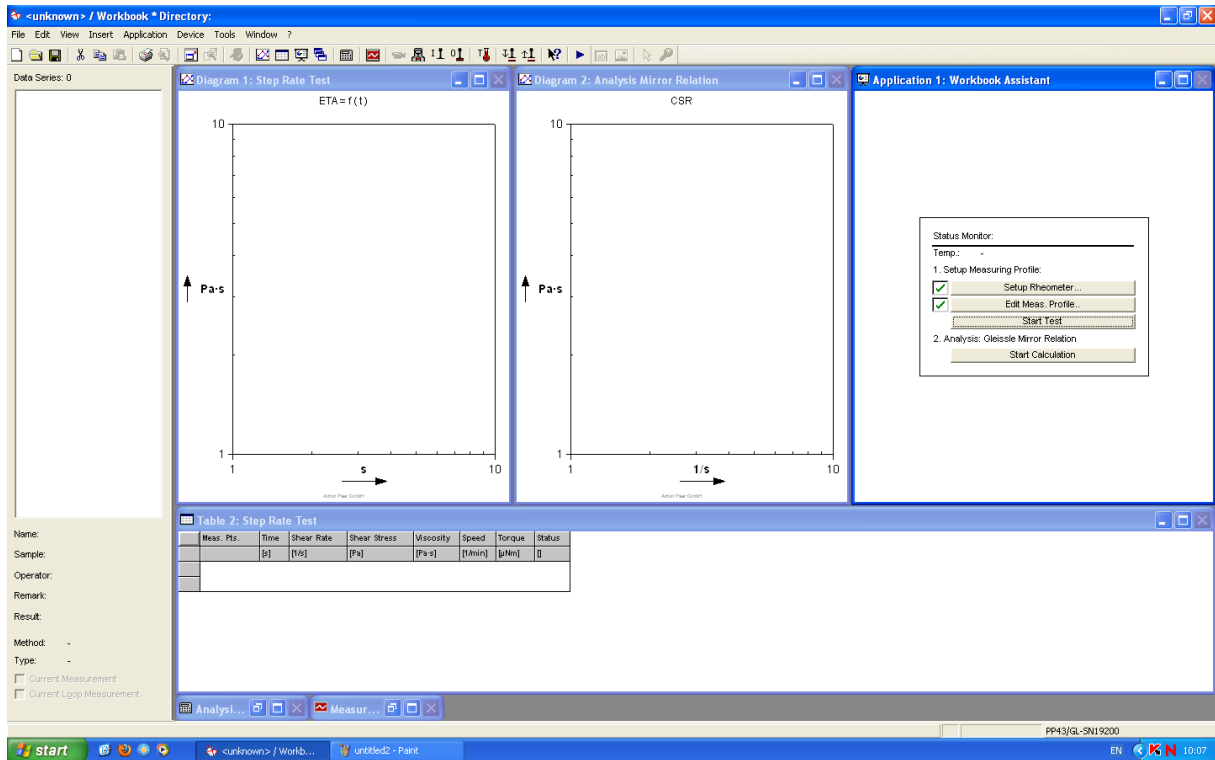


Fig. 16

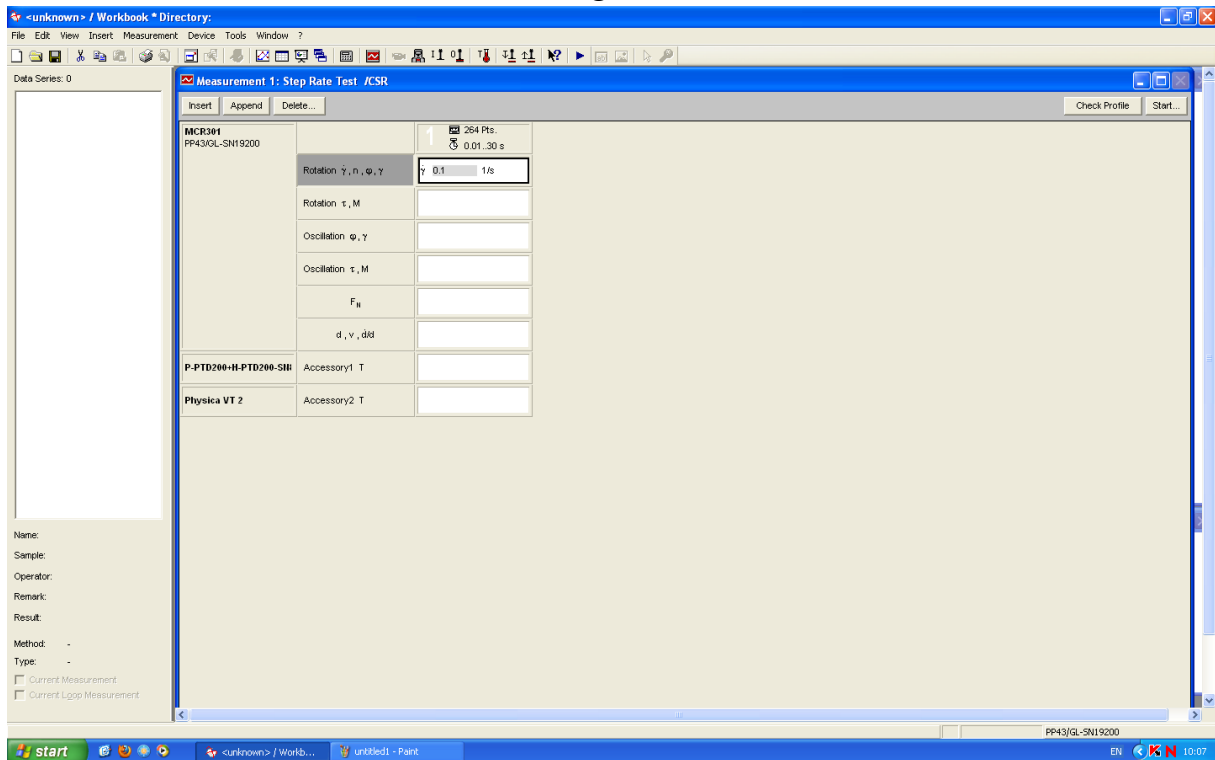


Fig. 17

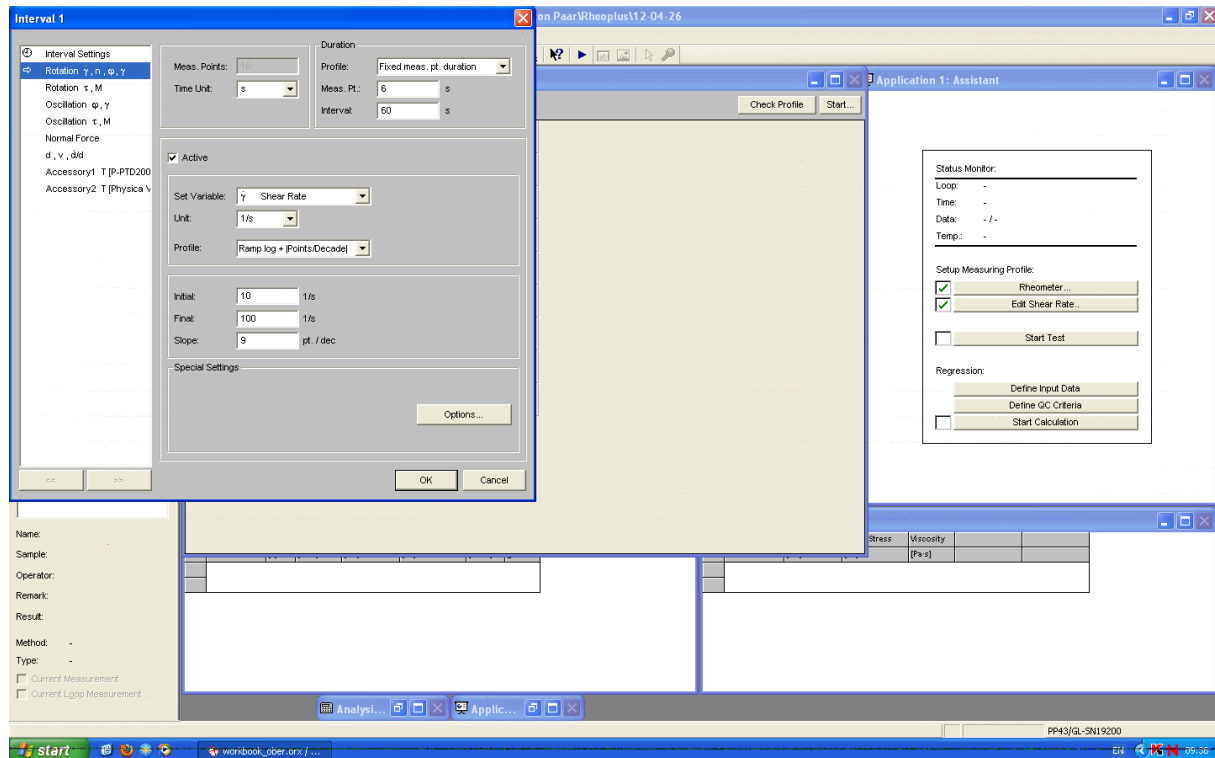


Fig. 18

6. Measuring

- In RheoPlus, we choose “Lift position”.
- If we have a measuring position of 0.3 mm and a diameter of the system of 43 mm, we can calculate the liquid volume we need (in our case ca. 0.45 mL).
- Make sure not to load too much nor too little sample. It will lead to large errors in the measurement data. In Fig. 19 you see the ideal sample volume for a plate-and-cone system. The same principle is applicable for parallel-plate-systems.
- The measuring position is set to 0.25 mm. This way the liquid is compressed a little bit. The measuring system should be fully wetted. To do so, adjust the measuring position. Click continue if asked.
- Next, we can start the test (after checking the profile in RheoPlus). Make sure, that the compressor does not pump. An exemplary output is shown in Fig. 21. You can also export the data in xls-format.
- To abort the test, click on the step symbol.
- Note: When making a measuring break, loose the screw and lift up the cap a little bit.
- Make sure to fill out the measurement documentation (xls-file) on the desktop.

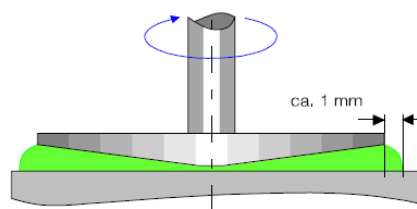


Fig. 19

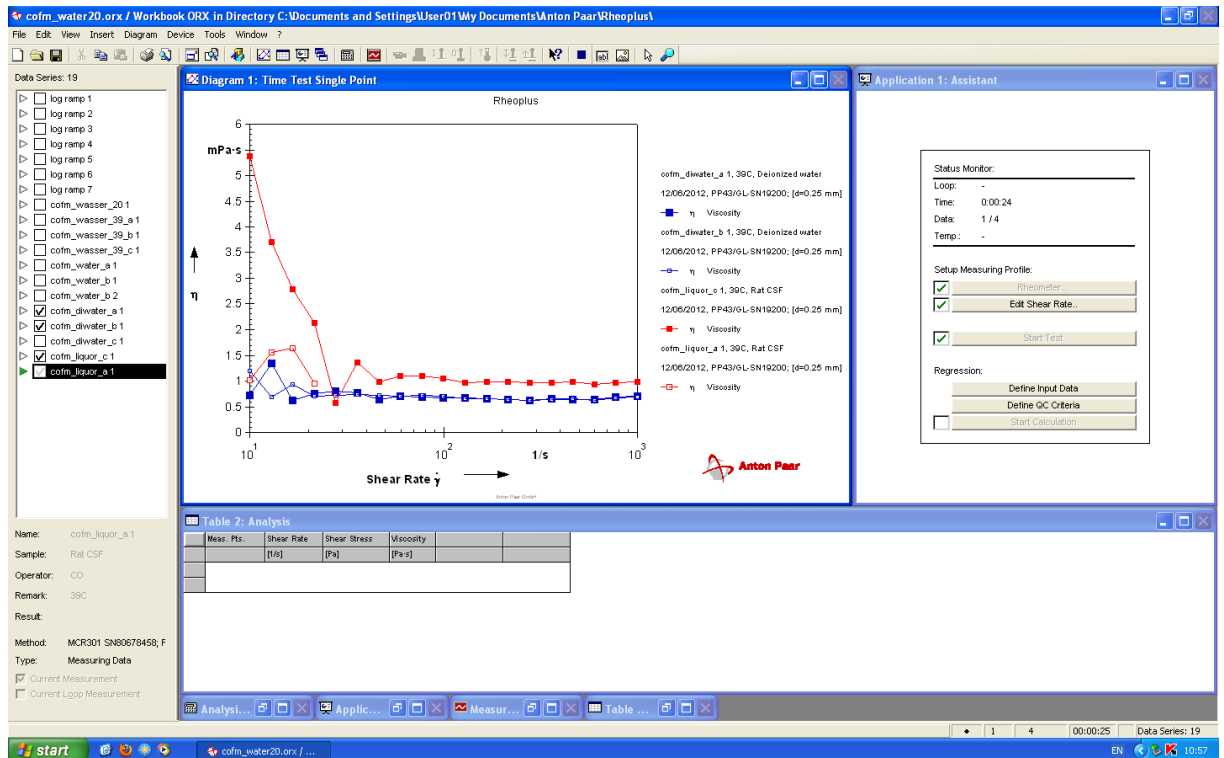


Fig. 20

7. After measuring

- Disconnect the rheometer from the PC ("Online").
- Shut down the devices.
- Clean the rheometer (see above).
- Empty the heating/cleaning system. To do so, open the water outlet using a screw. (Fig. 21)

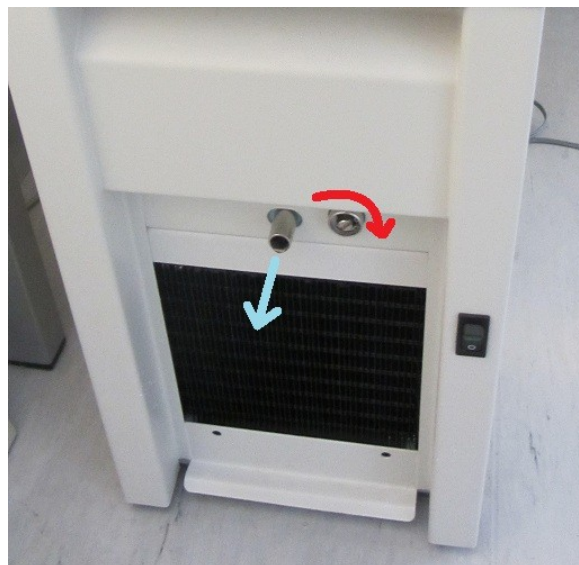


Fig. 21

Statutory Declaration

I declare that I have authored this Thesis independently, that I have not used other than the declared sources/resources, and that I have explicitly marked all material, which has been quoted by the relevant reference.

date

signature